UNCONVENTIONAL PHOTOELECTRON SPECTROSCOPIC STUDIES: PES OF SOME TRANSIENT SPECIES AND REACTIVE MOLECULES

by

SHUIT-TONG LEE

B.Sc., The Chinese University of Hong Kong, 1969

M.Sc., University of Rochester, New York, 1972

A THESIS SUBMITTED IN PARTIAL FULFILMENT OF
THE REQUIREMENTS FOR THE DEGREE OF

DOCTOR OF PHILOSOPHY

in the Department of

CHEMISTRY

We accept this thesis as conforming to the
required standard

THE UNIVERSITY OF BRITISH COLUMBIA

October, 1974

In presenting this thesis in partial fulfilment of the requirements for an advanced degree at the University of British Columbia, I agree that the Library shall make it freely available for reference and study. I further agree that permission for extensive copying of this thesis for scholarly purposes may be granted by the Head of my Department or by his representatives. It is understood that copying or publication of this thesis for financial gain shall not be allowed without my written permission.

Department of Chemistry

The University of British Columbia
Vancouver 8, Canada

Date Oct. 9 1974

ABSTRACT

A fast pumping, versatile photoelectron spectrometer suitable for the study of transient species and reactive molecules has been designed, constructed and tested. The photoelectron spectra of seventeen such compounds (CS, SO, S_2O, HN=NH, DN=ND, CH_3N=NH, HCP, OCSe, SCSe, CSe_2, O_3, FNO, ClNO, BrNO, HNO_3, $ClNO_2$ and FNO_2) have been obtained. The individual spectra have been assigned by using information supplied from vibrational analysis, by comparison with molecular orbital calculations and with related molecules. The experimental Franck-Condon factors have been utilized to estimate the geometries of the ionic states, and the procedure has been found to be quite reliable. The study has shown the potential of photoelectron spectroscopy in providing information on the electronic structure of transient species and reactive molecules, information that is difficult to obtain by other spectroscopic techniques.

TABLE OF CONTENTS

Page

Page

LIST OF FIGURES

Figure | Page

Figure | Page

LIST OF TABLES

ACKNOWLEDGEMENTS

I would like to express my sincere appreciation and gratitude to Dr. D. C. Frost and Dr. C. A. McDowell for their continued support, understanding and guidance throughout the course of this work.

I would also like to thank my many colleagues, Mr. A. Bain, Dr. J. C. Bunzli, Dr. M. Chiang, Mr. T. Chau, Dr. L. S. Chia, Dr. A. B. Cornford, Dr. A. Katrib, Dr. D. J. Smith, Dr. N. P. C. Westwood, Dr. G. Wight and Mr. D. Yee for their assistance on many occasions. Thanks are also due to Dr. R. Boyd, Dr. C. E. Brion, Dr. F. G. Herring, Dr. H. Kroto, Dr. A. J. Merer and Dr. R. Tapping for helpful discussions.

I wish to acknowledge gratefully the staff of the Electronic, Glass, Illustration and Mechanical Workshops. I am specially grateful to Mr. E. Matter for his precision construction of the spectrometer and to Mr. C. McCafferty for his skillful technical assistance.

I am thankful to Dr. N. P. C. Westwood for a careful

reading of this manuscript, to Mr. Paul Tang for typing part of the first draft and to Miss Patti Hon for typing the thesis.

I wish to extend my appreciation to all our friends who made our residence in Vancouver most enjoyable.

I am most grateful to my wife for her love, understanding and encouragement. I am indebted to my father for undergoing a lot of hardship in bringing me up. Our son Stanley should also be thanked for behaving himself during the writing of this thesis.

CHAPTER ONE

INTRODUCTION

Photoelectron spectroscopy is, essentially, a technique for measuring the binding energies or ionization potentials of electrons in molecules or atoms, by exposing the sample to a source of monochromatic photons of known energy $h\nu$ and analyzing the kinetic energies of the photoejected electrons. The binding energies E_b of the different groups of electrons can be obtained from the measured kinetic energies E_{kin} utilizing the Einstein photoelectric equation,

$$E_b = h\nu - E_{kin} . \qquad (1)$$

The essential requirements for a photon source which is to be used in photoelectron spectroscopy are that it be monochromatic, of usable intensity, and have sufficient energy to ionize the electrons of interest. A list of such photon sources, together with their characteristics is shown in Table I. Depending upon the energy of the photon source, the overall

TABLE 1. Monochromatic Photon Sources For Use in Photoelectron Spectroscopy

X-Ray Photon Source	Energy (eV)	Wave Length (Å)
Ag K_α	22162.9	0.55941
Mo K_α	17479.3	0.70930
Cu K_α	8048	1.5405
Cr K_α	5415	2.2896
Al K_α	1486.6	8.399
Mg K_α	1253.6	10.034
Na K_α	1041.0	11.910

VUV Photon Source	Energy (eV)	Wave Length (Å)
HeII	40.8126	303.781
HeI	21.2175	584.334
NeI doublet	16.8477*/16.6704	735.895*/743.718
ArI doublet	11.8278*/11.6233	1048.219*/10066.659
KrI doublet	10.6434/10.0321*	1164.867/1235.838*
H Lyman α	10.1986	1215.668
XeI doublet	9.5697/8.4363*	1295.586/1469.610*

* indicates the more intense line of the doublet.

field of photoelectron spectroscopy falls into two branches. One branch uses higher energy X-ray sources, and is termed Electron Spectroscopy for Chemical Analysis (ESCA)[1,2] or X-ray Photoelectron Spectroscopy (XPS). The other uses vacuum ultraviolet (VUV) radiation, and is called Molecular Photoelectron Spectroscopy[3], UV Photoelectron Spectroscopy (UPS), or simply Photoelectron Spectroscopy (PES). In ESCA, Aluminum K_α (1486.6 eV) and Magnesium K_α (1253.6 eV) are by far the most commonly used sources due to their narrower line widths, higher intensity and ease of operation, while the HeI resonance line (21.2175 eV) is most popularly used in PES for the same reasons. ESCA, because of its more energetic source and lower limiting resolution (>0.2 eV), is mainly concerned with the study of inner or core shell electrons. PES is exclusively concerned with outer or valence shell (up to about 40 eV) electrons. This leaves a gap between 40 eV and 1,000 eV where suitable photon sources are lacking, although recent developments indicate that this gap may be filled by the use of synchrotron radiation in conjunction with a monochromator[4-6]. Yttrium X-ray lines at about 130 eV developed by Krause[7] are also a promising source, although satellite lines are a complicating factor here. This thesis is concerned with PES using mainly the HeI resonance line.

In view of the fact that the basic principles of PES were well understood as early as 1905, when Einstein[8] successfully explained the photoelectric effect, it is surprising that the first set of such experiments appeared only as late as the

early 1960's[9-12]. Since then there has been an exponential growth in the field of PES as evidenced by the appearance of numerous extensive reviews[1-3, 13-37], and the gathering of several international conferences[38-41]. Within the past ten years or so, PES has developed from its exploratory stage to become one of the standard techniques of modern chemistry. Although the field is a young and developing one, it is generally acknowledged that it has at least reached its first stage of maturity[42]. The primary goal of PES, which is to obtain molecular ionization potentials with high precision and resolution, has certainly been met judging from the fact that hundreds of spectra have been recorded and discussed in books[10,11] and in the literature. Alerted by its potential, and with the availability of commercial photoelectron spectrometers[43], more and more researchers have begun to apply PES as a routine tool in molecular spectroscopy. In this respect, PES is essentially like any of the standard spectroscopic techniques, such as nmr, mass spectrometry, etc. To date, most of published PES work has been concerned with compounds that are stable under normal conditions, and have appreciable volatility (> .01 Torr) below 200° C. This kind of PES work will be called 'conventional' photoelectron spectroscopic studies in this thesis. On the other hand, PES studies of transient species and reactive molecules are rare because of the experimental difficulties involved. During the initial stages of this study, a few exploratory attempts[44-48] to study such systems with the technique of PES had revealed its great potential in providing information on the chemical

bonding of transient species, which would normally be very difficult to obtain by other methods. The extension of PES to study reactive molecules, which can be handled and studied only under appropriately controlled conditions, would be very fruitful since these molecules play a significant role in chemistry.

This thesis will describe an attempt to extend PES into the realms of these 'unconventional' photoelectron spectroscopic studies. A photoelectron spectrometer suitable for this kind of work has been designed and constructed. With this spectrometer, some transient species and reactive molecules have been studied. In addition, it has been possible to vary the temperature of the sample between -180°C and +1,200°C, where temperature dependent equilibrium systems may be studied.

CHAPTER TWO

THEORY OF PHOTOELECTRON SPECTROSCOPY

Although photoelectron spectroscopy (PES) is a relatively new technique, its theory is well documented and has been discussed in great detail in numerous reviews[1-3, 13-37]. Therefore, except for those aspects which are more pertinent to the study in this thesis, only a brief summary of the basic principles of the theory will be presented here. Greater attention will be paid to those areas where new developments have been achieved.

2.1 Characteristics Of A Photoelectron Spectrum

When a photoelectron is ejected by a photon of energy $h\nu$ from a molecule or atom, by the conservation of energy the following energy relation holds.

$$h\nu = E_{kin} + E_r + I_0 + \Delta E_{vib} + \Delta E_{rot} + \Delta E_{tran}, \quad (2.1.1)$$

where E_{kin} is the kinetic energy of the photoelectron,

E_r is the recoil energy of the ion,

I_0 is the difference in the electronic energy of the ion and molecule, and is termed the adiabatic ionization potential,

and ΔE_{vib}, ΔE_{rot} and ΔE_{tran} are respectively the difference in the vibrational, rotational and translational energy of the ion and the parent molecule.

Because of the large difference in the mass of the ion and the ejected electron, E_r is neglected through consideration of the conservation of momentum. Under the present level of experimental resolution (>10 meV, see section 2.3), rotational and translational energy level are usually not resolved, and thus ΔE_{rot} and ΔE_{tran} are also neglected. Usually the molecule is in the ground vibrational state, thus eq. (2.1.1) reduces to

$$h\nu = E_{kin} + I_0 + E_{vib}^{+} \qquad (2.1.2)$$

where E_{vib}^{+} is the vibrational energy of the ion. The measurement of the kinetic energy of the electron then gives the ionization potential of the molecule.

The photoelectron (PE) spectrum of a molecule thus consists of several PE bands, each of which corresponds to an ionization potential (IP) of the molecule, all the way up to the energy of the incident photons. The integrated area or the intensity of the individual band is related to the differential photoionization cross section corresponding to that

ionic state, and the shape of the band is an indication of the geometry change upon ionization. Each or some of these bands may show a series of resolved peaks corresponding to the different vibronic states. The separations between these peaks are then the vibrational frequencies of the ion. The lowest energy (first) peak, or the onset of the PE band is normally the adiabatic IP, while the most intense peak or the maximum of the band is referred to as the vertical IP. If the molecule is vibrationally excited or there is a large change in geometry during ionization, then care should be exercised in locating the exact position of the adiabatic IP. The intensity of each individual peak in a PE band is proportional to the probability of producing that particular vibronic state, giving the so-called Franck-Condon Factor.

In addition to the above-mentioned vibrational fine structure, further band structure may be due to spin-orbit coupling, Jahn-Teller distortion, or a mixture of the two, i.e. the spin-vibronic interactions. For quasi-linear ionic states the possibility of the Renner-Teller effect exists. Complications to simple band shapes may arise through auto-ionization or predissociation, and must be considered in a rigorous analysis. For molecules having IP's less than ∿11 eV, additional bands corresponding to low energy photo-electrons may arise due to the impurity lines in the light source (see section 3.3.3).

2.2 The Interpretation Of Molecular PE Spectra

2.2.1 A Brief Survey Of Assignment Criteria

Assuming an orbital description of a molecule, then at a certain level of approximation the molecular PE spectrum is a direct display of the energies of the various molecular orbitals (MO's). The individual PE bands then correspond to the removal of an electron from each MO leaving the ion in different ionic states. The lowest energy band is usually associated with the ground ionic state, while the others correspond to excited ionic states. In this way, the PE spectrum of a molecule is similar to the electronic spectrum of the ion with the transitions occuring only between its occupied MO's. The quantitive correspondence between the energies of the bands or IP's and that of the orbitals from which the electrons are removed is expressed in Koopmans' theorem[49] (see section 2.2.2) which states that the nth IP can be approximated to the negative of the nth orbital energy. With this theorem, the comparison of the calculated orbital energies and the experimental IP's is widely used in the interpretation of PE spectra.

The vibrational fine structures and the shapes of the individual PE bands frequently contain a great deal of information on the bonding characteristics of the orbital to which they relate. The relation between the band structures and orbital characteristics are derived from the Franck-Condon principle[50,51], which will be discussed in section 2.2.3. A further indication of the bonding character of the orbital may

be obtained from the change of the vibrational frequencies on going from the molecule to the ion. This makes use of the close relationship between the vibrational frequency, the force constant and the bond order. Thus, if a nonbonding electron is removed, there will be practically no change in vibrational frequency, whereas if a bonding or antibonding electron is removed, the vibrational frequency of the ion will be less or greater respectively than that of the neutral molecule. In larger polyatomics, several vibrational modes may be excited upon ionization, thus making vibrational assignments more difficult. Occasionally, the analysis of the spin orbit[52,53], Jahn-Teller[54-57] and Renner-Teller [58,59] splittings can be fruitful and lead to a better understanding of the structure of the ion.

A useful approach, especially for complex molecules, is to study a large number of homologous compounds[60,61]. By studying many such related compounds, and correlating and comparing the spectra down a series, one can usually gain some information that would not be obvious otherwise. In such studies, one may also make use of the resonance and inductive effects of the substituent groups. For planar molecules where applicable, the perfluoro effect[62,63] may sometimes be used to differentiate the π and σ orbitals.

Sometimes, the relative intensities of the bands may be used as an indication of the degeneracy of the states, i.e. the degenerate states have greater intensities than the non-degenerate states. This guideline must be used with

caution since it has been found invalid in many cases[17]. Quite recently the study of photoionization cross sections as a function of ionizing energy has shown high potential in providing information on the bonding character of orbitals. Both experimental[64,65] and theoretical[66] studies have indicated that usually the intensities of the orbitals mainly of s character tend to increase with respect to that of the orbitals mainly of p character when using higher energy light sources. The theoretical studies[66-69] have indicated some interesting relationships between the energy dependence of photoionization cross sections and the bonding character of orbitals. In view of the success of these studies, the comparison of measured and calculated values for relative band intensities may become an additional useful assignment criterion in PES. Another related and promising technique is the study of the intensity of the ejected photoelectrons as a function of the angle between the direction of the incoming photon and the outgoing photoelectron. This may also shed light on the nature of the molecular orbital, through the determination of the β factor[70,71].

PES is not a threshold technique, consequently the spectra are generally not complicated by autoionization processes. On the contrary, because of its resonant nature, autoionization in PES can usually be identified by using different light sources, and often leads to useful information about the autoionized state.

2.2.2 Koopmans' Theorem And The Calculation of Vertical IP's

(a) Koopmans' Theorem[49] And Its Implications

Consider a two-step process:

(1) Calculation of a Hartree-Fock (HF) Self-Consistent-Field (SCF) wave function for a molecule with n doubly occupied molecular orbitals and evaluation of its total energy E.

(2) Evaluation of the single determinant energy of the ion E^+ resulting from the removal of an electron from the kth molecular orbital, using the HF-SCF orbitals from the above calculation of the molecule for the remaining electrons.

Koopmans[49] showed that the energy difference or IP calculated in this way is just the negative of the kth orbital energy.

The mathematical proof of Koopmans' theorem (KT) is quite straightforward. For a molecule with n doubly occupied MO's ϕ_i, the single determinant wavefunction is

$$\psi = |\phi_1(1)\bar{\phi}_1(2)\cdots\phi_k(2k-1)\bar{\phi}_k(2k)\cdots\phi_n(2n-1)\bar{\phi}_n(2n)|, \quad (2.2.1)$$

and the Hamiltonian of the molecule is

$$H = \sum_{i=1}^{2n}\left(-\frac{\nabla_i^2}{2} - \sum_{\alpha=1}^{K}\frac{Z_\alpha}{R_{\alpha i}}\right) + \sum_{i<j}^{2n}\frac{1}{r_{ij}} \quad . \quad (2.2.2)$$

The corresponding wavefunction and the Hamiltonian for the ion with an electron removed from the kth MO are

$$\psi^{+} = |\phi_1(1)\bar{\phi}_1(2)\cdots \begin{Bmatrix} \phi_k(2k-1) \\ \bar{\phi}_k(2k-1) \end{Bmatrix} \cdots \phi_n(2n-1)\bar{\phi}_n(2n)| \tag{2.2.3}$$

and

$$H^{+} = \sum_{i=1}^{2n-1} \left(\frac{\nabla_i^2}{2} - \sum_{\alpha=1}^{K} \frac{Z_\alpha}{R_{\alpha i}} \right) + \sum_{i<j}^{2n-1} \frac{1}{r_{ij}} \quad . \tag{2.2.4}$$

In the expression for the Hamiltonians, Z_α is the charge on the nucleus α, $r_{\alpha i}$ is the distance of the electron i from the nucleus α, and r_{ij} is the distance between electron i and j. It can be shown[74] that the total energy of the molecule and the ion are

$$E = 2 \sum_{i=1}^{n} h_i + \sum_{i,j=1}^{n} (2J_{ij} - K_{ij}) \tag{2.2.5}$$

and

$$E^{+} = 2 \sum_{\substack{i=1 \\ i \neq k}}^{n} h_i + \sum_{\substack{i,j=1 \\ i,j \neq k}}^{n} (2J_{ij} - K_{ij}) + h_k + \sum_{\substack{i=1 \\ i \neq k}}^{n} (2J_{ik} - K_{ik}) \quad ; \tag{2.2.6}$$

where

$$h_i = \int \phi_i^*(1) \left(- \frac{\nabla_1^2}{2} - \sum_{\alpha=1}^{K} \frac{Z_\alpha}{R_{\alpha 1}} \right) \phi_i(1) dr_1 \tag{2.2.7}$$

= energy of an electron alone in the field of the bare nuclei; comprising the kinetic and electron-nuclear attraction energy,

$$J_{ij} = \iint \phi_i^*(1)\phi_j^*(2)\frac{1}{r_{12}}\phi_i(1)\phi_j(2)dr_1dr_2 \qquad (2.2.8)$$

= coulombic repulsion between any electron pair,

and

$$K_{ij} = \iint \phi_i^*(1)\phi_j^*(2)\frac{1}{r_{12}}\phi_i(2)\phi_j(1)dr_1dr_2 \qquad (2.2.9)$$

= exchange interaction between any electron pair of the same spin.

Noting $J_{ii} = K_{ii}$, one obtains

$$E^+ - E = -h_k - \sum_{i=1}^{n} (2J_{ik} - K_{ik}) \ . \qquad (2.2.10)$$

Since, however, the kth orbital energy ε_k is given by the solution of the SCF equation, i.e.

$$\left\{\left(-\frac{\nabla_1^2}{2} - \sum_{\alpha=1}^{K}\frac{Z_\alpha}{R_{\alpha 1}}\right) + \sum_{i=1}^{n}(2J_i - K_i)\right\}\phi_k = \varepsilon_k\phi_k \ , \qquad (2.2.11)$$

then one has

$$\varepsilon_k = h_k + \sum_{i=1}^{n} (2J_{ik} - K_{ik}) , \qquad (2.2.12)$$

and hence

$$E^+ - E = -\varepsilon_k . \qquad (2.2.13)$$

This thus illustrates the validity of KT.

There are three kinds of errors in the IP's calculated by this method due to[87]:

(1) The relaxation of the orbitals in the ion due to the perturbation caused by ionization.

(2) The difference in electron correlation energy in the ion and the molecule.

(3) The difference in relativistic energy in the ion and the molecule.

The neglect of (1) is inherent in KT and results in the calculated IP's being too large. Because of this neglect, the calculated IP should correspond to the vertical IP. (2) and (3) are introduced in the HF-SCF-MO method which is used to calculate the molecular wave function and the orbital energies. This method makes no attempt to calculate relativistic energy in both the ion and the molecule, with the IP being given only by the difference in electrostatic energy. Since the relativistic effect increases with the kinetic energy of the electron, the correction for this effect is usually negligible for outer shell electrons but is appreciable for

inner shell electrons. The HF theory includes some electron correlation by assuming that electron experiences an average potential created by the remaining (2n-1) electrons and through imposing the Pauli exclusion principle on the wave function. As such, the HF theory neglects the instantaneous (rather than average) repulsions between pairs of electrons. The contribution to the total energy due to instantaneous repulsions is called the correlation energy[73], since the motion of the electrons is correlated such that two electrons are unlikely to get very close to each other due to the coulombic repulsion. While the Pauli principle ensures the avoidance of electrons with parallel spins, in the independent-particle (one orbital per electron) HF scheme, the major part of the correlation error comes from the neglect of spatial correlation between the electrons with antiparallel spins. Since correlation effects arise to a large extent from pair interactions between electrons, the correlation energy is usually less in the ion than the molecule. As a result, generally too small an IP will be given by the difference of the good HF energies of the ion and molecule calculated independently.

(b) Application of Koopmans' Theorem in PES

Fortunately the errors introduced by the neglect of the relaxation and correlation effects are of opposite sign and very often tend to cancel each other. Therefore, IP's calculated by assuming KT frequently predict the experimental

values within a reasonable degree of accuracy. It has been shown[74,75] that the application of KT to calculations near HF accuracy of outer shell orbital energies often gives IP's too high by ~8%. This tends to indicate that, in general, the error due to relaxation energy is larger than the correlation energy. The ~92% agreement between experimental and calculated IP's is often sufficient to assign the photoelectron spectra unambiguously. Because of its simplicity and economy, KT IP's calculated by semi-empirical SCF-MO schemes such as the CNDO[76], INDO[76], MINDO[77] and extended Hückel[78] methods are more widely used than ab initio calculations. In addition to the assumptions of KT, the success of these methods depends on its inherent approximations. Very often, the relative ordering of the orbitals derived from the semi-empirical methods are the same as the ab initio result, although the orbital energies may be quite different. In such cases, the assignment of the PE spectrum would be the same. Experience[79] has shown the IP's calculated by CNDO/2[76] and INDO[76] methods are generally ~4 eV larger than the experimental values.

Despite the general success of KT for closed-shell molecules, its breakdown in predicting the right ordering of the ionic states is not uncommon. The classical case is N_2[80], where KT predicts $^2\Pi_u$ rather than $^2\Sigma_g^+$ being the ground ionic state. Other notable examples are in F_2[81], CO_2[3], CS_2[3], and OCS[3]. An extreme case is provided by bis(π-allyl)nickel,

whose first IP at 7.85 eV[82] corresponds to the almost pure Ni-3d orbital[83] ($9a_g$) of the neutral molecules. This, in fact, is the 13th orbital counted from the highest occupied orbital ($7a_u$). Ab initio calculations[44] showed that $\varepsilon(9a_g) = -18.3$ eV, whereas separate calculations[84] of the ion and molecule gave the same IP at 7.92 eV after relaxation of the electrons. This value is then in good agreement with experiment. Some guidelines in the safe use of KT and in forecasting the situations where KT is mostly likely to fail have been given in the literature[85-88]. In general, KT is mostly likely to fail when the ionization perturbation gives rise to large orbital reorganization. In particular, this includes the cases when the electron being removed is localized in one part of the molecule[88], either due to symmetry reasons or because it is a 'lone pair' electron. For the same reason, molecules containing electron-rich atoms like F tend to deviate from KT. Particular care must be exercised in the case where two or more orbitals lie close together, and where more often than not the relative ordering is problematical, leading to doubts in assigning the experimental IP's.

(c) <u>Other Methods For Calculating Vertical IP's</u>

It is obvious that the correct way of getting accurate IP's is to perform independent calculations for the molecule and the individual state of the ion, including the correlation energy and, perhaps, relativistic energy. Except for simple

molecules, this process is tedious and expensive, if feasible, and is not expected to be popular in the near future. Partly because of this, considerable effort has been recently attempted to correct the inefficiency of KT. One approach[89-96] has invoked the many-body techniques of second quantization[97,98], by which the vertical IP is directly related to the poles of the one particle Green's function[99]. Application of this method to N_2[92] and F_2[93] showed very good agreement with experiment. This method appears to be very promising in spite of its rather elaborate computations. Another approach[100,101] used the Rayleigh-Schrödinger perturbation theory[102] to correct the wavefunctions and energies of the ion and molecule. With first order corrections to the wavefunction, third order correction to the energy, and using a basis set of double or one and half zeta Slater orbitals for the calculation, this method was able to reproduce experimental IP's with an absolute deviation of less than 0.5 eV[101].

(d) Open Shell Molecules

For open shell molecules, there are two more difficulties in applying KT in addition to the three limitations mentioned in the case of closed shell molecules. First, if the restricted SCF formalism[103,104] is used, the off-diagonal multipliers ε_{ij}'s, which are introduced as the Lagrangian multipliers[105] by the constraints of the orthogonality of orbitals, cannot always be eliminated as they are in the

closed shell counterparts. Under such circumstances, as a result, no physical meaning can be attached to the diagonal ε_{ii}'s, which can be interpreted as orbital energies when ε_{ij}'s have been diagonalized. Therefore, in essence, KT does not hold. Even if the ε_{ij}'s can be eliminated, KT applies only in a limited sense. Generally, it holds for the open shell orbitals and not for the closed shell orbitals in the same molecule. If the unrestricted SCF formalism[103,106] is used, then ε_{ij}'s can be diagonalized, and the physical interpretation of orbital energies is possible. However, due to the fact that orbitals of different spins are different and thus have different energies, the one-to-one correspondence between the orbital energies and the IP's is lost. Secondly, in order that they be the eigenfunctions of the spin operators S^2 and S_z, the wave functions of the open shell states may not be single Slater determinants. As a result, the energy expression for such states contains cross terms due to the matrix elements between the component determinants, and thus KT usually does not apply. In practice, the first difficulty is not as bad as it looks since the orbital energies calculated in both formalisms often show qualitative agreements with the experimental IP's. An approximate way of estimating IP's for closed shell orbitals is to calculate them as excitation energies from the ground ionic state using its wave function (frozen orbital approximation). This was in fact the case in the study of the radicals NF_2[107], ClO_2[108] and NO_2[109], with

limited success. Naturally, the proper way would again be to carry out independent calculations for the molecule and the individual ionic states. But then, besides being tedious and expensive, the calculation may have the added problem of convergence. This difficulty was exemplified in the study of NO_2[109].

2.2.3 Franck-Condon Principle in PES

(a) Wave Mechanical Formulation of The Franck-Condon (FC) Principle[50,51].

The probability of a transition between two states is proportional to the square of the electric dipole transition integral R given by

$$R = \int \psi'(q,Q)(R_n + R_e)\psi''(q,Q)dqdQ \ . \qquad (2.2.14)$$

In this integral $\psi'(q,Q)$ and $\psi''(q,Q)$ are the total wavefunctions describing the upper and lower quantum states, respectively, indicated as functions of the totality of electronic coordinates q and the totality of nuclear coordinates Q, and R_n and R_e are the nuclear and electronic dipole moment operators respectively. Using the Born-Oppenheimer approximation[110], the wavefunction can be separated into a product of electronic and nuclear functions giving

$$\psi(q,Q) = \psi_e(q,Q)\psi_n(Q). \qquad (2.2.15)$$

Separating the nuclear function into the vibrational and rotational parts, the expression then becomes

$$\psi(q,Q) = \psi_e(q,Q)\psi_v(Q)\psi_{rot}(Q), \qquad (2.2.16)$$

where interactions between electronic, vibrational and rotational motion have been neglected. The rotational wavefunction can be neglected[111], since the relative intensities of the various vibrational peaks are of interest here. Thus we have

$$R = \int \psi_e' (q,Q)\psi_v' (Q)(R_n+R_e)\psi_e'' (q,Q)\psi_v'' (Q)dqdQ, \qquad (2.2.17)$$

which upon expanding gives

$$R = \int \psi_v' (Q)R_n\psi_v'' (Q)dQ\int \psi_e' (q,Q)\psi_e'' (q,Q)dq + \int \psi_v' (Q)\psi_v'' (Q)dQ\int \psi_e' (q,Q)R_e\psi_e'' (q,Q)dq. \qquad (2.2.18)$$

By the orthogonality of ψ_e' and ψ_e'', the first term vanishes. Denoting the electronic integral (the electronic transition moment) in the second term

$$R_e(Q) = \int \psi'_e\,(q,Q) R_e \psi''_e\,(q,Q) dq, \qquad (2.2.19)$$

and expanding it in a Taylor series about the equilibrium nuclear position Q_o gives

$$R_e(Q) = R_e(Q_o) + \left(\frac{dR_e}{dQ}\right)_{Q_o} (Q-Q_o) + \ldots . \qquad (2.2.20)$$

The FC principle is based on the assumption[51] that the variation of R_e with Q is slow, and thus all except the first term can be dropped, giving

$$R = R_e(Q_o) \int \psi'_v\ \psi''_v\ dQ. \qquad (2.2.21)$$

The vibrational transition probability or intensity is then

$$I_{v'\leftarrow v''} \propto \left| \int \psi'_v\ \psi''_v dQ \right|^2 . \qquad (2.2.22)$$

Equation (2.2.22) embodies the wave mechnical description of the FC principle: The intensity of a vibrational peak in an electronically allowed transition is proportional to the absolute square of the overlap integral, i.e. the FC factor, of the corresponding vibrational wavefunctions of the initial and final states. The FC factor is, in general, appreciable only when the maxima or minima of the two wavefunctions lie on top

of each other, i.e. at the same Q, and these maxima or minima for the higher vibrational levels appear near classical turning points of the motion, and thus vertical electronic transitions are usually the most favorable. This is in agreement with the result of the primitive form[50] of the FC principle, stating that the electronic transition is so rapid with respect to the vibrational motion that the molecule maintains a fixed geometry immediately after the transition.

(b) Qualitative Application Of The FC Principle In PES

The influence of this principle on the vibrational patterns and band shapes observed in the PE spectrum of a diatomic molecule is illustrated in Fig. 1. The shaded area, frequently called the FC region, represents the vertical transitions allowed by the FC principle. The different band structures are determined by the potential curve of the resulting ion, which is in turn determined by the equilibrium internuclear distance and vibrational frequency of the ion. Depending upon whether the ejected photoelectron came from a bonding, antibonding or nonbonding orbital, the equilibrium internuclear distance in the ion may be greater, smaller or approximately the same as that in the parent molecule, while the opposite is true for the vibrational frequency due to the corresponding change in force constant. These changes in geometry and vibrational frequency will then determine, through the FC principle (see also the following section), where the

THE FRANCK-CONDON PRINCIPLE IN PHOTOELECTRON SPECTROSCOPY

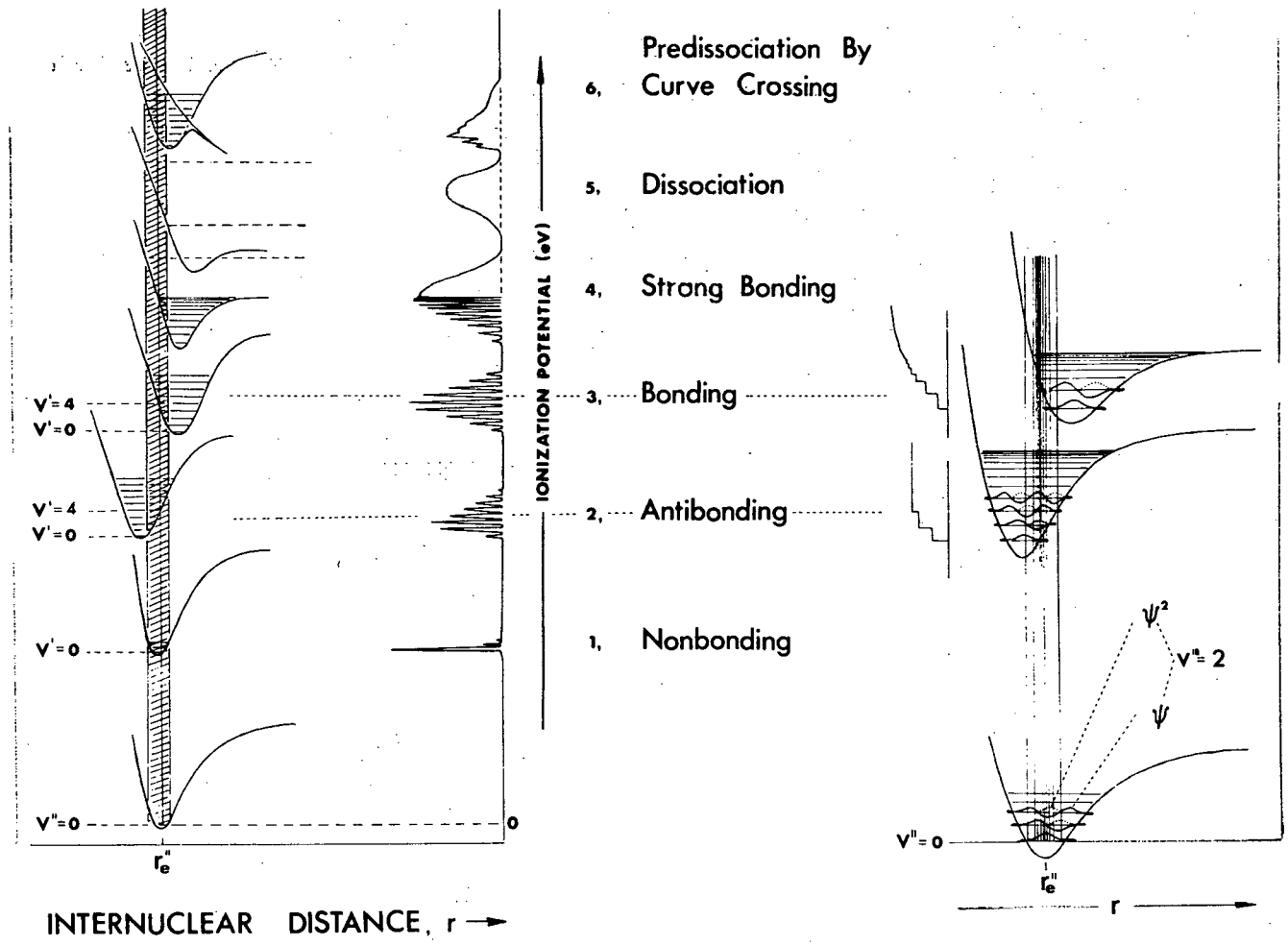

FIGURE 1

ion will be formed on the potential curve, giving rise to the various PE band structures as depicted in Fig. 1. Thus from the PE band shape and the vibrational frequency, the bonding character of the corresponding orbital from which the photoelectron is removed can frequently be deduced.

In the case of polyatomic molecules, the correlation between band shapes, vibrational frequencies, and bonding character becomes somewhat more complicated since the transitions now take place between multidimensional potential surfaces, and changes in bond lengths and bond angles are possible. Several vibrational modes may therefore be excited simultaneously. In addition, the bonding character of the MO's are now only meaningful between neighboring atom pairs in a molecule. Indeed, the same orbital can have different bonding character between different atom pairs, which means that, within the same band, one particular vibrational frequency may increase and another decrease, and the band structures of different vibrational progressions may be different. In general, however, the same principle applicable to the diatomic case may be used as a useful guide to the orbital nature in polyatomics.

(c) Quantitative Application Of The FC Principle In PES

According to the equation (2.2.22), the relative vibrational transition probabilities or intensities within a PE band are proportional to the corresponding FC factors.

These FC factors can be evaluated provided the appropriate vibrational wavefunctions are available. By calculating and fitting FC factors to the experimentally determined values, the geometry of the upper state can be estimated. This principle has, in fact, been frequently used to determine the geometries of excited electronic states observed in electronic spectra[112-115]. The same concept[116] is also applicable in PES for estimating the geometry of the ionic states. This is particularly attractive since the structures of ions are normally difficult to obtain, especially for polyatomics.

The main task in such a quantitative investigation is the evaluation of the overlap integral

$$M = \int \psi_v'(Q')\psi_v''(Q'')dQ', \qquad (2.2.23)$$

where Q' and Q" denote the totality of normal coordinates in the ionic and molecular states respectively. Assuming that the vibrational wavefunction of each state has the form

$$\psi_v = \prod_{i=1}^{n} \phi_i(Q_i), \qquad (2.2.24)$$

then the overlap integral becomes

$$M = \int [\prod_{i=1}^{n} \phi'(Q_i')][\prod_{i=1}^{n} \phi''(Q_j'')]\, dQ_1'\, dQ_2' \ldots dQ_n' \quad . \qquad (2.2.25)$$

In order to evaluate this integral it is necessary to specify the transformation between Q_j''s and Q_i'''s, which are related by[117]

$$Q' = AQ'' + d \qquad (2.2.26)$$

where A is an nXn square matrix and d is a column vector of order n. Normally A_{ij} is different from zero only when the ith and j^{th} normal coordinates have the same symmetry. For non-totally symmetric Q_i', d_i must be zero by symmetry.

Since ψ'' is usually a vibrationless ground state and is largely concentrated around the origin of the normal coordinates, the overlap integral is dominated by the contribution in the region of $Q'' = 0$ and $Q' = d$. In this case the integral will be insensitive to the nature of A, since the wavefunctions are the products of exponential terms. The integral may then be approximated by choosing A to be a unit matrix, giving

$$Q_i' = Q_i'' + d_i . \qquad (2.2.27)$$

Consequently, M separates into n component overlap integrals

$$M = \prod_{i=1}^{n} M_i(v_i' , v_j'') , \qquad (2.2.28)$$

where

$$M_i(v_i' , v_j'') = \int \phi'_{v'} (Q_i')\phi''_{v''} (Q_i' - d_i)dQ_i' \quad . \qquad (2.2.29)$$

The observed FC factors in the PE band may then be analyzed in terms of the squares of these one-dimensional integrals to give d_i's.

For symmetry coordinates, we have[118]

$$S' = S'' + D \quad , \qquad (2.2.30)$$

and if

$$S' = L'Q; \ , \ S'' = L''Q'' \quad , \qquad (2.2.31)$$

then

$$Q' = (L')^{-1}L''Q'' + (L')^{-1}D \qquad (2.2.32)$$

hence

$$A = (L')^{-1}L'' \qquad (2.2.33)$$

$$d = (L')^{-1}D \quad \text{or} \quad D = L'd \quad . \qquad (2.2.34)$$

Therefore, a knowledge of the d_i's can be related to the change in the symmetry coordinates D_i's, from which the change

in internal coordinates can in turn be calculated.

The L matrix, which is the eigenfunction of the FG secular equations[118], is a function of the vibrational frequencies and force fields, which are normally not available for the ionic states. However, it has been found that D is quite insensitive to L'. Therefore, for the approximate work undertaken here, the L' matrix for the ion is approximated by that of the neutral molecule.

In addition, for simplicity, the vibrational wavefunctions are approximated by that of a harmonic oscillator, i.e.

$$\phi_i = N_{v_i} H_{v_i}(\alpha_i Q_i) \exp[-1/2\ \alpha_i^2 Q_i^2] \quad , \qquad (2.2.35)$$

in which

$$N_{v_i} = (\alpha_i/\pi^{\frac{1}{2}}\ 2^{v_i}\ v_i!)^{\frac{1}{2}} \quad ,$$

and

$$\alpha_i^2 = 4\pi^2 c\nu_i/h \quad .$$

The $H_{v_i}(\alpha_i Q_i)$ are Hermite polynomials, v_i the vibrational quantum numbers, ν_i vibrational frequencies in cm^{-1}, and c is the speed of light. The component integral can then be expressed in the closed form[119],

$$M(v',v'') = K_{v'v''}\left(\frac{1-\beta^2}{1+\beta^2}\right)^{(v'+v'')/2}\sum_{\ell=0}^{[v',v'']}\left(\frac{4\beta}{1-\beta^2}\right)^{\ell}\cdot$$

$$\frac{(-i)^{v'-\ell}}{\ell!(v'-\ell)!(v''-\ell)!}\,H_{v'-\ell}[i\beta^2\gamma(1-\beta^4)^{-\frac{1}{2}}]\cdot$$

$$H_{v''-\ell}[-\beta^2\gamma(1-\beta^4)^{-\frac{1}{2}}] \quad , \qquad (2.2.36)$$

where

$$K_{v'v''} = (v'!v''!)^{\frac{1}{2}}\,2^{-(v'+v''-1)/2}(\beta/(1+\beta^2))^{\frac{1}{2}}\cdot$$

$$\exp[(-1/2)\beta^2\gamma^2/(1+\beta^2)] \quad ,$$

$[v',v'']$ designates the smaller of the two integers v' and v'', and

$$\beta = \alpha''/\alpha' \quad , \gamma = -\alpha' d \quad . \qquad (2.2.37)$$

Eq. (2.2.36) reduces, when $v'' = 0$, to

$$M(v',0) = \frac{(-i)^{v'}2^{(1-v')/2}}{(v'!)^{\frac{1}{2}}}\left(\frac{\beta}{1+\beta^2}\right)^{\frac{1}{2}}\exp[-\tfrac{1}{2}\,\frac{\gamma^2\beta^2}{1+\beta^2}]\cdot$$

$$\left(\frac{1-\beta^2}{1+\beta^2}\right)^{v'/2} H_{v'}[i\beta^2\gamma(1-\beta^4)^{-\frac{1}{2}}] \quad . \qquad (2.2.38)$$

The main calculation is carried out by a computer program (Appendix) and the procedure is summarized:-

(1) d_i is set equal to zero for the vibrational mode not excited in the ion.

(2) The FC factors (FCF) for any combination level are calculated as the product of those for the corresponding overtone levels.

(3) For each excited vibration, the FCF are calculated at a series of d_i values. The best d_i value is then chosen on the basis of two criteria:- (a) The overall qualitative features of the experimental FCF are followed in the calculated FCF. (b) The standard deviation of the calculated FCF from the experimental FCF is a minimum.

(4) D_i's are evaluated from the d_i's.

(5) The change in internal coordinates are calculated from the D_i's.

(6) Since the sign of each d_i is undetermined there are 2^N possible ionic state models consistent with the observed FCF, where N is the number of vibrational modes of the same symmetry excited. The choice of the model is based on the bonding character of the MO from which the electron is removed.

The method outlined above has been used wherever applicable in this study to estimate the geometry of the ions. By comparing with the experimental data, it will be shown (section 5.2.4) that this method is quite reliable in deter-

mining the ionic geometries, with a maximum deviation of 0.006 Å in bond lengths.

2.2.4 Selection Rules In PES

(a) Selection Rules In Electronic Excitations

It is usually assumed that the initial (neutral) and final (ionic) states are represented by single Slater determinants. The ith photoionization process can then be described as the excitation of an electron from the orbital ϕ_i to a continum photoelectron orbital ϕ_{ph}. The transition probability for the process is proportional to the square of the electronic transition moment R_e (eq. (2.2.19)), and using the above assumption, we have,

$$\text{Transition probability} \propto \left|\int \psi_e^i (N) R_e \psi_e^f (N) dq\right|^2$$

$$= \left|\int \phi_i R_e \phi_{Ph} dq\right|^2 \left|\int \psi_e^i (N-1) \psi_e^f (N-1) dq\right|^2 \qquad (2.2.39)$$

$$= \left|\int \phi_i R_e \phi_{Ph} dq\right|^2 \cdot \prod_{j \neq i}^{N-1} \left|\int \phi_j \phi_j^f \, dq\right|^2 , \qquad (2.2.40)$$

where ψ_e^i (N-1) is the N-1 electron remainder of the initial state function ψ_e^i (N) of an N electron molecule and ψ_e^f (N-1) is the wavefunction of the ion. The properties of the integrals in equations (2.2.39) and (2.2.40) dictate the following

selection rules on the difference between ψ_e^i (N) (molecule) and ψ_e^f (N-1) (ion).

(1) The change in the total spin angular momentum must be ±½ due to the dipole matrix.

(2) The overlap integral in eq. (2.2.39) requires that the 'passive' orbitals have the same symmetry.

(3) In the frozen orbital approximation (KT), the overlap integral in eq. (2.2.40) requires that the ion and molecule differ only in one orbital.

In short, under the assumptions of the frozen orbital approximation and that the wavefunctions are described by single Slater determinants of one electron orbitals, photoionization is a single step one electron process, and the PE spectrum of a closed shell molecule may be assigned on the basis of one IP per orbital.

However, multi-electron (i.e. two or more) processes may be allowed if electron correlation is taken into account in the wavefunctions. The inclusion of electron correlation is usually accomplished by the method of configuration interaction (CI)[120-125], in that the ionic wavefunction is constructed as a linear combination of the configurations corresponding to the possible excited ionic states of the same symmetry, i.e.

$$\psi_j^{CI}(N-1) = \sum_i C_{ij}\psi_i^f (N-1) \quad . \qquad (2.2.41)$$

The transition probability to a CI state is given by

$$|\int \phi_i R_e \phi_{Ph} dq|^2 |\int \psi_e^i (N-1) \cdot \sum_i c_{ij} \psi_i^f (N-1) dq|^2 . \quad (2.2.42)$$

The overlap integral, and thus the transition probability will not be zero if the CI wavefunction contains at least one ionic state which is formed by a single electron process. For such a CI state the probability then reduces to

$$|\int \phi_i R_e \phi_{Ph} dq|^2 |\int \psi_e^i (N-1) \psi_o^f (N-1) dq|^2 c_{io}^2 , \quad (2.2.43)$$

where ψ_o^f is the wavefunction of the allowed ionic state, and its value relative to that of the latter ψ_o^f is given by the square of their overlap integral, i.e.

$$|\int \psi_o^f (N-1) \psi_i^{CI} (N-1) dq|^2 = c_{io}^2 \quad (2.2.44)$$

Qualitatively, multi-electron processes can be thought to occur due to perturbations induced by the photo-ionization process. Therefore, one would expect these processes to become more probable when more energetic ionic states are formed by using more energetic light sources. In practice this is what is observed. Thus multi-electron processes are quite common in ESCA[1,2] (>1000 eV), but exceptionally few have been claimed[125-127] to occur in HeI (21.22 eV) PES. However, two electron processes have recently been found

to occur quite frequently in HeII (40.8 eV) PES[128].

(b) Selection Rules In Vibrational Excitations

The selection rules in vibrational excitations are determined by the vibrational overlap integral (eq. (2.2.25)),

$$M = \int [\prod_{i=1}^{n} \phi'(Q_i')][\prod_{j=1}^{n} \phi''(Q_j'')]dQ_1' \, dQ_2' \ldots dQ_n' \quad .$$

In order for M not be zero, the integral must be totally symmetric. Usually the initial state is a vibrationless ground state, whose vibrational wavefunction is totally symmetric. Hence the vibrational wavefunction of the ion must be totally symmetric as well. This requirement leads to the following selection rules[129].

(1) Totally symmetric vibrations may assume any quantum number.

(2) Non-totally symmetric vibrations can only assume zero or even quantum numbers, whose wavefunctions are then totally symmetric.

(3) For combination bands, i.e. simultaneous excitation of two or more vibrational modes, of non-totally symmetric modes, the transition is allowed if the total wavefunction is totally symmetric.

For a vibrationally excited initial state, the requirement that the overlap integral must be totally symmetric can be used to select the allowed transitions.

2.3 Linewidths And Resolution In PES

Like any other kind of spectroscopic measurements, the observed linewidth of a peak in PES is a convolution of the instrumental function and the inherent linewidth of the transition. The former is a measure of the instrumental resolution, while the latter is a function of the nature of the transition and the molecule under consideration. It is immediately obvious that the observed linewith can only be reduced at the expense of the instrumental resolution, and if the latter has been reduced to the negligible limit, the observed linewidth will then be the inherent linewidth.

The inherent linewidth is determined through the Heisenberg uncertainty principle by the lifetime of the ionic state. Depending upon the lifetimes encountered, this[130] may range from a line broadening of 10^{-7} eV for a fluorescent ionic state, up to 0.4 eV for a rapidly dissociating ionic state. Because the ultimate theoretical instrumental resolution obtainable is greater than 1 meV (see below), one may also consider the line structures which are comparable to this limit to be inherent linewidths. For complex molecules, the inherent linewidth may then include rotational envelopes, closely spaced unresolved vibrational structures, spin-orbit splittings, Jahn-Teller and Renner-Teller splittings.

In PES, the instrumental resolution is usually defined as $\Delta E_{1/2}/E$, where $\Delta E_{1/2}$ and E are respectively the full width at half maximum (FWHM) and the kinetic energy of the

electrons, both measured in eV. However, it is customary to use simply $\Delta E_{1/2}$ as a measure of resolution, and in general the FWHM of the argon doublet ($^2P_{3/2}$,$^2P_{1/2}$) is used as a universal test. The various possible factors that limit the ultimate instrumental resolution have been discussed in detail by Turner[130] and Samson[131]. In practice, the following are the most influential and pose the major problems.

(1) The Doppler effect due to the thermal motion of the molecule and the velocity of the photoelectron - These two parameters couple to give the Doppler width according to the formula[131]

$$\Delta E_{1/2} = 0.723(ET/M)^{\frac{1}{2}} \text{ meV} \quad , \qquad (2.3.1)$$

where M is the molecular weight of the ion, T is the absolute temperature, and E the kinetic energy of the photoelectron. To give a better feeling for the magnitude of this broadening, $\Delta E_{1/2}$ is plotted in Fig. 2 for various values of M as a function of electron kinetic energy and temperature. This broadening can be reduced by cooling the sample or using less energetic light sources, e.g. NeI instead of HeI to produce photoelectrons of lower energy. The Doppler width can, in principle, be completely eliminated by forming the sample into molecular beam and analyzing the photoelectrons ejected perpendicular to it.

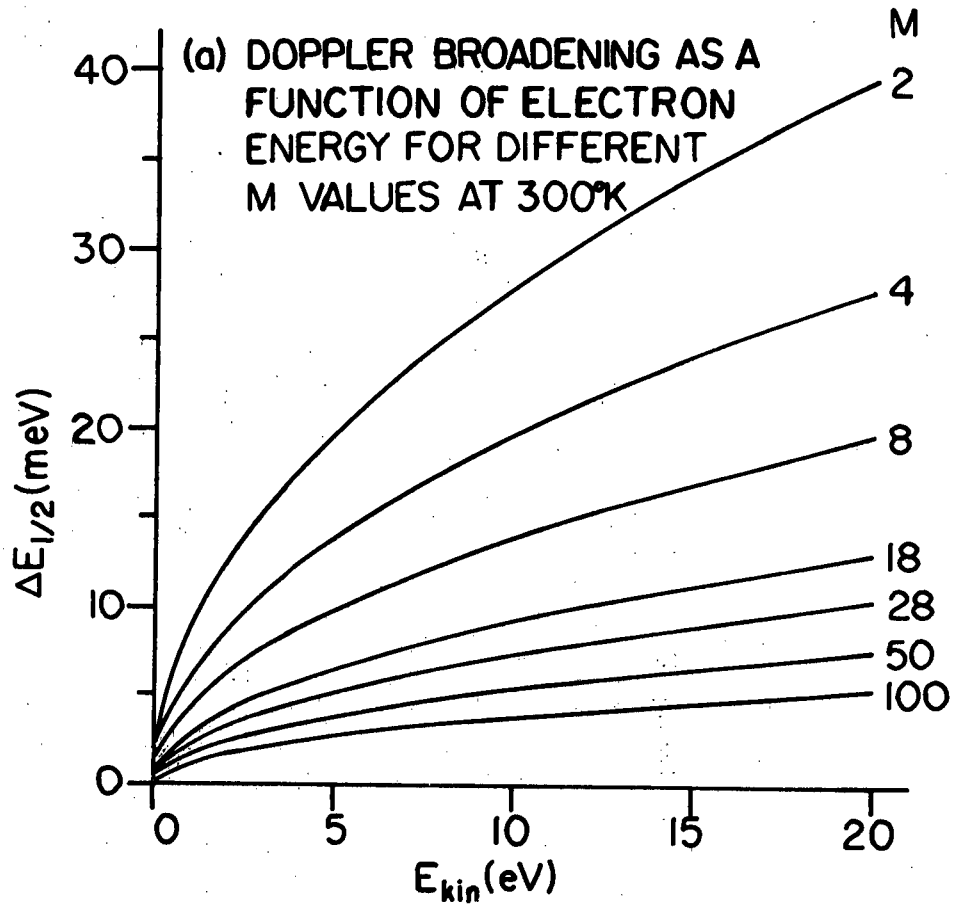
(a) DOPPLER BROADENING AS A FUNCTION OF ELECTRON ENERGY FOR DIFFERENT M VALUES AT 300°K
M
2
4
8
18
28
50
100
40
30
20
10
0
$\Delta E_{1/2}$ (meV)
0
5
10
15
20
E_{kin} (eV)

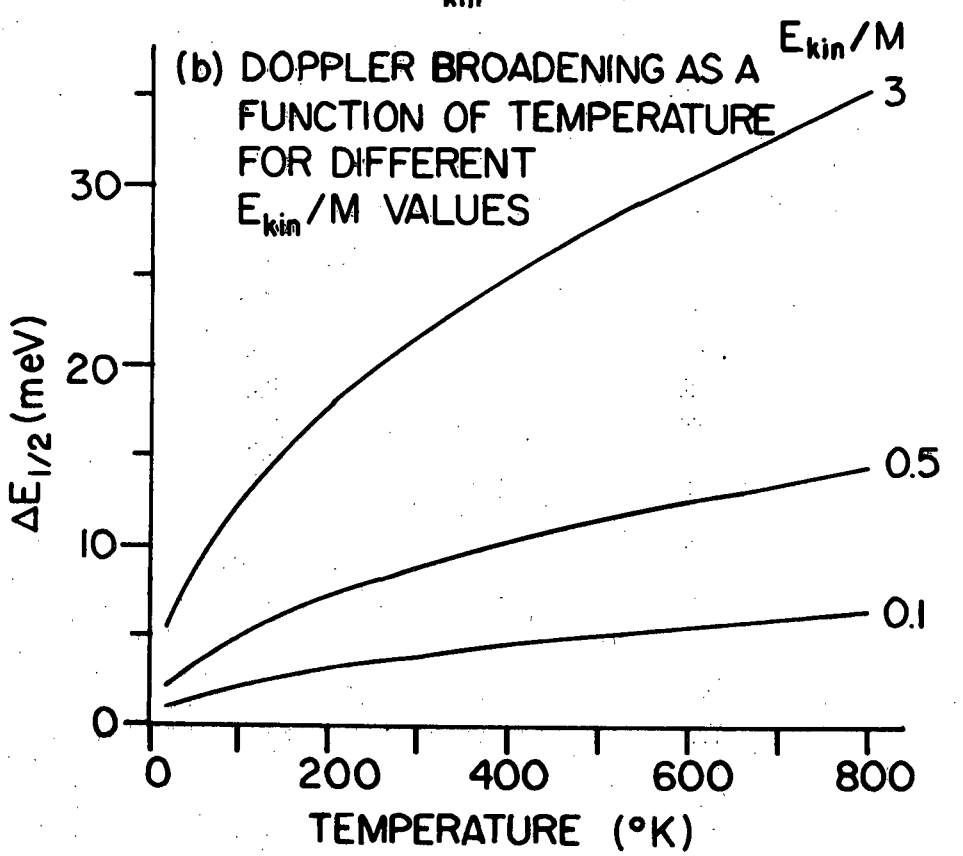
(b) DOPPLER BROADENING AS A FUNCTION OF TEMPERATURE FOR DIFFERENT E_{kin}/M VALUES
E_{kin}/M
3
0.5
0.1
30
20
10
0
$\Delta E_{1/2}$ (meV)
0
200
400
600
800
TEMPERATURE (°K)

FIGURE 2

(2) Linewidth of the light source due to self-absorption - It has been shown[131] that the common types of line broadening encountered in a light source such as natural, Doppler, pressure and stark broadenings are far too small ($<10^{-3}$ eV) compared to that due to self-absorption for the HeI resonance line. The linewidth due to the latter increases with the pressure, the length of the discharge region, and that of the undischarged gas column. Surprisingly, the broadening[131] does not seem to depend on the nature of the light source nor the diameter of the discharge capillary. Dependent upon the above factors, linewidth can vary from 1 meV up to 7 meV. The lower limit can be obtained at the lowest possible pressure by a microwave discharge, although at the expense of the available light intensity.

(3) Line broadening due to the inhomogeneity of the electrostatic and magnetic fields - This includes the effects due to the residual earth magnetic field, inhomogeneous analzer surface potential, and the micropotentials on the apertures. The last effect is particularly important in the case of transient species, and is difficult to remedy.

However, if careful precautions are taken to eliminate or reduce these limiting factors, an ultimate resolution of ~1 meV is possible, which would be sufficient to resolve rotational structure in some cases. To date, the best instrumental resolution achieved has been between 4-7 meV with the argon doublet[132], however, a nominal resolution of 10-25 meV is

conveniently obtainable in most laboratories, this being considered as 'high resolution' PES (much above 30-40 meV is considered medium resolution).

Besides the experimental considerations, the working resolution can be improved by the analytical analysis of the raw data. The method is to eliminate the linewidth due to instrumental function by deconvolution[133-137]. The success of deconvolution requires an accurate estimation of the instrumental function, and that the data has a favorable signal to noise ratio. This technique has been used successfully[137] to recover the spin-orbit splitting in the $X^2\pi_g$ state of O_2^+, and the result is comparable to the very high resolution study[132].

CHAPTER THREE

THE SPECTROMETER AND PERFORMANCE

3.1 Introduction

During the course of this study, two spectrometers have been employed. The first system was used for the initial exploratory work and except for some notable modifications, its detailed features were described in Cornford's thesis[138]. The experience gained through exhausting the capabilities of that unit has subsequently played a significant role in the development of the second system, which is the focus of this chapter.

3.2 General Design Considerations

One of the purposes of this study was to design and construct a photoelectron spectrometer that would be suitable for the study of transient species and reactive molecules. In the design of such a spectrometer, there are several significant considerations:

(1) The spectrometer must have a fast pumping system. This is essential since the species of interest here are either short lived or tend to decompose easily on contact with surfaces. By faster pumping and hence reducing the time between the photoionization region (ionization chamber) and the region where they are produced (transient species) or stored (reactive molecules), the greater the chance of successfully recording a PE spectrum. A useful additional feature is the short pump-down cycle of the spectrometer, which involves a shorter time elapse before the unit is again in operating condition after venting and servicing. A further bonus of the fast pumping system is a reduction in the build-up of deposits which may decrease the efficiency of the analysis system.

(2) The spectrometer should have a versatile sample inlet system and an easily accessible ionization chamber. The individual transient species that are of interest may be produced by one of several completely different methods, such as microwave discharge, pyrolysis etc, or may, for reasons of of chemical reactivity, require the use of a specific material for the inlet system and sample holder. It is therefore of the essence that the spectrometer can handle all these differing situations. Easy access to the ionization chamber region is of particular importance, since most samples, by virtue of their short lifetimes or reactivity, must be generated as close to the chamber as possible.

(3) The spectrometer should have high sensitivity and the capability of high resolution (better than 25 meV). It is absolutely essential to have high sensitivity since more often than not the transient species are produced only with low partial vapor pressure, e.g. sometimes as low as 1% of the parent molecule. High resolution is necessary to resolve any fine band structure which is necessary for a rigorous analysis of the spectrum.

(4) The spectrometer should be as durable as possible with respect to corrosive vapors and yet as simple as possible in construction. It should also be easily assembled and dissembled so that cleaning, repairing and modifying become straightforward procedures.

(5) In addition to the earth's magnetic field, other magnetic fields may be introduced by certain experimental arrangements, e.g. by the current generated in a wire-wound furnace. The source of this field is usually so close to the electron trajectory in the analyzer, that it makes the magnetic shielding by Mu-metal infeasible. Consequently, the elimination of stray magnetic fields is best achieved by three pairs of Helmholtz coils mounted at right angles to each other. These may be individually adjusted to compensate for any such field effects.

(6) A minor, but equally important consideration is the siting of the spectrometer in a relatively field-free

room, with independent power supplies thus limiting the interference of other electrical apparatus.

3.3 The Spectrometer

3.3.1 The Vacuum System

The vertical cross-section of the spectrometer through the entrance and exit apertures of the electron analyzer is shown in Fig. 4. One distinct feature of the vacuum system is that it does not have a separate vacuum housing for the analyzer, in contrast to other conventional spectrometers. As a result, the ionization chamber is within easy access and the pumping volume is reduced considerable, a favorable condition for fast and efficient pumping. The ionization chamber and the analyzer are separated by the circular apertures in the ionization chamber, lens and entrance slit as shown in Fig. 4. The diameters of the apertures in the above-mentioned order are respectively 0.030", 0.100" and 0.020". The ionization chamber is connected through a 2" i.d. vacuum throttle valve (Varian Associates) to a 4" oil diffusion pump (Cooke Vacuum Prod., DPD 4-1000B) with a pumping speed of 1000 l/sec (air). The analyzer and the housing for the channel electron multiplier are pumped through a 1 5/8" i.d. vacuum throttle valve (Veeco forged brass angle valve, type SL 150S) by a 2" oil diffusion pump (NRC HS2) with

THE PHOTOELECTRON SPECTROMETER

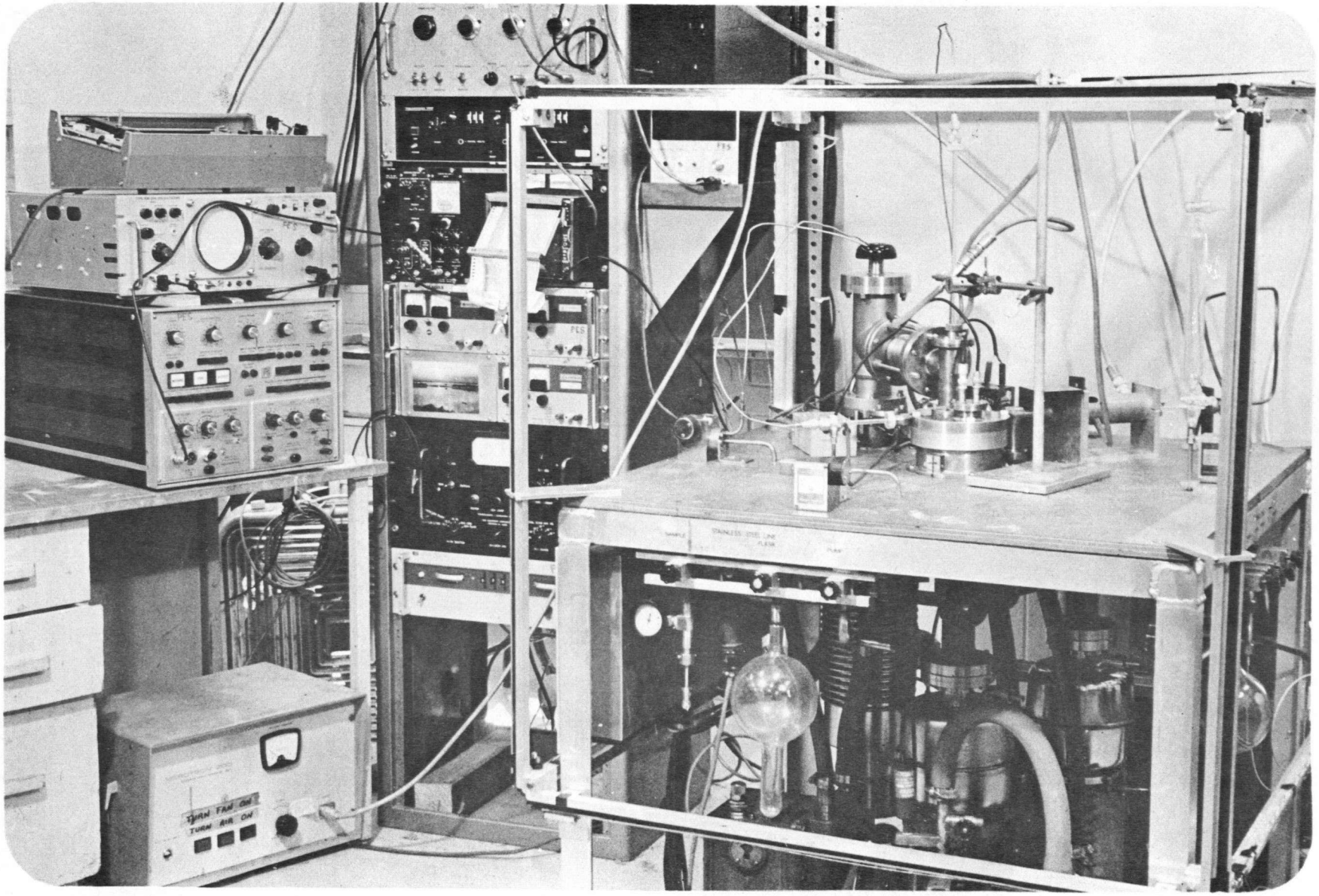

VERTICAL CROSS-SECTION OF PE SPECTROMETER

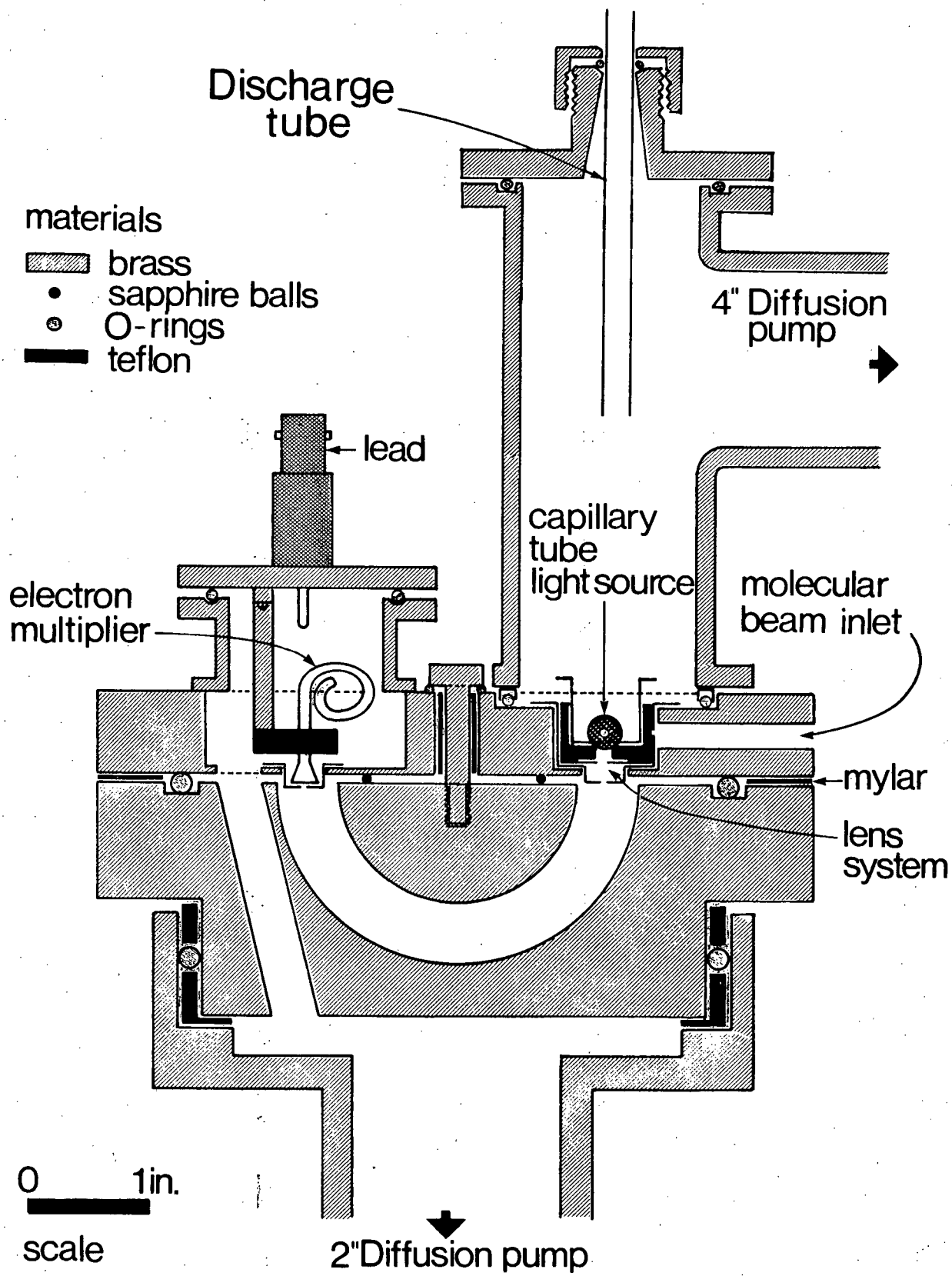

FIGURE 4

PUMPING PORTS FOR THE ANALYZER UNIT AND GENERAL SAMPLE INLETS

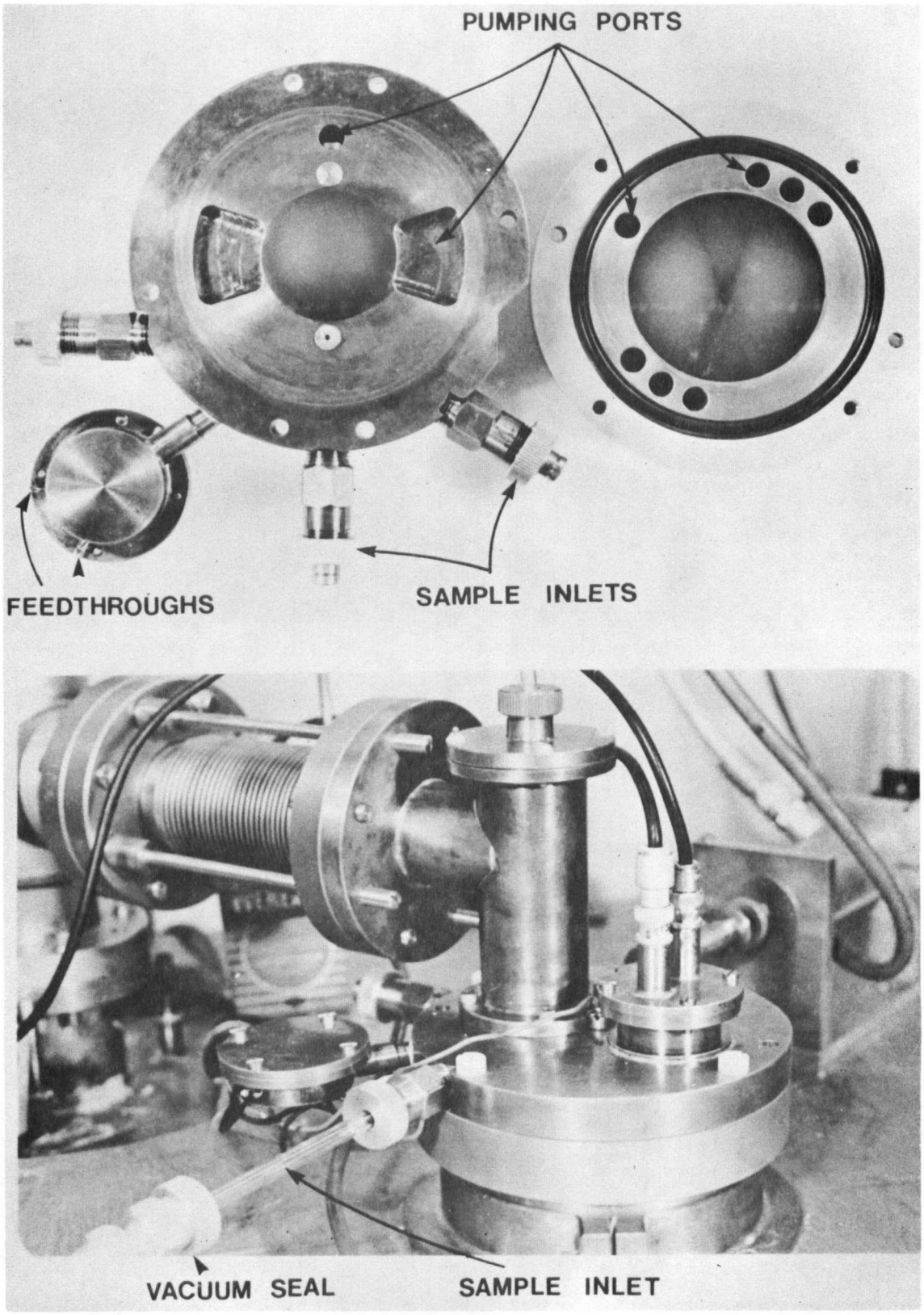

FIGURE 5

a pumping speed of 285 l/sec (air). These diffusion pumps are respectively backed by Duo-Seal rotary pumps (Welch Scientific, model 1397 and 1402). The six pumping ports for the analyzer are shown in Fig. 5 and are arranged so as to have the least possible disturbance on the electron trajectory. These ports and the one for the multiplier housing are long cylinders of 3/8" in diameter drilled at an angle through the solid brass block which is also an integral part of the analyzer. An ionization gauge (NRC 538P) situated below these ports is used to measure the pressure of the system. The vacuum seals are effected by Viton O-rings, with the help of bolts wherever necessary.

3.3.2 The Electron Energy Analyzer

A 180° hemispherical electrostatic analyzer was selected for the spectrometer for the following reasons:

(1) The design of the vacuum system depends upon it.

(2) The ionization chamber can be readily accessible.

(3) An electrostatic analyzer was chosen over a magnetic analyzer because the energy (electrostatic) analysis is more straightforward than the momentum (magnetic) analysis in that the deflecting electric potential is a linear function of the electron energy. However, the magnetic analysis is convenient to use at relatively

high electron energies ($\sim 10^4$ eV, thus their use in ESCA is more popular)[139,140].

The energy dispersion properties and focusing action of hemispherical electrostatic analyzers was first discussed by Purcell[141]. It has subsequently been developed and its properties discussed by a number of researchers[142-146]. A schematic diagram of the analyzer unit is shown in Fig. 6. The potential V_{12} applied between the two hemispherical surfaces of radii $R_2 > R_1$, produces at radius r a radial electrostatic field

$$E(r) = A/r^2 , \qquad (3.3.1)$$

and a potential

$$V(r) = A/r + B , \qquad (3.3.2)$$

where A and B are constants. For an electron with a velocity v_o which enters the analyzer at $x_1 = 0$ and at launch angle $\alpha = 0°$, and exits after being deflected by 180°, the following relationship holds,

Centrifugal force = Electric force

$$\frac{m_e v_o^2}{R_o} = \frac{eA}{R_o^2} . \qquad (3.3.3)$$

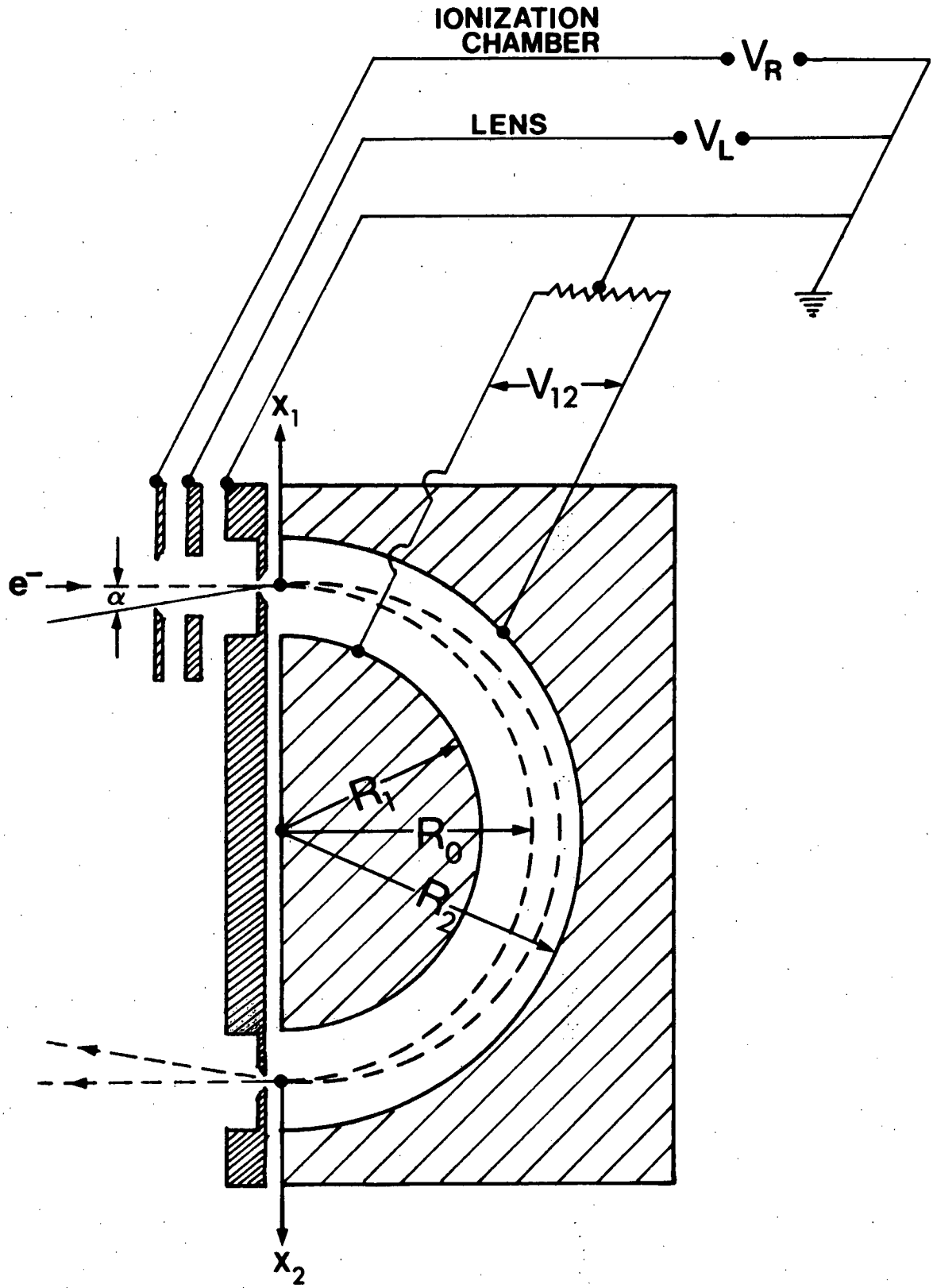

180° HEMISPHERICAL ANALYZER UNIT

FIGURE 6

If eV_o in electron volts (eV) is set equal to the kinetic energy of the electron, $E_o = m_e v_o^2/2$, then

$$A = 2R_oV_o = (R_1 + R_2)V_o \ , \qquad (3.3.4)$$

where R_o is the radius of the circle travelled by the electron. From eq. (3.3.2), the potentials of the inner and outer hemispheres with respect to R_o, which is also the midpoint, are then

$$V(R_1) - V(R_o) = A/R_1 - A/R_o, \qquad (3.3.5)$$

$$V(R_o) - V(R_2) = A/R_o - A/R_2, \qquad (3.3.6)$$

and consequently V_{12} is given by

$$V_{12} = V(R_1) - V(R_2) = A/R_1 - A/R_2$$

$$= V_o[(R_2/R_1 - (R_1/R_2)] \ . \qquad (3.3.7)$$

In addition, for the hemispherical analyzer, other properties[145] that are worthy of note include;

(1) The analyzer has first order angle (α) focusing.

(2) The analyzer has two dimensional focusing because of spherical symmetry.

(3) Neglecting the α^2 term, the energy resolution of the analyzer can be approximated by

$$\Delta E_{1/2} / E_o = w/2R_o , \qquad (3.3.8)$$

where w is the diameter of the entrance and exit apertures.

The particular analyzer employed for the present spectrometer has the following parameters; R_1 = 1", R_o = 1.25", R_2 = 1.5" and w = 0.020". Therefore the working conditions of the analyzer are

$$V_1/V_2 = (+3)/(-2) , \qquad (3.3.9)$$

(eq. (3.3.5) and (3.3.6))

$$V_{12} = (5/6)V_o , \quad \text{(eq. (3.3.7))} \qquad (3.3.10)$$

and $\Delta E_{1/2}/E_o = 0.8\%$. (eq. (3.3.8)) (3.3.11)

The outer and inner hemispheres of the analyzer were both machined from solid brass. The outer hemisphere is screwed to the supporting plate by four nylon screws and

is insulated by mylar and teflon spacers (Fig. 4). The inner hemisphere is held in position by three sapphire balls and is also screwed to the supporting plate, while its insulation is effected by the Viton O-ring and the teflon sheathing (Fig. 4). The hemispherical surfaces are gold plated and then coated with colloidal graphite (Crown, 8078 Dry Graphite Lubricant). This coating improves the experimental resolution considerably and also greatly reduces the background due to scattered electrons. Moreover, it acts as a protective coating for the hemispheres, since the analyzer efficiency can be completely restored after sample poisoning by removal of the old coating with an organic solvent and application of a new coating.

3.3.3 The Light Source Unit

The 584 Å HeI resonance line is produced by a low pressure microwave discharge in unpurified helium (Canadian Liquid Air) powered by a Microtron-200 Generator (Electro-Medical Supplies) with a maximum output of 200 watts at 2450 MHz. The microwave resonant cavity is of the type described by Zelikoff et al[147], and its design specifications were fully reported in Vroom's[148] thesis. The characteristics of such a source have been described by Samson[149]. While the 584 Å line is the most intense, small amounts of 537 Å (23.09 eV), 522 Å (23.8 eV) and 304 Å (40.8 eV) are also present in

the light source. In addition, the presence of impurity lines due to H_α(1215 Å), H_β(1025 Å), NI(1134, 1200 Å) and OI(989, 1304 Å) is quite common, and frequently gives rise to extra bands in the PE spectra.

The vertical cross-section of the light source unit is shown in Fig. 7. The discharge is produced in a quartz tube (5 mm o.d.), the radiation emerging through a boron nitride constriction, into the collimating capillary tube (1 mm i.d.), and thence into the ionization chamber in a direction perpendicular to a line joining the entrance and exit apertures of the analyzer. The pumping port for the unwanted helium is also used for aligning the discharge tube and the capillary. The alignment is effected by constraining the two brass sheathings, one of which fits snugly over the discharge tube and the other over the capillary, into a linear configuration by the solid brass housing, and is further assisted by the Viton O-rings (Fig. 7), which also serve as vacuum seals. The undischarged helium is pumped either by a rotary or a 2" oil diffusion pump. However, the former has been found to be sufficient for the removal of excess He, thereby giving an efficient and intense source of HeI radiation. The more efficient diffusion pump is anticipated to be more effective for the production of the HeII line.

VERTICAL CROSS-SECTION OF THE LIGHT SOURCE UNIT

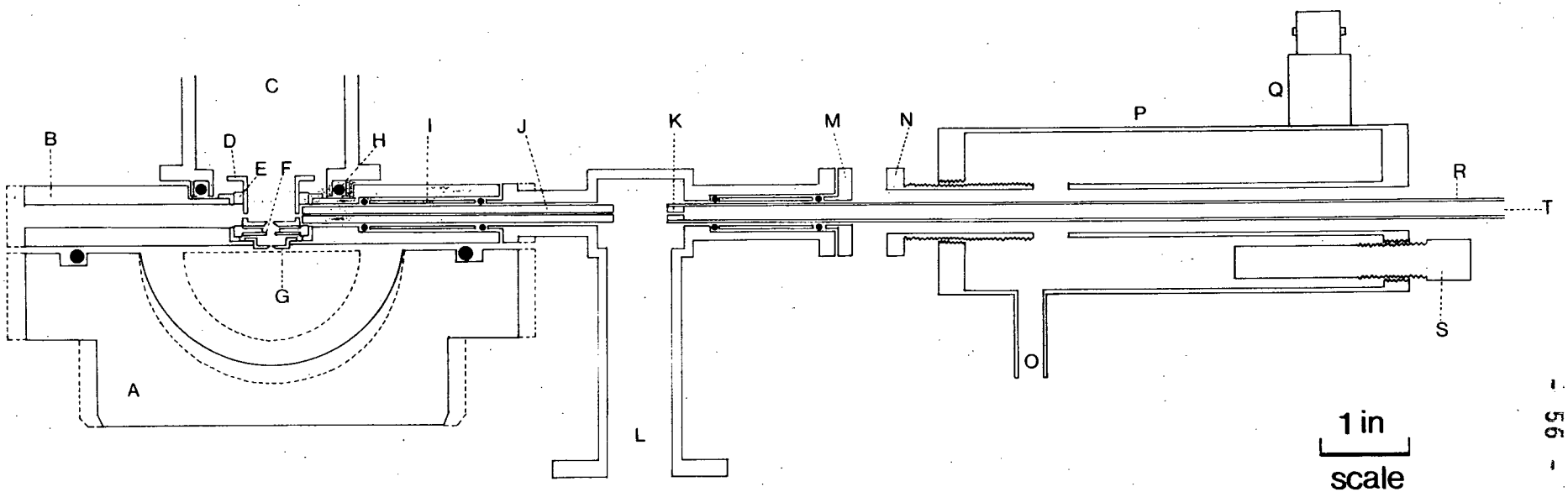

A. 180° HEMISPHERICAL ANALYSER
B. SUPPORTING PLATE
C. IONIZATION CHAMBER PUMPING PORT
D. IONIZATION CHAMBER
E. TEFLON
F. LENS
G. ENTRANCE APERTURE
H. O-RING SEAL
I. ALIGNMENT SHEATHING
J. COLLIMATING CAPILLARY (BRASS)
K. BORON NITRIDE CONSTRICTION
L. HELIUM PUMP OFF
M. SEALING FLANGE
N. TUNING STUB
O. FORCED AIR COOLING
P. MICROWAVE CAVITY
Q. POWER INPUT
R. QUARTZ DISCHARGE TUBE
S. QUARTER WAVE ADJUSTER
T. HELIUM INLET

FIGURE 7

3.3.4 The Sample System

(a) General Sample Inlet System

Stable samples are handled and stored in two separate but similarly constructed vacuum lines. Except for the one-litre glass storage flask, one of them is made of stainless steel and the other is of brass. Stainless steel or brass veeco angle valves are used in these lines for isolation purposes. A thermocouple (Varian NRC type 501) and a pressure gauge (Marsh type 3 2" Compound Gauge) in each line measure the vacuum and the sample pressure respectively. The control of the sample pressure into the ionization chamber is regulated by a variable leak valve (Granville Philips Series 203). The connection between the leak valve and the ionization chamber is made very flexible for simple disconnection by using 1/8" o.d. stainless steel or brass tubing and screw-on type O-ring vacuum seals (Fig. 5). This flexibility ensures lack of strain, and enables the various inlets to be set into any desired configuration.

(b) Direct Inlets For Reactive Molecules

The considerations for reducing the decomposition of reactive molecules before they are photoionized include:

(1) Choice of the right kind of material for the sample holder,

(2) Reduction in collisions with the walls, and hence

reduction in time between source and photoionization, and

(3) Cooling of the sample.

Three direct inlets, which are made of Kel-F, pyrex, and stainless steel respectively, have been constructed and used in this study, and they have been successful on all the occasions so far encountered. The configuration of the spectrometer when these units are in use is exemplified in the cases of the pyrex and Kel-F units, both shown in Fig. 8. When these units are used, the sample is held in the liquid or solid phase by immersing it in a suitable slush bath, and the operating sample pressure in the ionization chamber is controlled by the combined use of the 4" oil diffusion pump and the regulating valve (Kel-F, Teflon or stainless steel) (note - under such conditions the most volatile component comes off first, but by careful monitoring of the spectrum the course of the experiment can be followed.)

(c) Microwave Discharge Unit For Producing Transients

The configuration of the discharge apparatus is shown in Fig. 3. If necessary, the discharge cavity (Evenson type can be brought closer than 5 cm to the photoionization region (Fig. 9). The screw-on Viton O-ring vacuum seal is so designed that the discharge tube can be tilted as much as 15° to prevent stray electrons produced in the discharge

DIRECT SAMPLE INLETS

KEL-F INLET

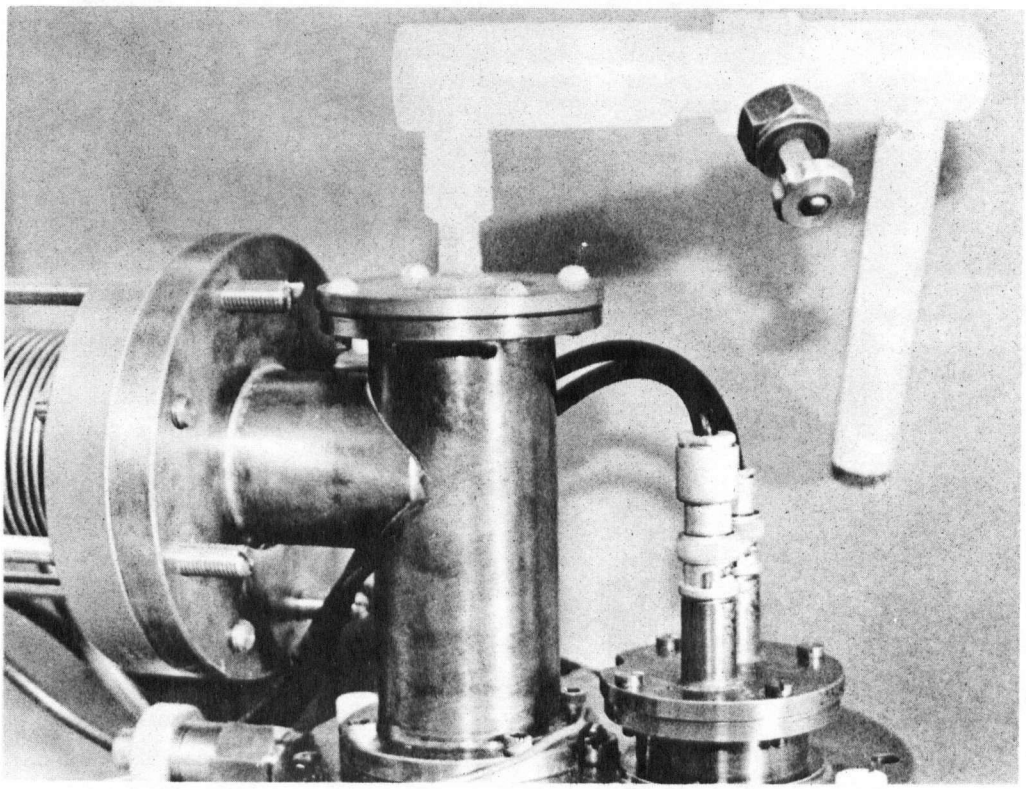

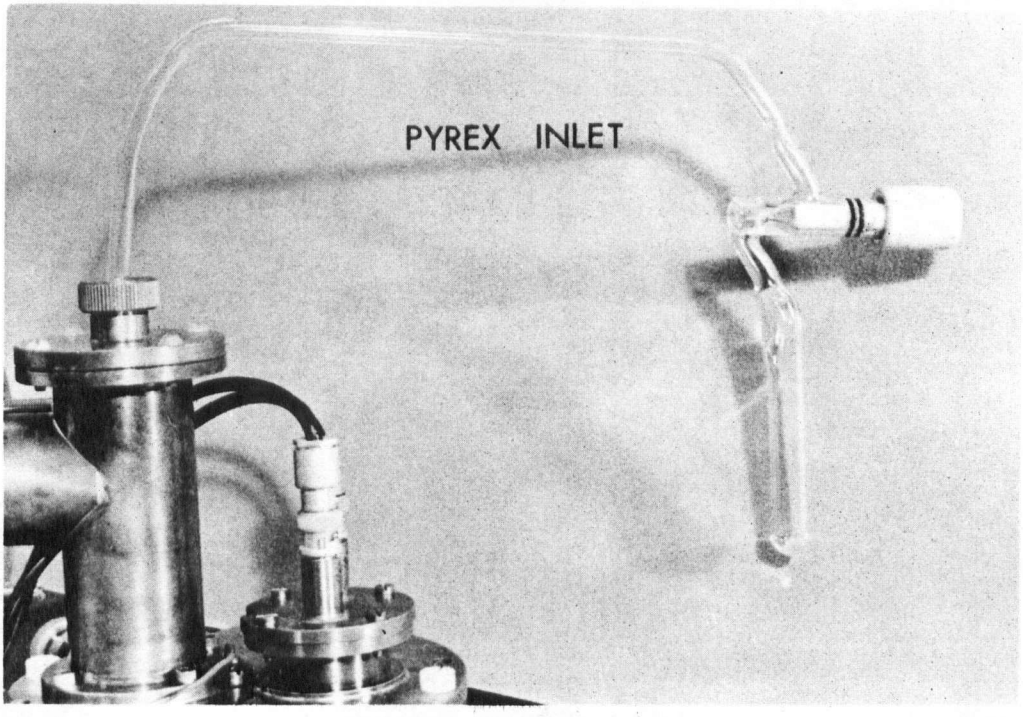

FIGURE 8

MICROWAVE DISCHARGE ASSEMBLY

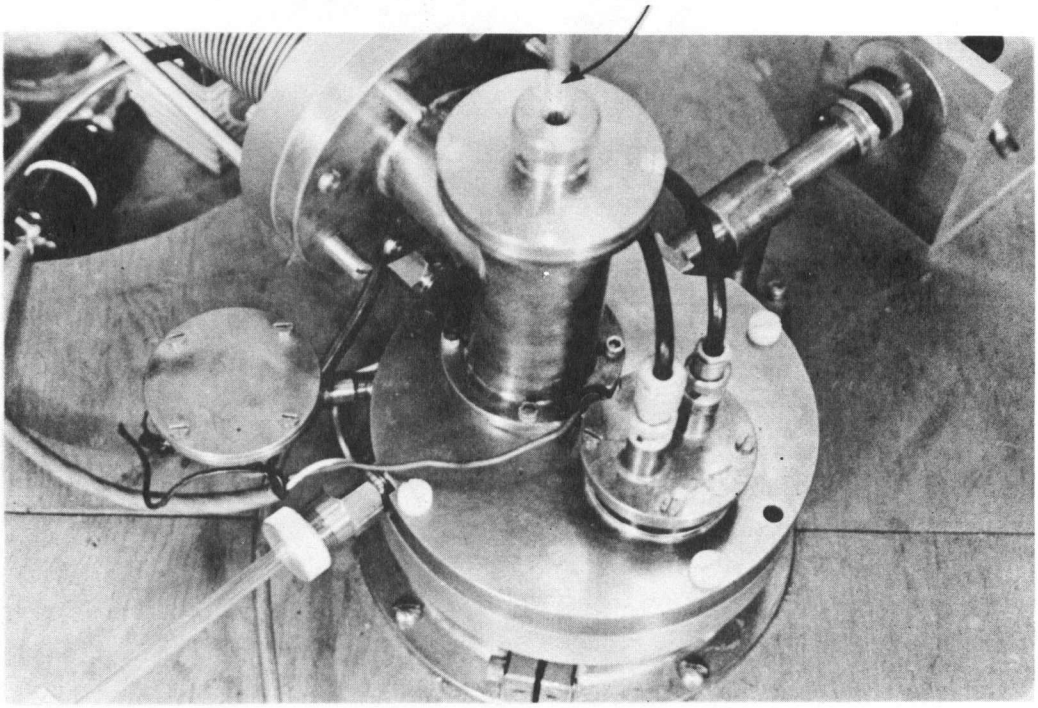

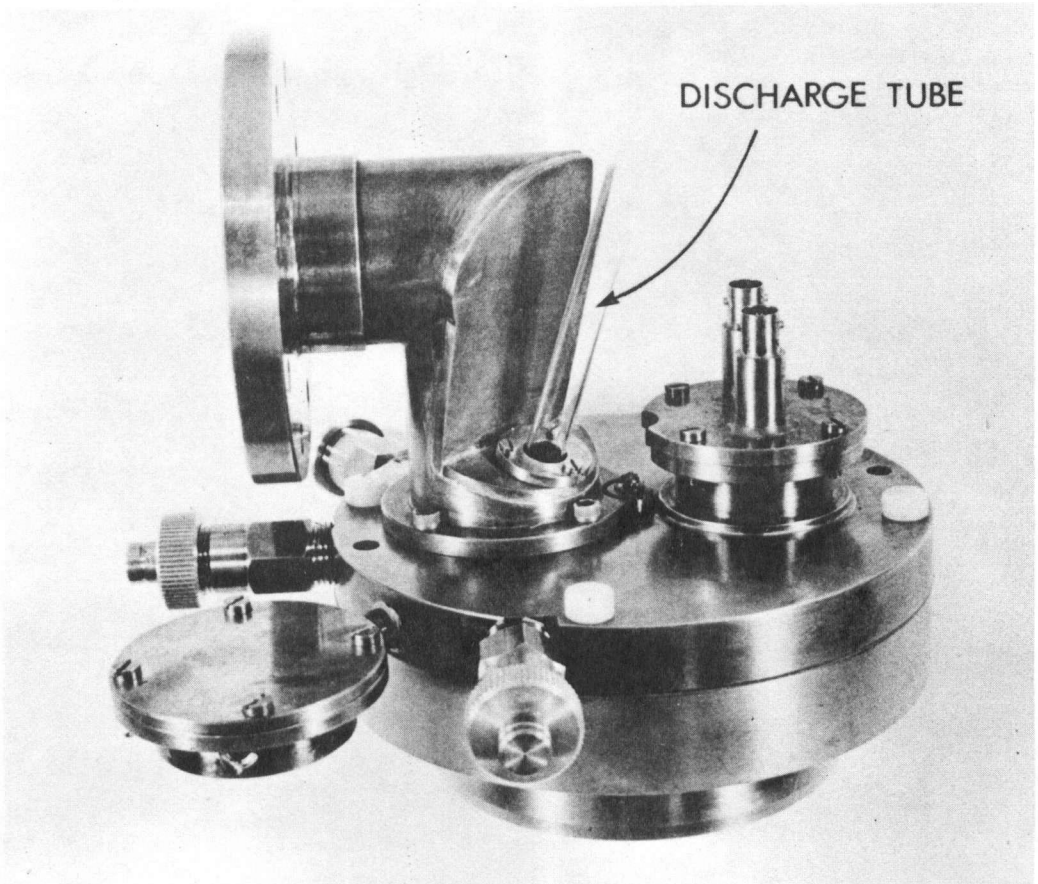

FIGURE 9

from going directly into the analyzer and causing high background counts. These stray electrons can further be reduced through collimation and enhanced wall collisions by inserting the discharge tube closer to the ionization chamber. By use of a nozzle (0.5 mm) in the discharge tube immediately above or below the discharge cavity, the production of the transient species can frequently be dramatically increased, as a result of the formation of a nozzle type molecular beam.

(d) High Temperature Pyrolysis Unit For Producing Transients

The components (the heater, the quartz and cooling units) of the pyrolysis unit are shown in Fig. 10. The 7 cm heater is made of 0.10" thick platinum wire noninductively wound on a grooved boron nitride (BN) thin-walled former, which fits snugly into another BN sheathing for positioning the wires and reducing heat loss. The quartz unit is made from two quartz tubes of 3 mm o.d. and 20 mm i.d. respectively, by sealing them at one end to form a nozzle. The other end of the outer tube is joined through a Kovar seal to the stainless steel vacuum-sealing flange which has three adjustable screws resting on the cooling unit for raising, lowering or tilting the quartz unit. The cooling unit is made of copper with an opening for differential pumping, and the cooling is effected by flowing cold water through it. The heater slides over the inner tube to sit at the bottom of the quartz unit, which in turn fits into the cooling unit. The whole assembly sits on the pumping port for the ionization chamber. All vacuum seals

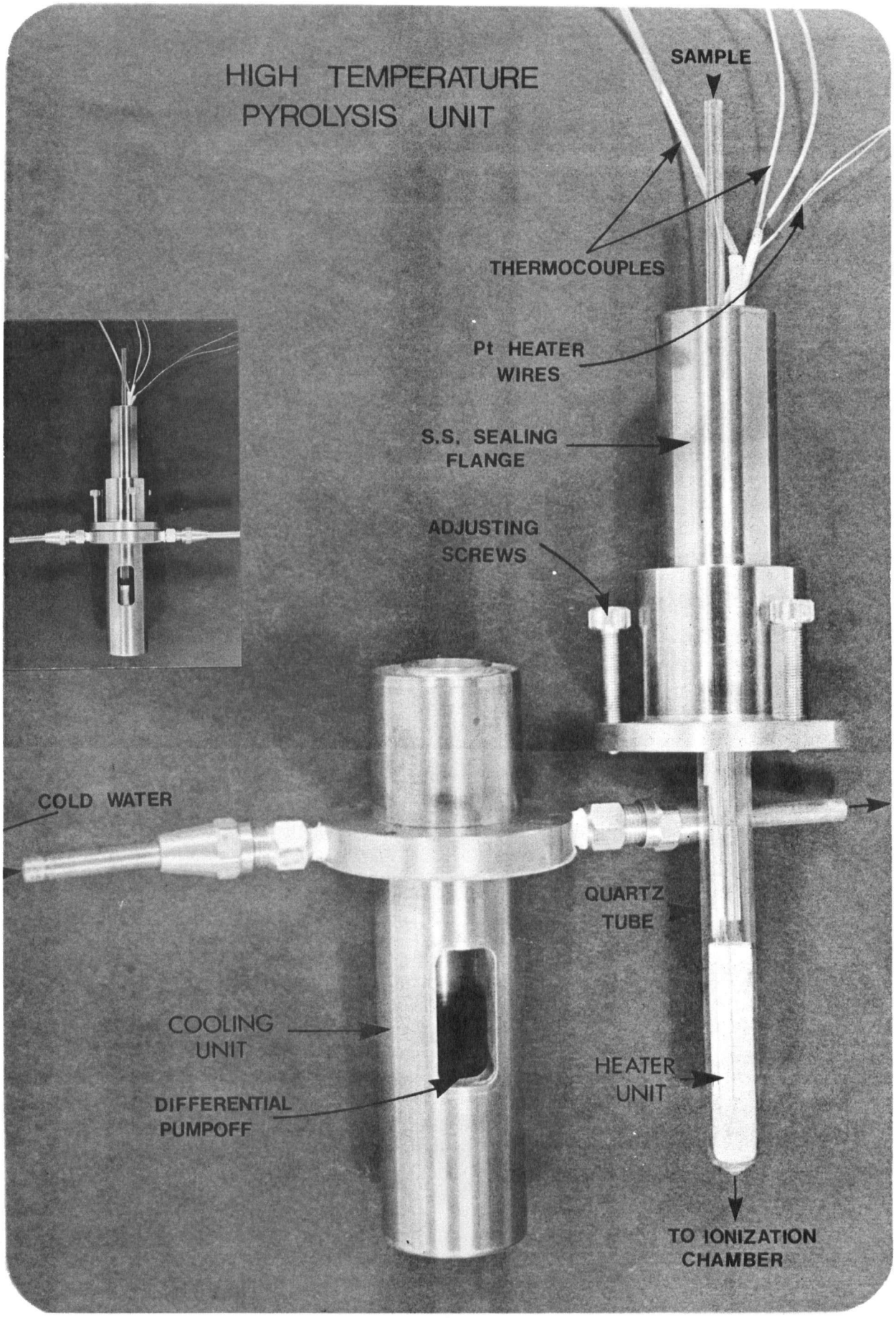
HIGH TEMPERATURE
PYROLYSIS UNIT
SAMPLE
THERMOCOUPLES
Pt HEATER
WIRES
S.S. SEALING
FLANGE
ADJUSTING
SCREWS
COLD WATER
QUARTZ
TUBE
COOLING
UNIT
DIFFERENTIAL
PUMPOFF
HEATER
UNIT
TO IONIZATION
CHAMBER

FIGURE 10

are accomplished by Viton O-rings. The lengths of the quartz and cooling units are so chosen that the nozzle is just a few mm above the photoionization point. An Alumel-Chromel thermocouple for temperature measurement is inserted halfway up the BN heating unit. The power for the heater is supplied through a Variac from an ordinary 110 volt AC line. A steady temperature of 1200°C is obtained with 250 watts at 3 amps. Under these conditions, the temperature of the spectrometer is merely warm to the touch, indicating that the cooling is sufficient. A slight adjustment of the Helmholtz coil settings is all that is necessary to retune the spectrometer. However, it has been found necessary to tilt the heater a little by means of the 3 adjusting screws in order to reduce the large background counts which presumably arise from the thermally emitted electrons emerging directly into the analyzer.

(e) Variable Temperature Unit For Equilibrium Studies

The components (before being welded together) of the variable temperature unit are shown in Fig. 11. The heater, which is wound noninductively around the coiled stainless steel (s.s.) inlet tubing, is made of 0.013" non-magnetic chromel-P wires. The sample gas flowing through the s.s. tubing is cooled by cold nitrogen gas generated by vaporizing liquid nitrogen from a dewar, or heated by the heater wires, and its temperature is measured by an Alumel-Chromel thermocouple spot-welded onto the tubing. By controlling the cold nitrogen flow rate or the power supplied to the heater, the temperature of the sample can be varied between -180°C and 500°C, with a fluctuation of ±5°C. The

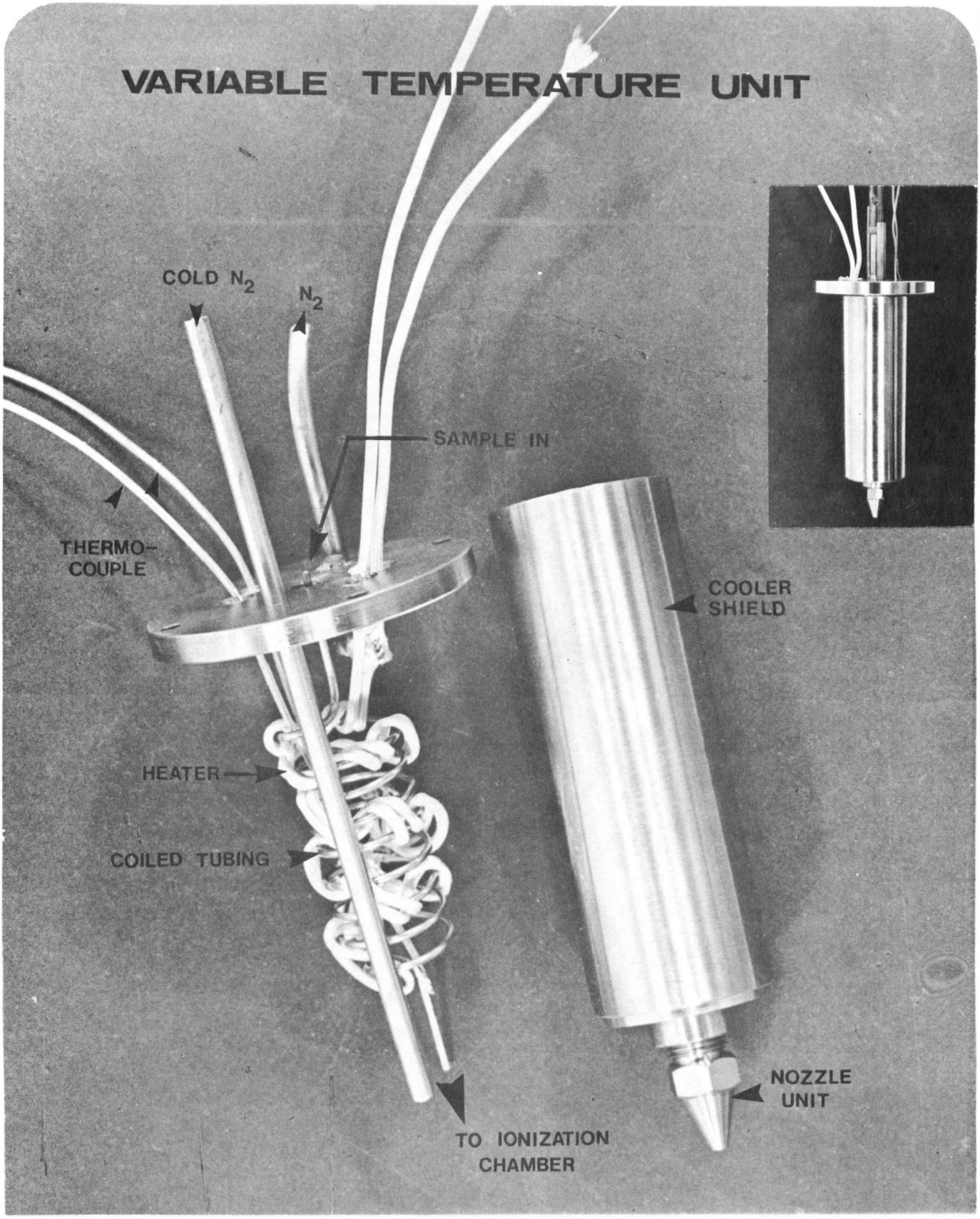
VARIABLE TEMPERATURE UNIT
COLD N_2
N_2
SAMPLE IN
THERMO-
COUPLE
COOLER
SHIELD
HEATER
COILED TUBING
NOZZLE
UNIT
TO IONIZATION
CHAMBER

FIGURE 11

demountable nozzle is designed for the study of supercooled molecular jets[150]. The unit sits on the pumping port of the ionization chamber, with the nozzle being about 2 mm above the photoionization point. The vacuum seal and insulation are again obtained by the Viton O-rings and the plexiglass washer.

3.3.5 The Scanning And Detecting System

The control circuitry for the spectrometer is shown in Fig. 12. For reasons of simplicity and economy, all voltages are supplied by the use of batteries, which are grounded on one side (except that for the analyzer). Voltage adjustments are accomplished using vernier-drive potentiometers (TRW Trimmers-Potentiometers). The power for each Helmholtz coil is supplied by a DC power supply (Lambda LH122A FM).

The analyzer can be operated in one of two possible scanning modes: (1) The potential difference (V_{12}) between the hemispheres is scanned, while keeping the ionization chamber at ground potential. (2) The potential difference (V_R) between the ionization chamber and the grounded entrance aperture of the analyzer is scanned, while keeping that between the hemispheres at a selected value. This selected value depends upon the desired resolution and intensity. The scanning potentials are respectively supplied by a programmable sweep (first mode) or by amplifying a 4 volt ramp originating from a multichannel analyzer (Fabritek 1072) (second mode), and their ranges can be respectively varied in steps of 0.1 volts or linearly up

PE SPECTROMETER CONTROL

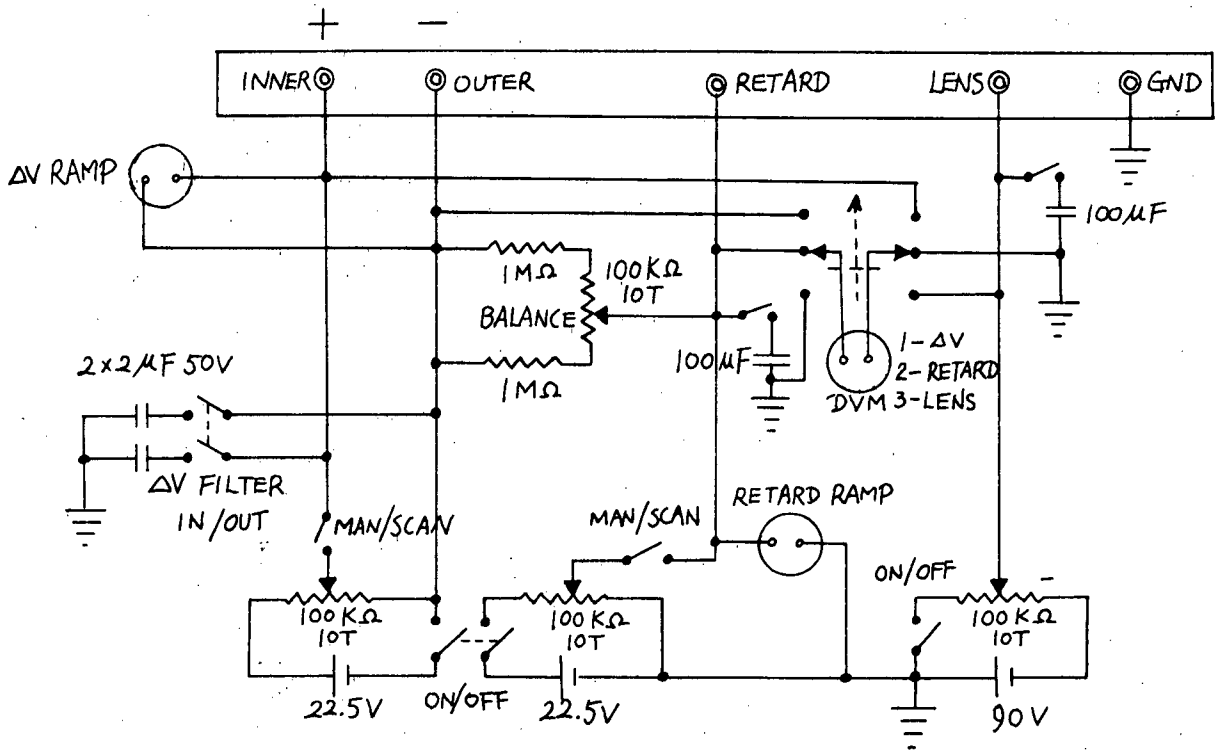

RAMP AMPLIFIER

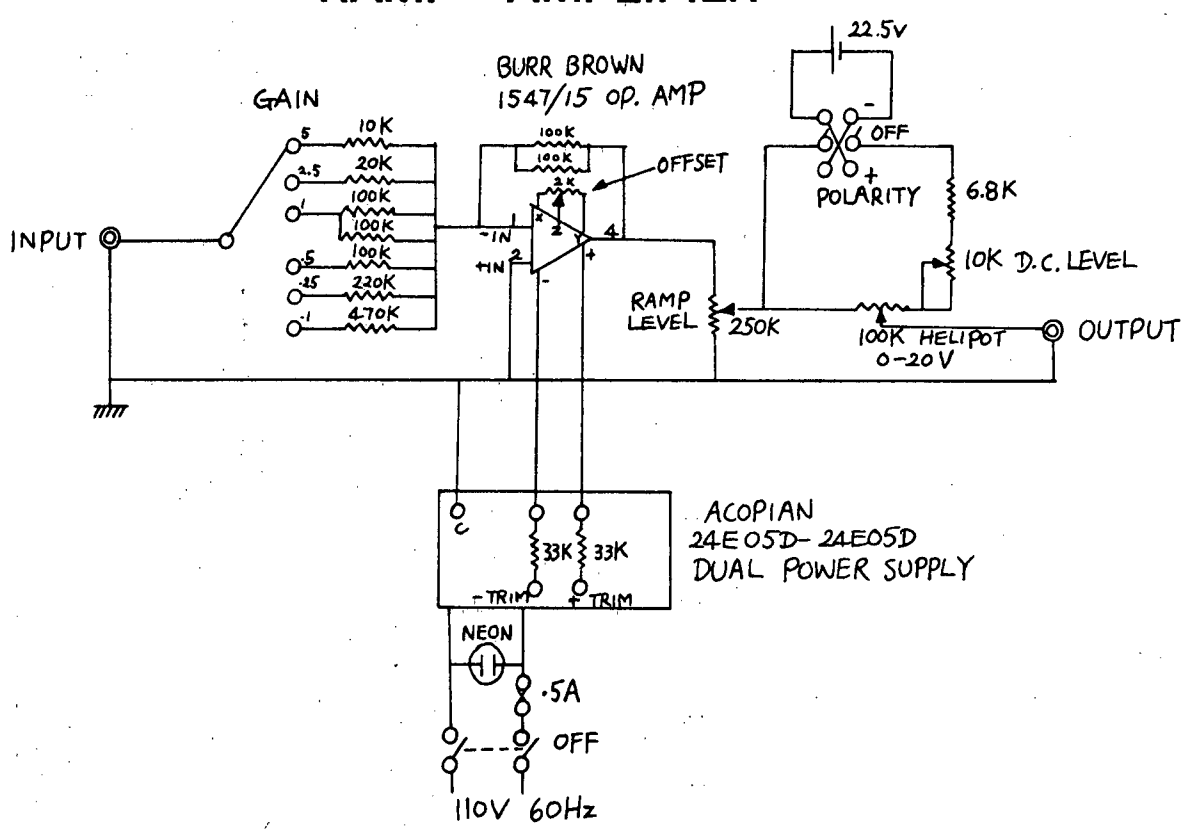

FIGURE 12

to 20 volts. In the first scanning mode, electrons of different energies are successively focused and thus are analyzed at different resolutions (refer eq. (3.3.8)), while in the second mode, they are pre-accelerated or pre-decelerated to the selected focusing energy of the analyzer, and thus are analyzed at constant resolution.

A channel electron multiplier (Mullard B319AL) operating in saturated mode is used for electron detection. A positive voltage of ∿3000 volts (Hewlett Packard 6525 DC Power Supply) is applied to its output while the input is held at 300 V above ground (by battery) to accelerate the electrons. Pulse counting is used for data acquisition and conventional pulse counting equipment is used for this purpose, namely, a preamplifier, an amplifier and a discriminator (Harshaw NA-15, NH-34A). The data readout system may involve a multichannel analyzer (Fabritek 1072), ratemeter (Harshaw NR-10), chart recorder (Hewlett Packard 680 Strip Chart Recorder) and X-Y plotter (MFE Plotamatic 715).

3.4 Operation And Performance Of The Spectrometer

The base vacuum is in the region of 1-3 x 10^{-6} mm Hg, which can normally be obtained starting from atmospheric pressure in about one hour, provided that the system has not been exposed to the air too long for appreciable adsorption to have occurred. The helium gas in the light source hardly

increases the base pressure, since it is being differentially pumped (section 3.3.3). The pressure of the sample at the ionization chamber is not measured directly, but is instead monitored by the ionization gauge (section 3.3.1). The operating pressure as read at the ionization gauge is between 0.4-3 x 10^{-5} mm Hg (ca. 0.01-1 Torr in the ionization chamber). The differential pump on the ionization chamber is isolated when stable samples are being run since large quantities of sample would be consumed, and is partially or completely opened for running reactive molecules or transients.

The advantages and disadvantages of operating the analyzer in the two scanning modes (section 3.3.5) are shown by recording the PE spectrum of oxygen in the respective mode (Fig. 13). In the first mode (scan V_{12}), very low energy electrons (0-2 eV) are badly discriminated against, with the result that the fourth band of O_2 can only be detected after applying a positive potential to the lens (Fig. 13), and variable resolution (linewidths) is obtained in the same spectrum because of the constant $\Delta E_{\frac{1}{2}}/E$ (eq. (3.3.8)). In the second mode (scan V_R), a rising background normally occurs on the low kinetic energy side, and occasionally is so strong to obscure any bands in this region. The second mode is superior in that very high resolution can be obtained by decreasing V_{12}, although at the expense of signal intensity, while the second mode may be used as a check that all bands are detected at fairly low electron energy region (1-4 eV). Consequently, in

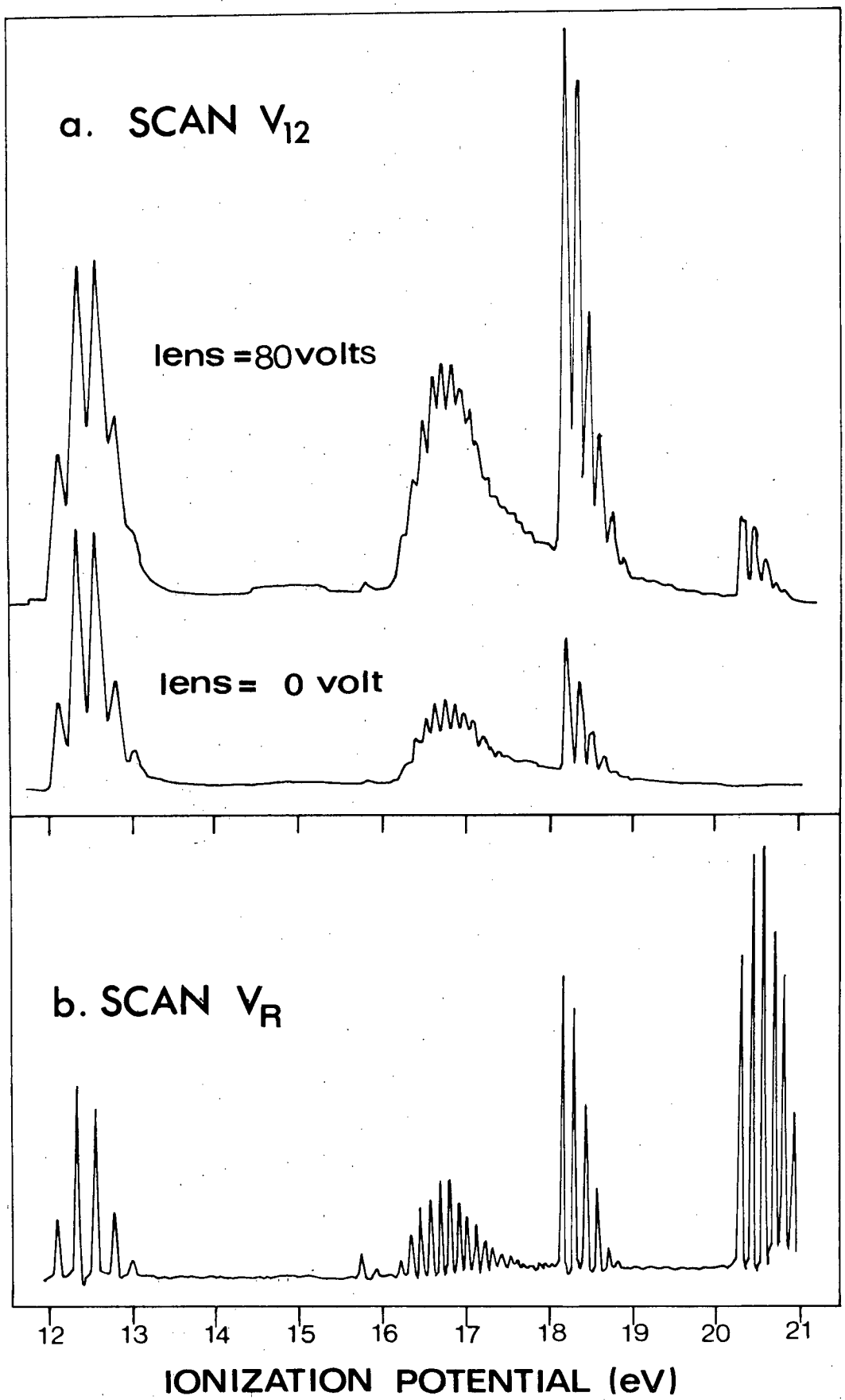
a. SCAN V_{12}
lens =80volts
lens = 0 volt
b. SCAN V_R
12
13
14
15
16
17
18
19
20
21
IONIZATION POTENTIAL (eV)

FIGURE 13

practice, the analyzer is always operated in the second mode, with the energy of the focused electrons chosen to give the best compromise between resolution and intensity, and whenever necessary the second mode is used as a cross check. In the second scanning mode a negative lens at a selected potential, presumably due to its focussing action on the electrons, has been found to increase the intensity drastically and is thus always used.

As discussed in section 2.3, the major stumbling block to very high resolution is the inhomogeneous surface potential and micropotentials at the apertures. This is especially detrimental in the present study since the spectrometer is constantly exposed to corrosive or reactive vapors, making it extremely difficult to obtain the theoretical resolution (0.8%). The kind of resolution and sensitivity which is typical of the present spectrometer when it is relatively clean is given in Table 2, where is shown the observed half width of the Ar $^2P_{3/2}$ peak and its intensity at different focusing conditions. The best resolution obtained has been 15 meV with an intensity of 10,000 counts/sec. Normally the spectrometer is operated at a resolution of 20-30 meV with counts of ∿30,000 per sec.

The potential of the present system for studying transient species is tested on some atomic species, e.g. H,N and F, and O_2 ($^1\Delta_g$), which have been reported by Jonathan

TABLE 2* FWHM and Intensity Of The Argon $^2P_{3/2}$ Peak at Different Focusing Conditions

$\Delta E_{1/2}$ (meV)	I (counts/sec)	E (eV)	V_{12} (volt)	V_R (volt)	V_L (volt)
19	2,000	0.251	0.209	5.015	-0.065
20	6,000	0.370	0.308	4.826	-0.299
20	9,000	0.490	0.408	4.678	-0.428
20	11,000	0.607	0.506	4.523	-0.650
21	15,000	0.727	0.606	4.369	-0.754
22	19,000	0.847	0.706	4.220	-0.904
23	25,000	0.966	0.805	4.046	-1.124
24	29,500	1.085	0.904	3.907	-1.278
25	38,000	1.201	1.001	3.746	-1.426
30	43,000	1.321	1.101	3.597	-1.586
31	48,000	1.441	1.200	3.441	-1,726

* $\Delta E_{1/2}$: FWHM of the peak; I: Intensity; E: Energy of the focused electrons; V_{12}: Potential across the analyzer hemispheres; V_R: Retarding potential and V_L: Potential of the lens.

et al.[44-47]. The PE spectra of these species are shown in Figs. 14, 15 and 16, and were obtained by a microwave discharge in the indicated molecules without the use of any diluent gas. In all cases, our results are at least comparable to those of Jonathan et al.[44-47], but with a significant improvement in resolution. This merit has enabled us to detect some new features in the PE spectra of CS (section 4.1) and $SO(^3\Sigma^-)$ (section 4.2).

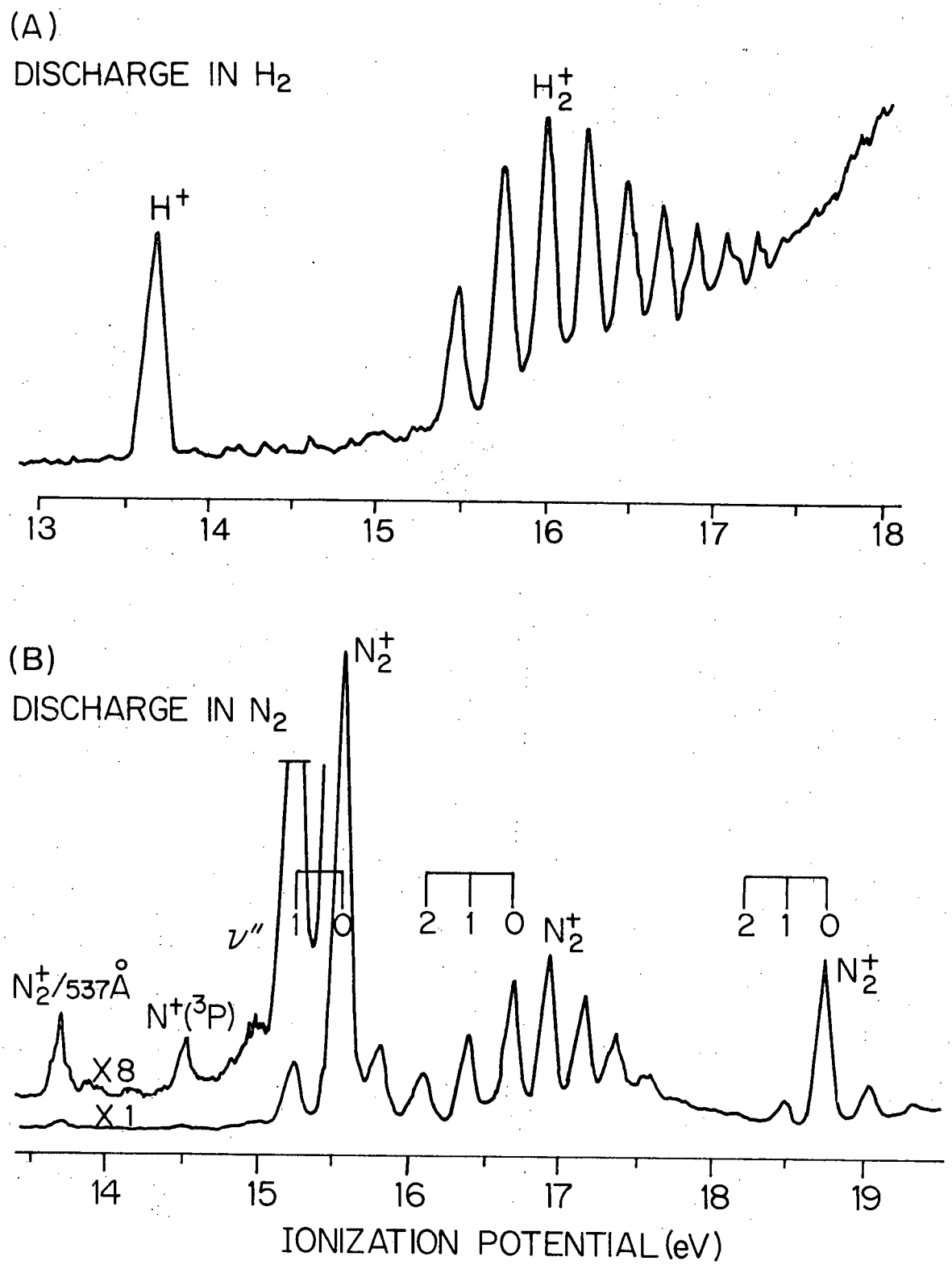
(A)
DISCHARGE IN H_2
H^+
H_2^+
13
14
15
16
17
18
(B)
DISCHARGE IN N_2
N_2^+
ν''
1
0
2
1
0
N_2^+
2
1
0
N_2^+
$N_2^+/537Å$
$N^+(^3P)$
X8
X1
14
15
16
17
18
19
IONIZATION POTENTIAL (eV)

FIGURE 14

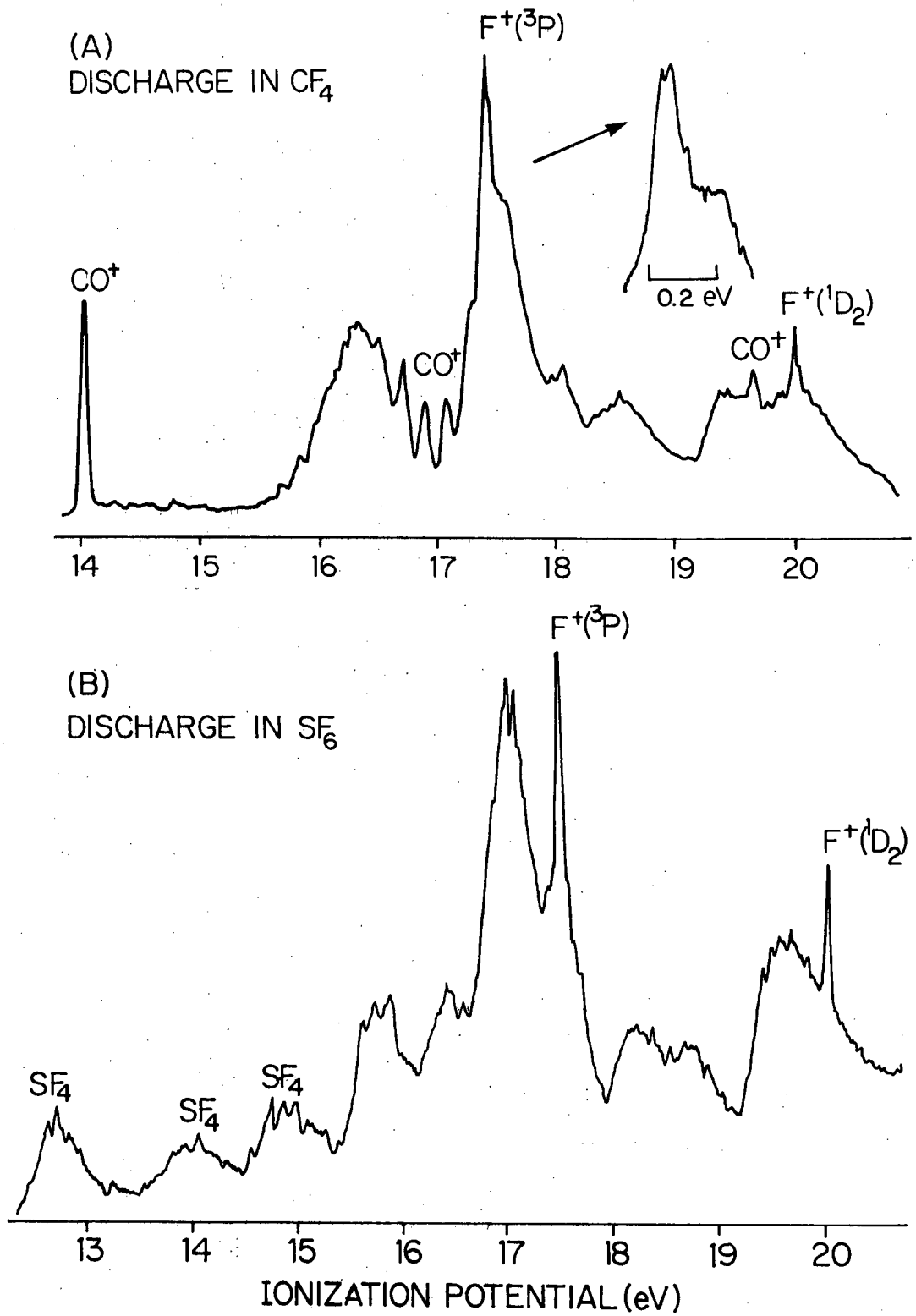
(A)
DISCHARGE IN CF_4
$F^+(^3P)$
CO^+
CO^+
0.2 eV
$F^+(^1D_2)$
CO^+
14
15
16
17
18
19
20
(B)
DISCHARGE IN SF_6
$F^+(^3P)$
$F^+(^1D_2)$
SF_4
SF_4
SF_4
13
14
15
16
17
18
19
20
IONIZATION POTENTIAL (eV)

FIGURE 15

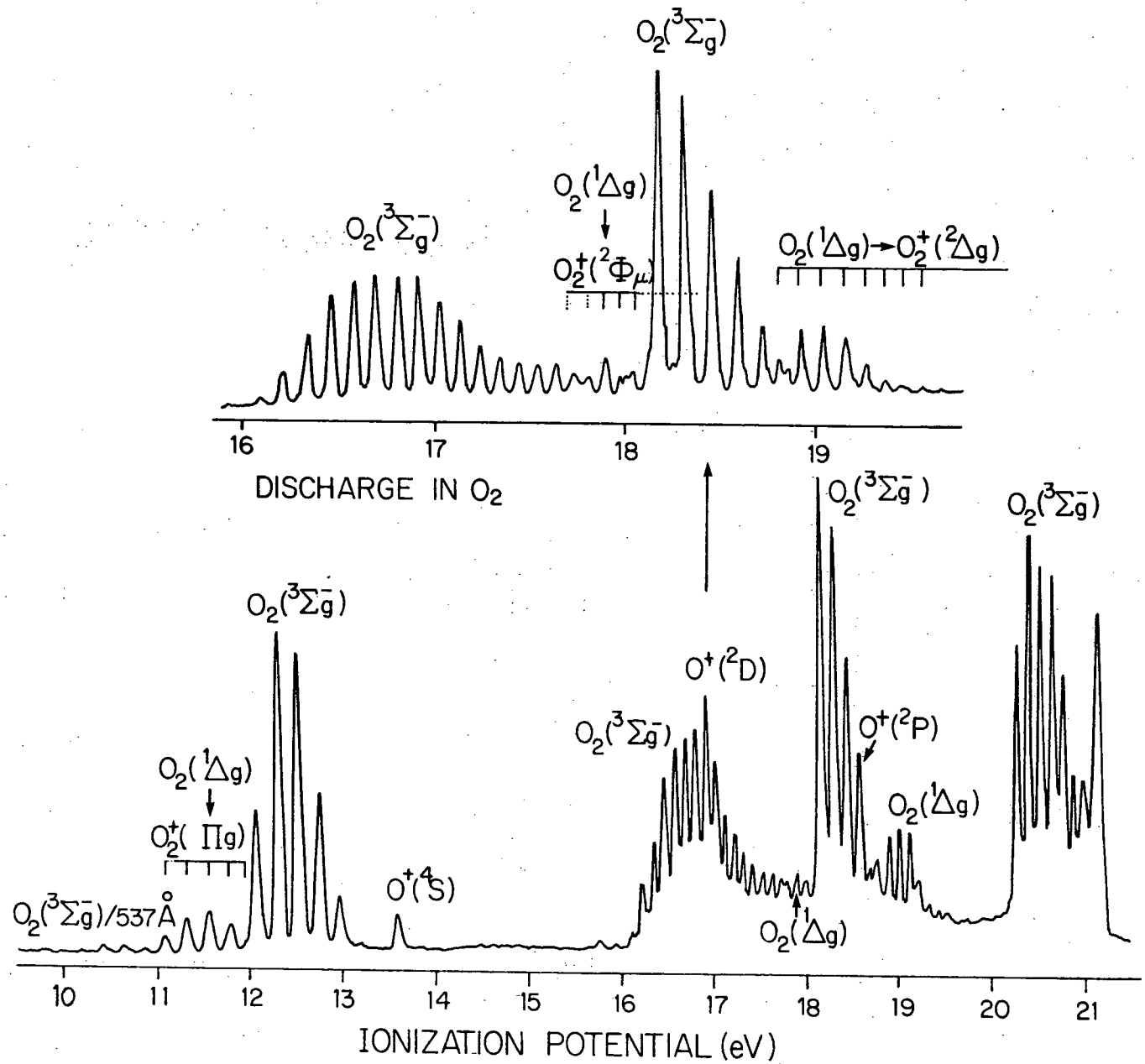
$O_2(^3\Sigma_g^-)$
$O_2(^1\Delta g)$
$O_2^+(^2\Phi_\mu)$
$O_2(^1\Delta g) \rightarrow O_2^+(^2\Delta g)$
16
17
18
19
DISCHARGE IN O_2
$O_2(^3\Sigma_g^-)$
$O_2(^3\Sigma_g^-)$
$O_2(^3\Sigma_g^-)$
$O^+(^2D)$
$O_2(^3\Sigma_g^-)$
$O^+(^2P)$
$O_2(^1\Delta g)$
$O_2(^1\Delta g)$
$O_2^+(\Pi g)$
$O_2(^3\Sigma_g^-)/537$ Å
$O^+(^4S)$
$O_2(^1\Delta g)$
10
11
12
13
14
15
16
17
18
19
20
21
IONIZATION POTENTIAL (eV)

FIGURE 10

CHAPTER FOUR

PHOTOELECTRON SPECTROSCOPY OF SOME TRANSIENT SPECIES

4.1 Carbon Monosulfide (CS)

4.1.1 Introduction

Carbon monosulfide (CS) has been extensively studied by spectroscopic methods[151]. The species can be produced in good yield by either the discharge or photolysis of CS_2[151g]. The first ionization potential (IP) of CS was reported by several groups using either electron impact[152a], mass-spectrometry[152b] or conventional optical methods[151j]. Very recently, two groups[153] have obtained the photoelectron (PE) spectrum of CS giving the first two IP's. The first IP was identified[153] as referring to the ground ionic state ($X^2\Sigma$), and the second was tentatively assigned[153a] to the ionic $^2\Pi$ state.

Considering the similar electronic structure of CS to CO, we should expect each IP of CS to be lower than the

corresponding one of CO in view of the lower IP's of S than that of O. Therefore it is surprising that a third IP was not obtained by photoelectron spectroscopy. The PE spectrum of a neutral molecule resembles closely the electronic spectrum of the ion. It is instructive to compare the electronic states of CP, an isoelectronic species of CS^+, with that of CS^+. Two conclusions may be safely drawn. First, for CP[111], excited states $A^2\Pi$ and $B^2\Sigma$ are respectively 0.855 and 3.608 eV above the ground state $X^2\Sigma$, while as for CS^+, $A^2\Pi$[153a] is 1.46 eV above $X^2\Sigma$. The ordering of the first two electronic states of the two molecules are the same, and the separations are reasonably close. Hence it is reasonable to expect CS to have at least another IP below 21.22 eV. Secondly, the spin-orbit splitting for the $^2\Pi$ state of CP is 158.3 cm^{-1} [111], and so the $^2\Pi$ state of CS^+ should have a spin-orbit splitting of a similar order of magnitude, probably larger. In the light of this, the reported spin-orbit splitting[153a] for the $^2\Pi$ state of CS^+ of $\sim$30 cm^{-1} seems rather small.

In the following, it will be shown that these expectations are indeed well borne out, and that the second IP can be unambiguously assigned to the $^2\Pi$ state of the ion[154].

4.1.2 Experimental

CS was produced by microwave discharge of CS_2. No attempt was made to remove CS_2 by trapping because no compli-

cations occurred due to its presence. Previously, we noticed the discharge in CS_2 was rather unstable and CS was produced in a measurable amount only for about an hour. A modified discharge cavity[155] which has been claimed to give better performance, was used instead. Great care was taken to ensure a very stable CS_2 pressure. Power as low as 50 W was found sufficient to produce maximum yield of CS. A quartz tube of 5 mm i.d. was used and the discharge cavity placed 27 cm from the ionization region. Under these conditions, a stable supply of CS with its first peak more intense than that of CS_2 was obtained continuously for six hours. Multiple scans for each IP of CS were possible. The spectra were recorded at a resolution between 25-30 meV (measured by FWHM of Ar peaks). Calibration was effected using the values for CS_2 which are in turn calibrated using argon.

4.1.3 Results and Discussion

The PE spectra of CS_2 with and without the discharge are depicted in Figs. 17a and 17b respectively. In addition to the two bands observed before[153], two more bands due to CS^+ are obtained. The IP's and the vibrational frequencies are collected in Table 3. Our values are in good agreement with the previous ones[153].

If an orbital description of the electronic structure is assumed, CS has a configuration

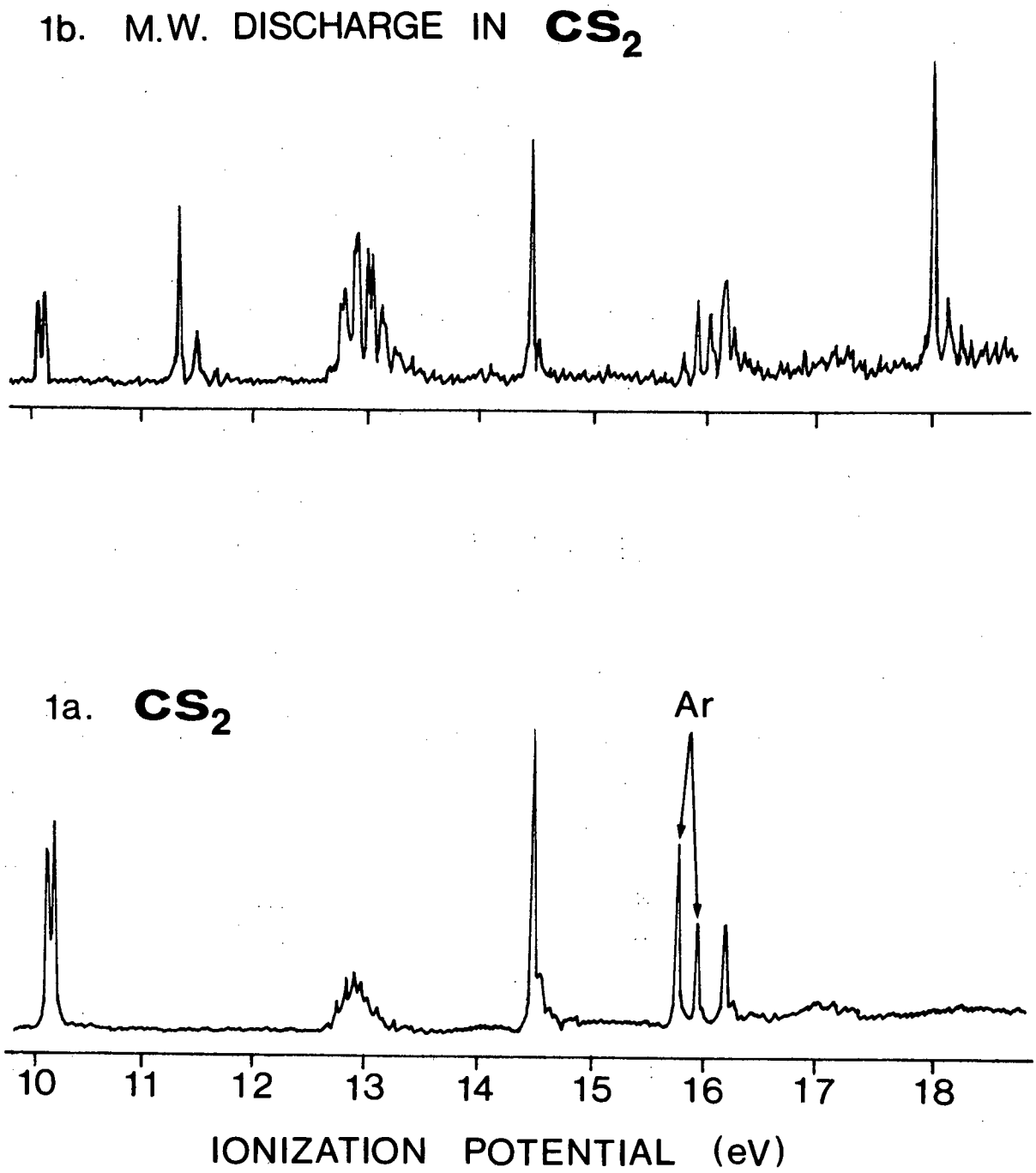
1b. M.W. DISCHARGE IN CS_2
1a. CS_2
Ar
10
11
12
13
14
15
16
17
18
IONIZATION POTENTIAL (eV)

FIGURE 17

ABLE 3 PES and Theoretical Data of CS

Ionic state	Ionization potentials (eV)					Vibrational frequency (cm^{-1})		
	PES[a]			Theoretical		PES		
	This work[b]	Ref. 153a	Ref. 1536	CNDO/2[d]	Ref. 158	This work[c]	Ref.153a	Ref.153b
$X^2\Sigma$	11.34	11.33	11.33	10.10	12.80	1380	1325	1290
$A^2\Pi$	12.78 (12.90)	12.79 (12.92)	12.76	11.24	12.61	970	1050	980
$B^2\Sigma$	15.83 (16.06)			16.56	18.83	870		
$C^2\Sigma$	18.03			24.64	30.12	1060		

a) adiabatic IP's are given, vertical IP in parentheses.

b) estimated experimental error ± 0.02 eV.

c) estimated experimental error ± 30 cm^{-1}.

d) with 4 eV adjustment.

$$(1\sigma)^2(2\sigma)^2(3\sigma)^2(4\sigma)^2(1\pi)^4(5\sigma)^2(6\sigma)^2(2\pi)^4(7\sigma)^2.$$

The four observed bands will then correspond to the removal of electrons from three σ and one π molecular orbitals (MO).

The spin-orbit splitting for the second band is resolved clearly (Fig. 18b) and has a value (A) of 280 ± 30 cm^{-1}. This value is in excellent agreement with a very recent result[156] (301.283 cm^{-1}) obtained from the electronic spectrum of CS^+. This then leaves no doubt that the second band corresponds to the $^2\Pi$ state and the other three to the $^2\Sigma$ states of CS^+.

The first band, giving a coincident adiabatic and vertical IP at 11.34 eV, has at least three observable vibrational components (Fig. 18a). The sharpness of the first peak, together with the increase in the vibrational spacing compared to the ground molecular state, i.e. from 1275 to 1380 cm^{-1}, indicates ionization of an antibonding σ MO.

The second band (Fig. 18b) overlaps with one from CS_2. Because of the difference in vibrational spacings and the splitting of fine structure for CS, we are able to determine the adiabatic and vertical IP's accurately. This band has a vibrational series of at least six components, and the decrease in the vibrational spacing, together with the length of the series clearly indicates the removal of a

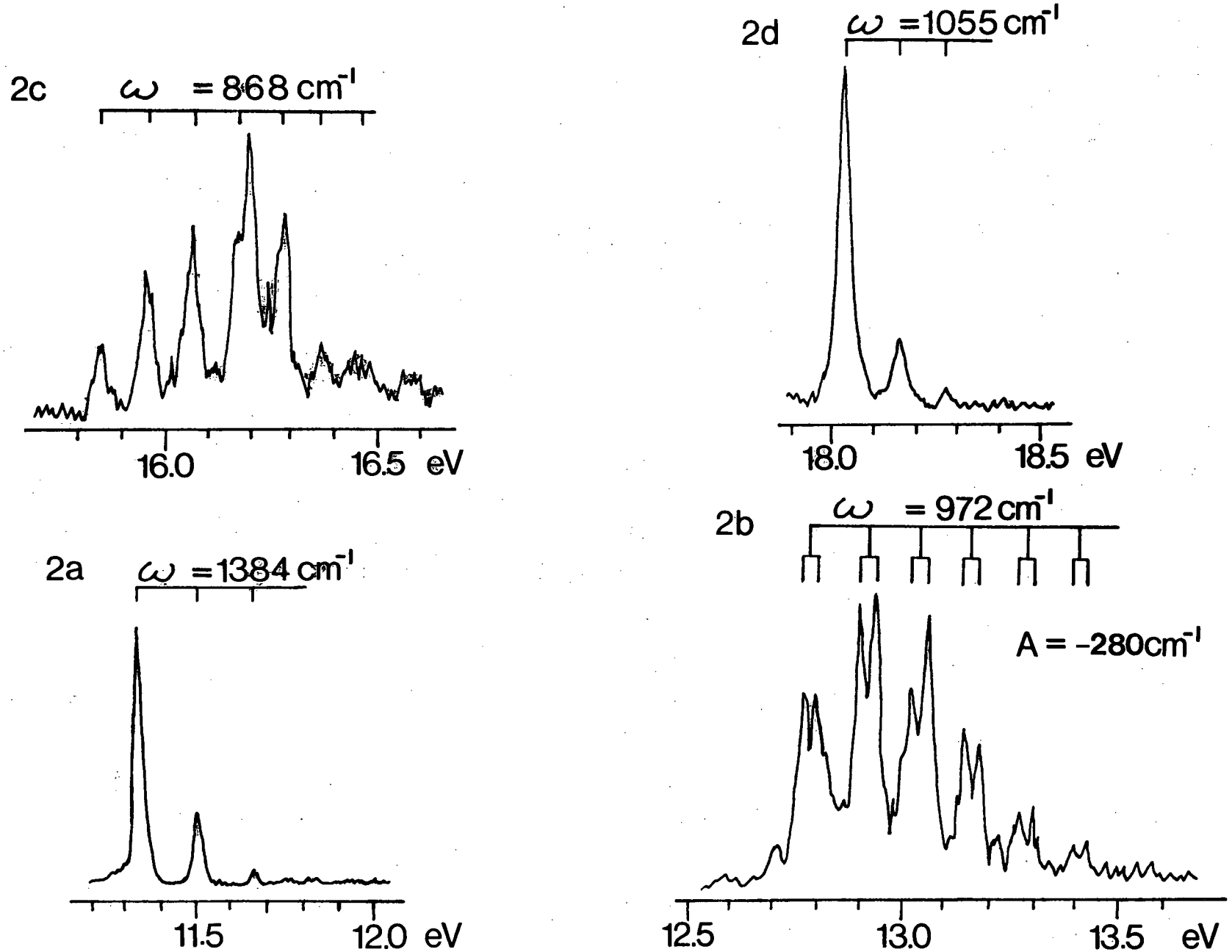
2c
ω = 868 cm⁻¹
16.0
16.5 eV
2d
ω = 1055 cm⁻¹
18.0
18.5 eV
2a
ω = 1384 cm⁻¹
11.5
12.0 eV
2b
ω = 972 cm⁻¹
A = -280cm⁻¹
12.5
13.0
13.5 eV

FIGURE 18

strongly bonding (π) electron.

The third band (Fig. 18c) is also overlapped by one from CS_2. The resolution is good enough to enable an accurate determination of the adiabatic and vertical IP's at 15.83 and 16.06 eV respectively. The band shows at least six vibrational components and a large decrease in vibrational spacing. The MO involved appears to be even more bonding than the second.

The decrease in the vibrational spacing of the fourth band is in line with the removal of a bonding electron, yet the sharpness of the first peak (Fig. 18d) is unexpected. The corresponding IP has not been obtained for CO, but a fourth IP at 23.60 eV for N_2 has recently been obtained from Rydberg series[157]. Hence by comparing with N_2, it is reasonable to assign the fourth band, with an identical adiabatic and vertical IP at 18.03 eV, to the $C^2\Sigma$ state of the ion.

In order to obtain more confirmation for the assignment, we resort to theoretical calculations. An ab initio SCF-LCAO-MO calculation using an extended basis set of Slater type orbitals[158] has been carried out for CS. By applying Koopmans' theorem[49], the IP's are calculated (Table 3). The agreement between the experimental and theoretical results is not satisfactory, notably in the ordering of the ionic Π state. This points to the fact that Koopmans' theorem must be applied cautiously. Never-

theless, the bonding character of individual MO's agrees with the experimental finding. We have performed a CNDO/2[76] calculation and surprisingly the predicted IP's are in better agreement with experiment, except that a bonding electron is indicated to be involved in the first IP.

4.2 Sulfur Monoxide (SO)

4.2.1 Introduction

The PE spectrum of SO($^3\Sigma^-$) has been studied by Jonathan et al.[47,159], who identified three IP's below 21.2 eV. It is clear that the spectrum of SO is far from complete and raises several points that need to be clarified. First, considering the similarity in electronic structure between O_2 and SO, one notes that the reported spectrum of SO[159] is far too simple in that some ionic states accessible in HeI PES may have been undetected. Secondly, the $X^2\Pi$ ionic state should have a spin-orbit splitting greater than that of O_2^+ $X^2\Pi_g$ state (A = +195 cm^{-1} [111]) and at least comparable to that of CS^+ $A^2\Pi$ state[160] (A = -280 cm^{-1}, section 4.1.3). Therefore, with better resolution one should be able to resolve this splitting. Thirdly, in the study of S_2O[161] (section 4.3.3), we have raised the point that the 'second IP' of SO at 11.3 eV may be due instead to the second PE band of S_2O. The present section is aimed at

attempting to answer these important questions.

4.2.2 Experimental

$SO(^2\Sigma^-)$ was produced by a MW discharge (100W) in SO_2 without or with the addition of varying amounts of sulfur vapor. The amount of the latter was controlled by a heating tape wound around a side-arm of the discharge tube into which some (sublimed) sulfur powder was placed. The PE spectrum was calibrated using the spectroscopic IP's of the oxygen atoms[162] produced in the discharge.

4.2.3 Results and Discussion

The PE spectra of $SO_2(A)$ and the products of the discharge in SO_2 with different amounts of S vapor is shown in Fig. 19, with the amount of S increasing from B to D. The discharge in SO_2 alone gave a PE spectrum (Fig. 19B) which shows, in addition to the O^+ peaks, two additional bands due to SO[47, 159] at 10.33 eV and 14.94 eV. The spectrum is identical to that of Jonathan et al, except that the PE band at 11.3 eV is hardly detectable in Fig. 19B . With a little S vapor added into the discharge (Fig. 19C), the peaks due to O^+ disappeared. In addition, two new bands at 10.6 eV and 11.3 eV began to appear, and they increased dramatically with respect to those of SO^+ with increasing S vapor pressure (Fig. 19D). Moreover, at high S vapor pressure two more bands at 14.7 eV and 16.0 eV (Fig. 19D) could be

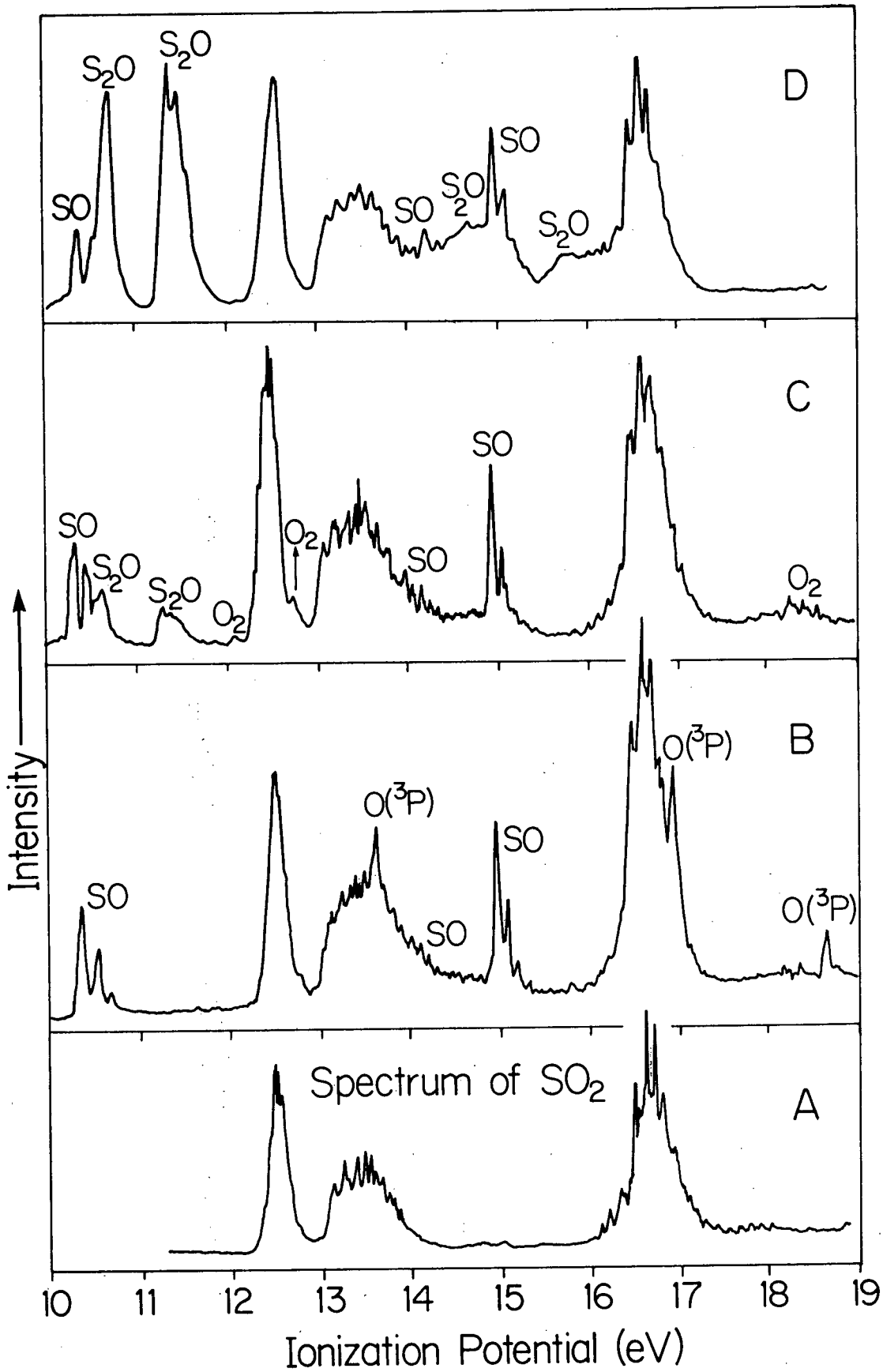
D
C
B
A
SO
S_2O
O_2
$O(^3P)$
Spectrum of SO_2
Intensity
10
11
12
13
14
15
16
17
18
19
Ionization Potential (eV)

FIGURE 19

identified. Comparing with the PE spectrum of S_2O[161] (section 4.3.3), these four bands can be assigned unambiguously to those of S_2O. This thus confirms our previous claim[161] that the 2nd band (11.3 eV) of SO observed by Jonathan et al[159] was actually the 2nd band of S_2O, which was formed by the reaction of SO with S deposited on the walls. The partial overlap of the first band of SO by that of S_2O explains the unexpected broadening[159] of v' = 1 and 2 peaks of the former. The observation that the intensities of the bands of S_2O grow with increasing S concentration is in complete accord with the fact[163] that SO ($^3\Sigma^-$) formed in the discharge reacts rapidly with S to form S_2O. Indeed, with less efficient pumping SO can be eliminated from the spectrum as a result of its complete reaction with S.

The 1st band of SO was recorded at high resolution and is shown in Fig. 20. The expected spin-orbit components are clearly resolved, with an average splitting of 320 ± 20 cm^{-1} (40 meV) which then leaves no doubt that the 1st IP is due to the $^2\Pi$ ionic state. The IP's and vibrational frequencies corresponding to the two distinct bands at 10.33 eV and 14.94 eV are collected in Table 4, and these values are in good agreement with the previous results[47,159].

The average total half-widths of the overlapped ($^2\Pi_{1/2}$,$^2\Pi_{3/2}$) peaks in the 0-0 and 0-1 components of the $X^2\Pi$ state are 85 ± 3 meV. Using the observed spin-orbit splitting and assuming the peaks of the two spin states $^2\Pi_{1/2}$ and $^2\Pi_{3/2}$ are equally intense, have the same half-widths, and are of

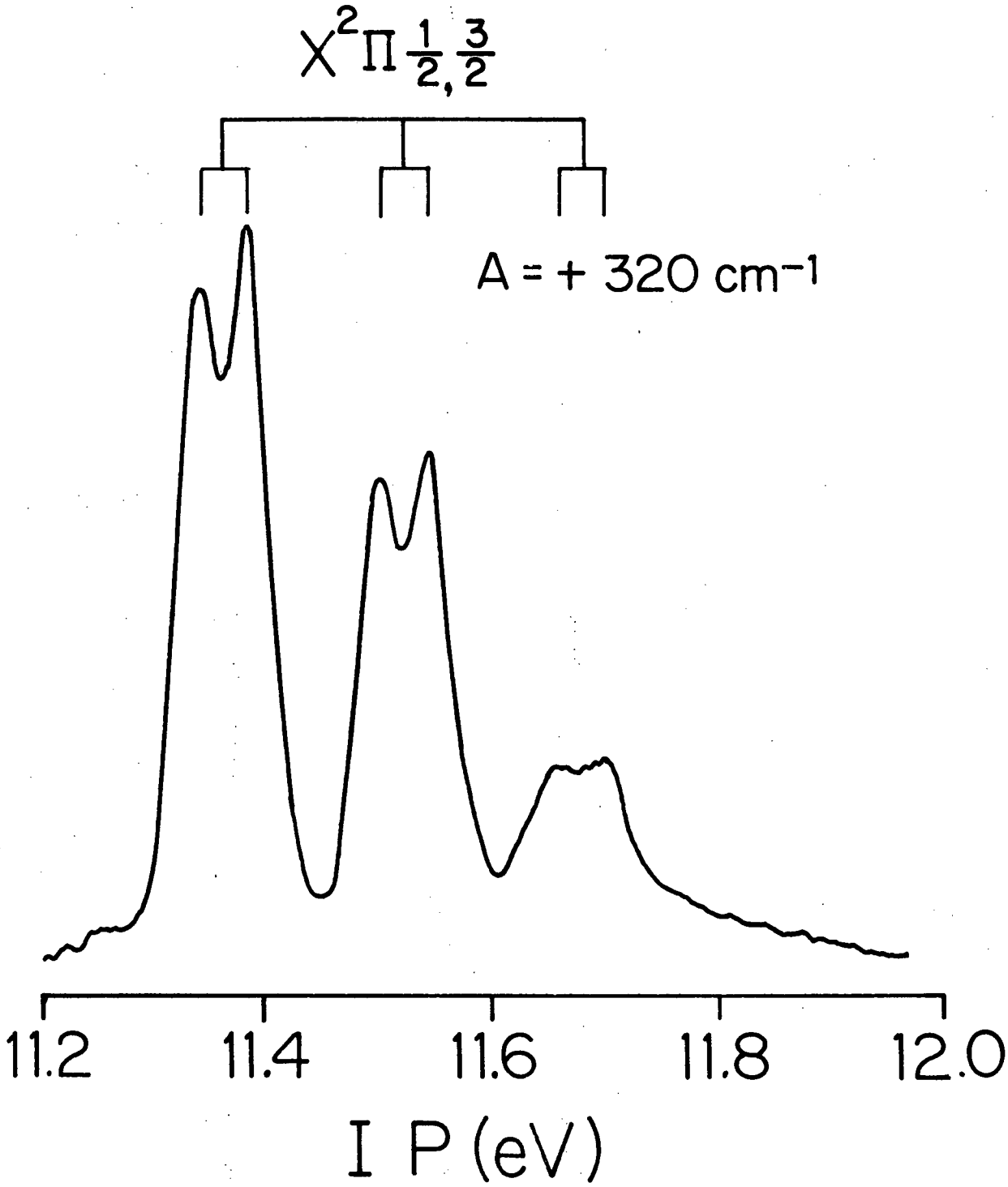

FIGURE 20

TABLE 4 PES Data for SO

Ionic state	Vertical IP (eV)	(adiabatic)	Vibrational frequency (cm^{-1})	
	This work	Ref. 159	This work	Ref. 159
$X^2\Pi_{1/2,3/2}$	10.33±0.01 10.37±0.01	10.32	1270±30 1270±30	1210
$a^4\Pi$	13.90 (13.39)±0.10	--	750±100	--
$A^2\Pi$	∿14.6 (∿14.0)	--	700±100	--
$b^4\Sigma^-$	14.94±0.01	14.96	920±30	970

gaussian type, the half-widths of these individual peaks can then be estimated[164] to be 54 ± 4 meV. This value is significantly larger than the observed half-widths of the peaks in the band at 14.94 eV, which are 45 ± 3 meV. The smaller half-widths of the latter tend to suggest that this band is probably due to a state with no spin-orbit splitting, i.e. a Σ state (or a Π state with a very small spin-orbit splitting which is unlikely in view of the 40 meV splitting for the $X^2\Pi$ state). Comparing with O_2^+[132], the assignment of this band to the $b^4\Sigma^-$ state of SO^+ is most probable, as suggested previously[159].

Comparing the 13.5 - 15.0 eV region of the PE spectrum (Fig. 21) recorded with (B) and without (A) the MW discharge in SO_2 alone, we have observed that there are extra peak intensities and some additional peaks in the former. These features were also evident in the spectra measured by Jonathan et al[159] but had not been mentioned in their discussion. While the 2nd band of SO_2^+ (Fig. 21A) drops to the baseline beyond 14.1 eV, there are, however, some distinct peaks (Fig. 21B) in the same region which seem to correlate with the presence of SO in the spectrum. By manually subtracting the intensity of the 2nd band of SO_2^+ from the spectrum of the discharge products, the extra peak intensities are shown as vertical lines in Fig. 22. These peaks must then be due to SO since their intensities follow the other bands of SO. The spacing between peaks varies between 850 cm^{-1} and 700 cm^{-1} with an average

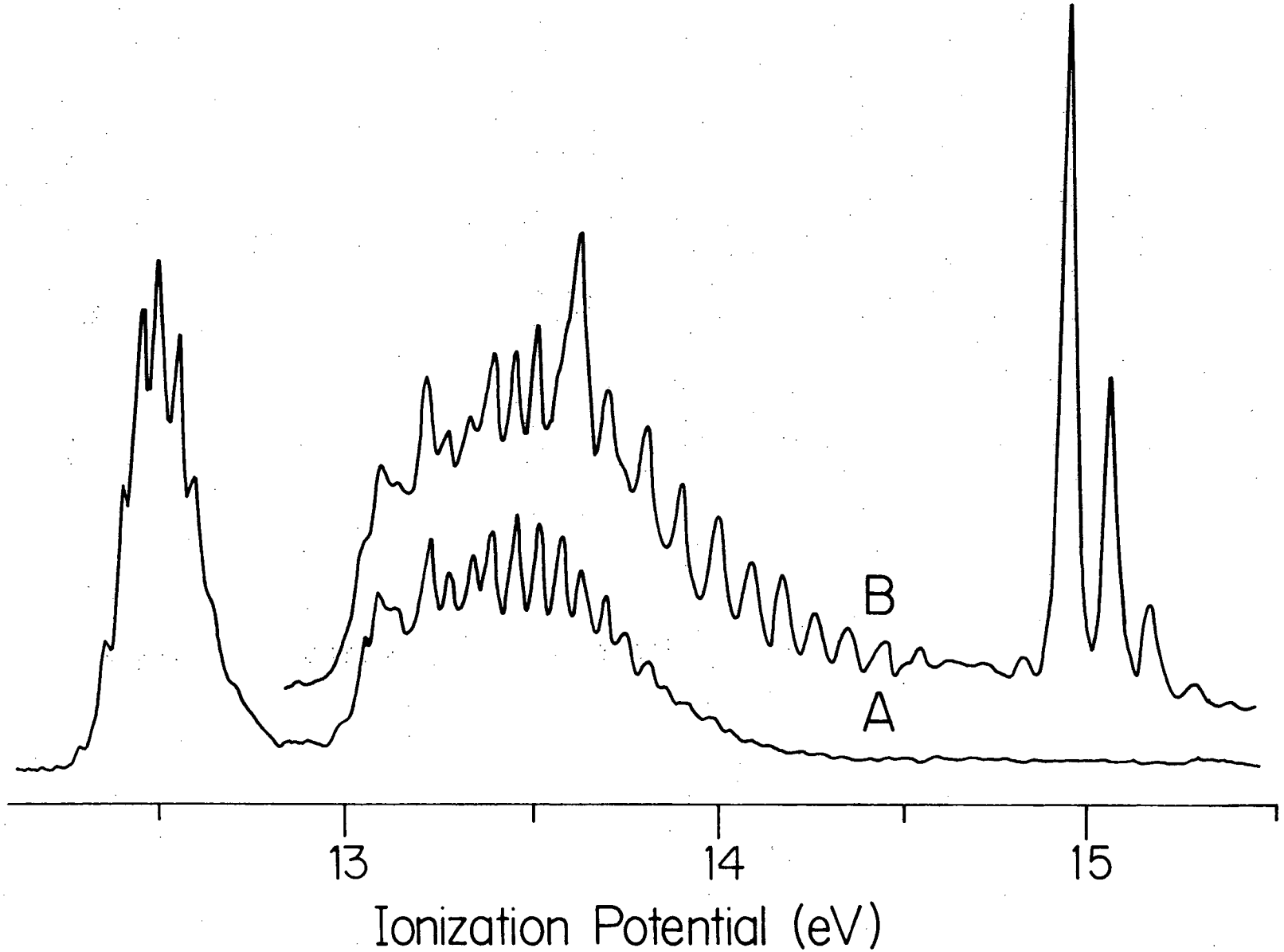

FIGURE 21

of 750 cm^{-1} compared with the ground state value of 1111 cm^{-1} [111]. The drastic reduction in vibrational frequency and the length of the progression (at least ca. 12 components) is indicative of the removal of a strongly bonding electron. By comparing with O_2^{+}[132], it seems reasonable to assign this band to be due to the $a^4\Pi$ state, since the corresponding transition in O_2 also shows an extensive vibrational progression with a large decrease in the vibrational frequency, from 1780 cm^{-1} to ~900 cm^{-1} [111] (for the molecule and ion). The adiabatic and vertical IP's of this band are estimated to be at 13.39 eV and 13.90 eV (v' = 5) respectively. Because of the overlap from the second band of SO_2^{+}, these quoted IP values may be in error by as much as one vibrational quantum.

Upon close examination, it is noted that peaks of the $a^4\Pi$ state broaden at and beyond v' = 6, and irregular structure appears around 14.6 eV (Fig. 22). In view of the fact that this is reproduceable and folows the SO band intensities, and guided by the spectrum of O_2^{+}[132], where a similar phenomenon occurs on the high energy side of the $a^4\Pi_u$ band, we are inclined to suggest there may be an additional band in the mentioned region, which overlaps strongly with the $a^4\Pi$ state of SO^{+}. If this is genuine, it will then be the $A^2\Pi$ ionic state. The corresponding adiabatic and vertical IP's cannot be determined with certainty but are estimated to be at 14.0 eV and 14.6 eV respectively (Fig. 22) and the

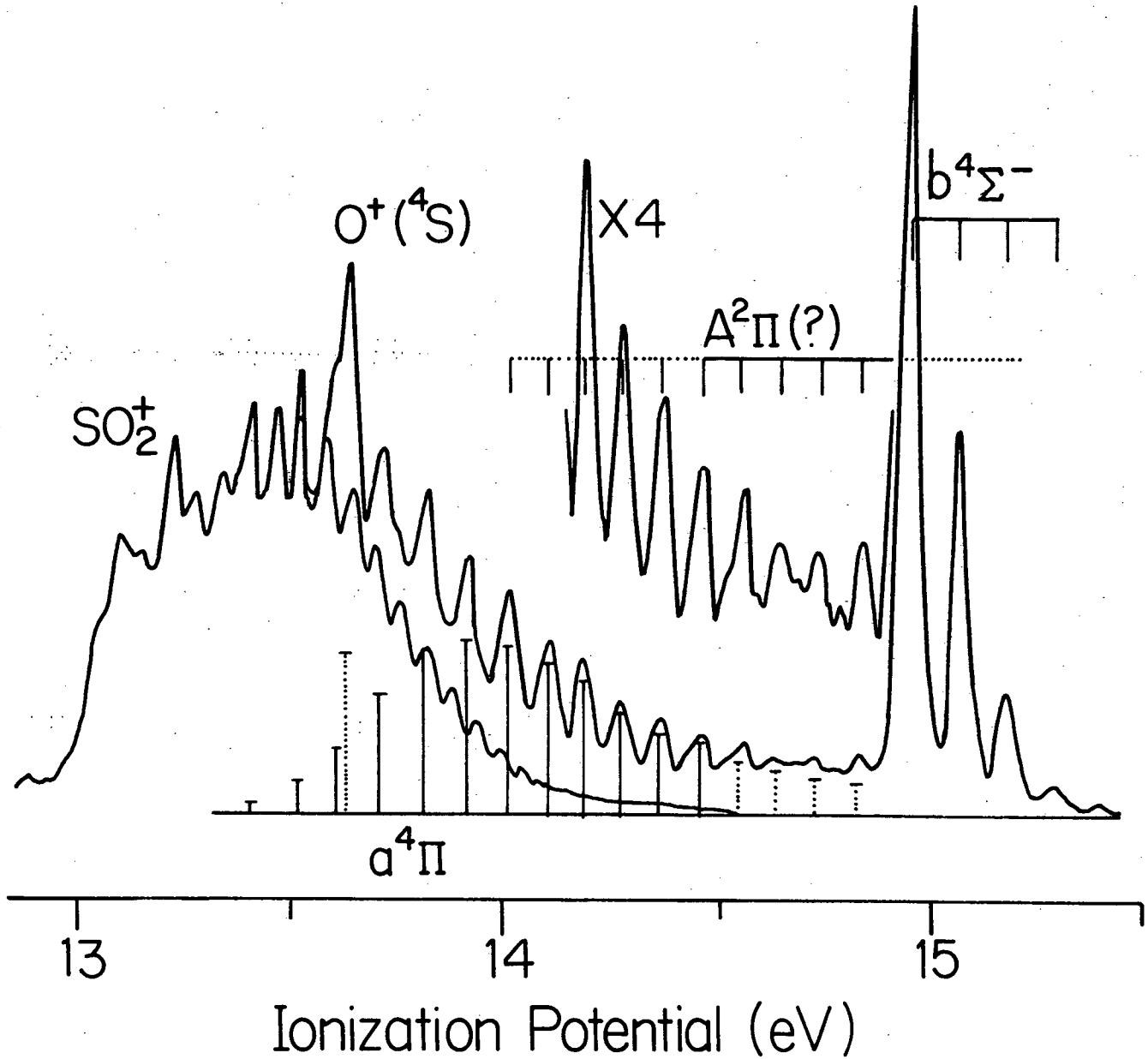
$O^+(^4S)$
X4
$b^4\Sigma^-$
$A^2\Pi(?)$
SO_2^+
$a^4\Pi$
13
14
15
Ionization Potential (eV)

FIGURE 22

vibrational spacing is approximately 700 cm^{-1} compared with 1111 cm^{-1} [111] for the ground state. This compares with the values of 1780 cm^{-1} and ~800 cm^{-1} for the $A^2\Pi_u$ state of O_2.

With the identification of the $a^4\Pi$ and $A^2\Pi$ states, the PE spectrum of SO^+ then, as expected, closely resembles that of O_2^+ except for the absence of the $B^2\Sigma^-_{(g)}$ state in the former (O_2^+,20.4 eV). We suspect this state to be buried underneath the intense third band of SO_2^+ (at 16.6 eV).

In conclusion, it may be added that attempts to remove SO_2 from the discharge products either by selective cold-trapping or by using an excess of S vapor resulted in the complete disappearance of SO as well.

4.3 Disulfur Monoxide (S_2O)

4.3.1 Introduction

The chemistry of S_2O has been reviewed by Schenk and Steudel[163]. In the vapor phase and at low pressures of ca. one torr or less, S_2O can be stable for a few hours[163], and SO formed as an intermediate in a reaction is almost always the precursor of S_2O[163]. Historically, S_2O was actually mistaken for SO for more than a decade until its identity was finally established in 1956.

The PE spectrum of S_2O is, moreover, of additional interest because it is isoelectronic with the molecules NSF and SO_2, the PE spectra of which have recently been the

subject of extensive studies[167-170]. The related compound NSCl has also been investigated[167] because of disagreements regarding the assignment of various ionization potentials[168,169]. It will be shown that our results and assignments lead to a resolution and definite confirmation of the order of the orbitals in this series of molecules.

4.3.2 Experimental

S_2O was produced by two separate methods.

(1) By the microwave discharge of sulfur dioxide (SO_2) in the presence of sulfur, which was coated on the wall of the discharge tube. Depending on the pressure of SO_2, various proportions of S_2O/SO_2 could be obtained. At a certain pressure, the PE spectrum of SO_2 disappeared completely, yet when the supply of SO_2 was turned off, the bands due to S_2O also disappeared.

(2) By passing thionyl chloride ($SOCl_2$) vapor through a 4 cm column of silver sulfide (Ag_2S) powder heated to about 150°C[171]. The heater was made by winding chromel-P wires non-inductively around a quartz tube. The direct inlet system made of pyrex (section 3.3.4.b) was used for $SOCl_2$ because of its ready decomposition. The PE spectrum of $SOCl_2$ disappeared completely when Ag_2S was heated and the new bands appeared could be identified as due to S_2O and SO_2. The best yield was obtained at around 150°C.

The PE spectra obtained from the two methods were

identical except for a difference in the S_2O/SO_2 intensity ratio, with the second method giving consistently better yields of S_2O as expected[163]. This leaves no doubt that the new species we observed is S_2O.

The resolution as measured by the FWHM of the argon $^2P_{3/2}$ peak is between 25-30 meV. Calibration of the spectrum was effected using argon and oxygen. The estimated error is ± 20 meV for ionization potentials (IP's) and ± 30 cm^{-1} for vibrational frequencies.

4.3.3 Results and Discussion

The PE spectrum obtained by passing $SOCl_2$ over heated Ag_2S is shown in Fig. 23, where the PE spectra of pure SO_2 and $SOCl_2$ are also included for comparison. Although it was not possible to get rid of SO_2 from the spectrum of S_2O, fortunately its existence caused little problem. The PE spectrum of S_2O (Fig. 23b) consists of four distinguishable bands with vibrational fine structure resolved in two of them. The IP's and vibrational frequencies are collected in Table 5.

The interpretation of the PE spectrum of S_2O is aided by comparison with those of NSF[167-170] and SO_2[172], which are isoelectronic to S_2O. Comparison with the PE spectra of NSCl[167] is also helpful, since this has similar valence electronic structure to S_2O. The deductions drawn from these intermolecular comparisons and the MO calculations

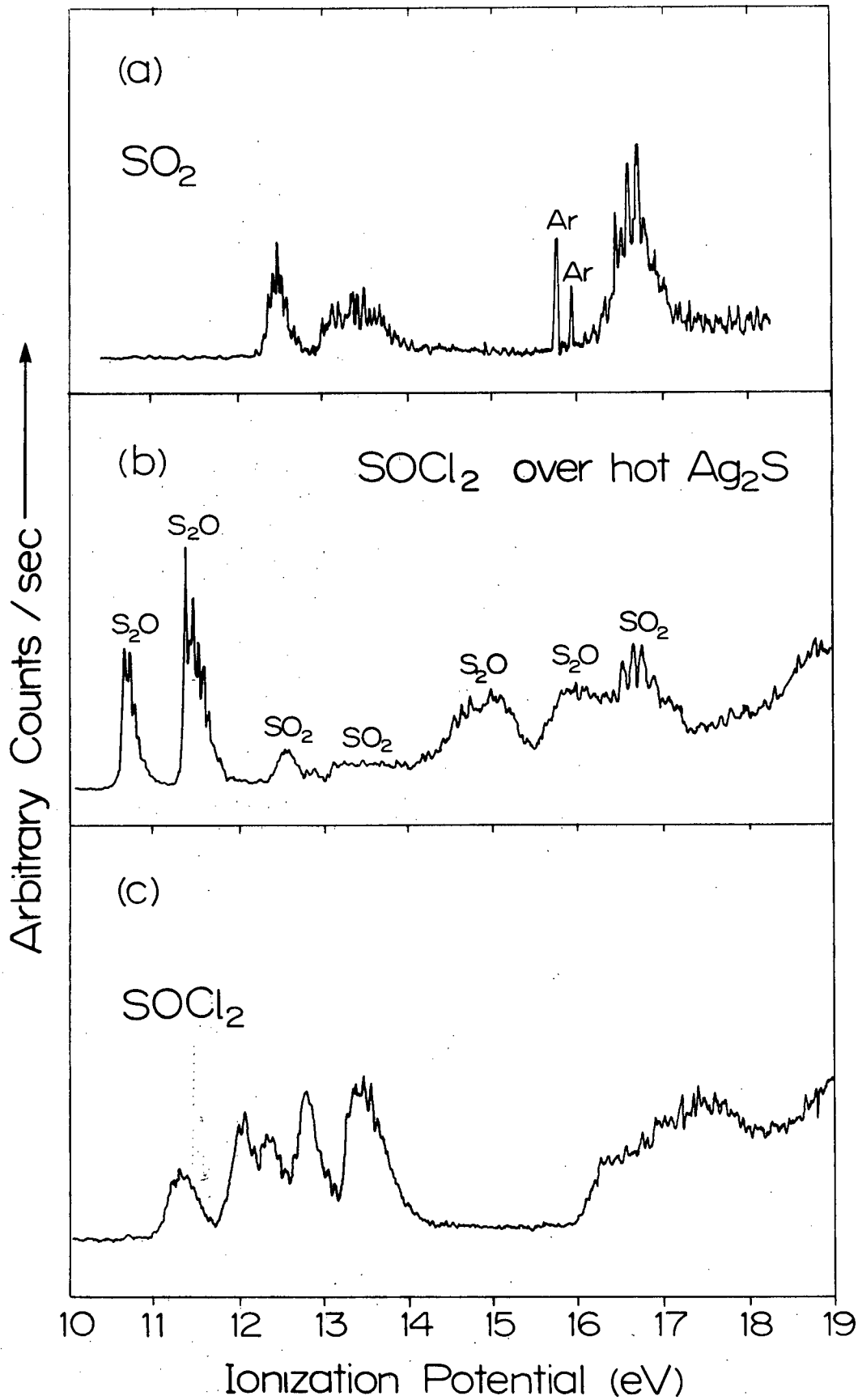
(a)
SO2
Ar
Ar
(b)
SOCl2 over hot Ag2S
S2O
S2O
SO2
SO2
S2O
S2O
SO2
(c)
SOCl2
Arbitrary Counts / sec
10
11
12
13
14
15
16
17
18
19
Ionization Potential (eV)

FIGURE 23

TABLE 5 PES and Theoretical Data for S_2O

CNDO/2		PES	
MO symmetry	IP[a] (eV)	IP[b] (eV)	ν[c] (cm^{-1})
7a'	9.68	10.53 (10.59)	480 (679)
6a'	10.36	11.25	930 (1165)
2a"	10.71	11.31 (11.42)	940 (1165)
5a'	14.11	14.3 (14.7)	----
1a"	14.13	14.9	----
4a'	15.44	15.5 (16.0)	----
3a'	18.39	18.7 (?)	----

a) IP's obtained by subtracting 4 eV from the corresponding absolute MO energy.

b) vertical IP's are in parentheses.

c) values in parentheses are the corresponding vibrational frequencies in the neutral molecule from ref. 166.

(see below) suggest six to seven accessible IP's and that the orbital configuration of S_2O is

$$KKKLL\ (1a')^2(2a')^2(3a')^2(4a')^2(1a'')^2(5a')^2(2a'')^2(6a')^2(7a')^2.$$

In addition, the calculation shows, provided Koopmans' theorem holds, for S_2O the second and third IP's are close, and the fourth and fifth IP's are degenerate within experimental accuracy. The fact that the second and third IP's of SO_2[172], NSF[168-169] and NSCl[167] are close and the fourth and fifth IP's of SO_2 are also close leads one to expect similar behavior from S_2O, and lends support to the MO calculations. In fact, the PE spectra of these compounds are remarkably similar, as exemplified in the ionization potential correlation diagram depicted in Fig. 24. Namely, the PE bands of each compound can be grouped into three regions, i.e. the first IP, the second and third IP's, and the higher IP's. Consequently, the analysis for the spectrum of S_2O appears to be fairly straightforward using this intermolecular correlation. In order to strengthen the basis of the above expectation and to obtain more information for the analysis, we turn to MO calculations. A CNDO/2 MO calculation[76] was performed on S_2O with the experimental geometry[166] and the results colected in Table 5. The deductions from the intermolecular comparisons and the MO calculations are encouragingly consistent, and thus lend support to the MO calculation. Furthermore, the success with which the earlier approximate MO calculations predicted the

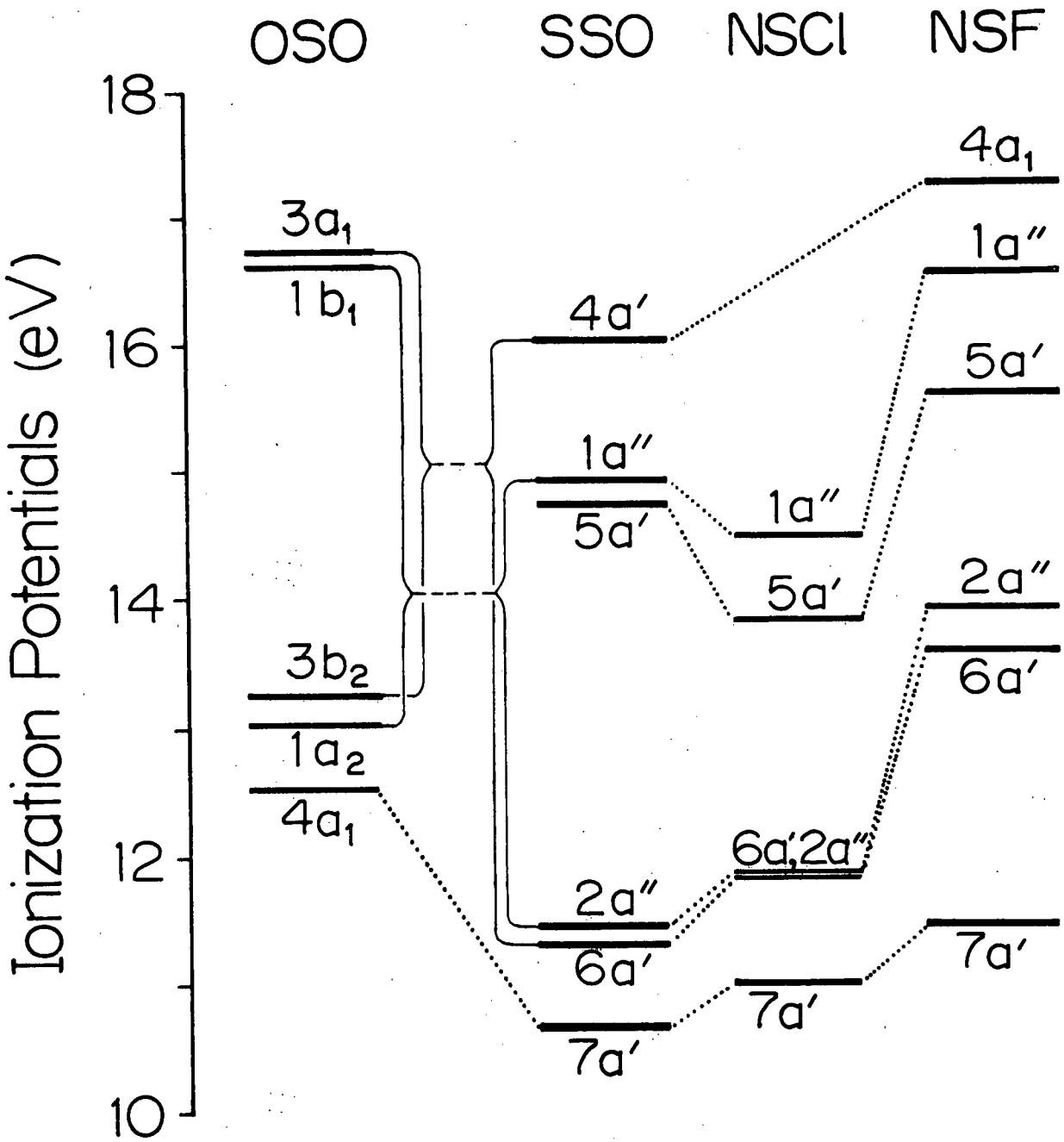
OSO
SSO
NSCI
NSF
Ionization Potentials (eV)
18
16
14
12
10
3a1
1b1
3b2
1a2
4a1
4a′
1a″
5a′
2a″
6a′
7a′
1a″
5a′
6a′,2a″
7a′
4a1
1a″
5a′
2a″
6a′
7a′

FIGURE 24

IP's of NSF[168-170], NSCl[167] and SO_2[173] makes it evident that we can affect similar success in the case of S_2O.

The first band in the PE spectrum of S_2O (Fig. 25) consists of one IP, with the adiabatic and vertical values at 10.53 and 10.59 eV respectively. This is compared to 10.3±0.1 eV, the only observed IP of S_2O, obtained from mass spectrometry[174]. The four clearly discernible vibrational components with an average spacing of 480 cm^{-1} are assigned to ν_3 which is mainly the S-S stretch. The calculation indicates the 7a' MO is S-S bonding in accord with the decrease of the vibrational frequence from 679 cm^{-1} [166] in the neutral molecule to 480 cm^{-1} in the X^2A' ionic state. The assignment of the vibration 480 cm^{-1} to the bending mode ν_2 (388 cm^{-1} [166] in the neutral molecule) is ruled out because the Walsh rules predict an increase in bond angle accompanying the removal of orbital 7a' and hence a decrease in bending frequency (as occurred in SO_2[172] and NSF[170]). However, the shape of the high energy end of the band may indicate an additional, but very weak vibrational progression of spacing ca. 200 cm^{-1}, which if real should be the ionic bending frequency.

It is difficult to decide whether one or two IP's are involved in the second PE band (Fig. 25). As discussed above, we prefer to assign two IP's to this band and propose that electrons from the MO's 6a' and 2a" respectively are removed. The corresponding IP's and vibrational frequencies are summarized in Table 5. The vibrational structure on

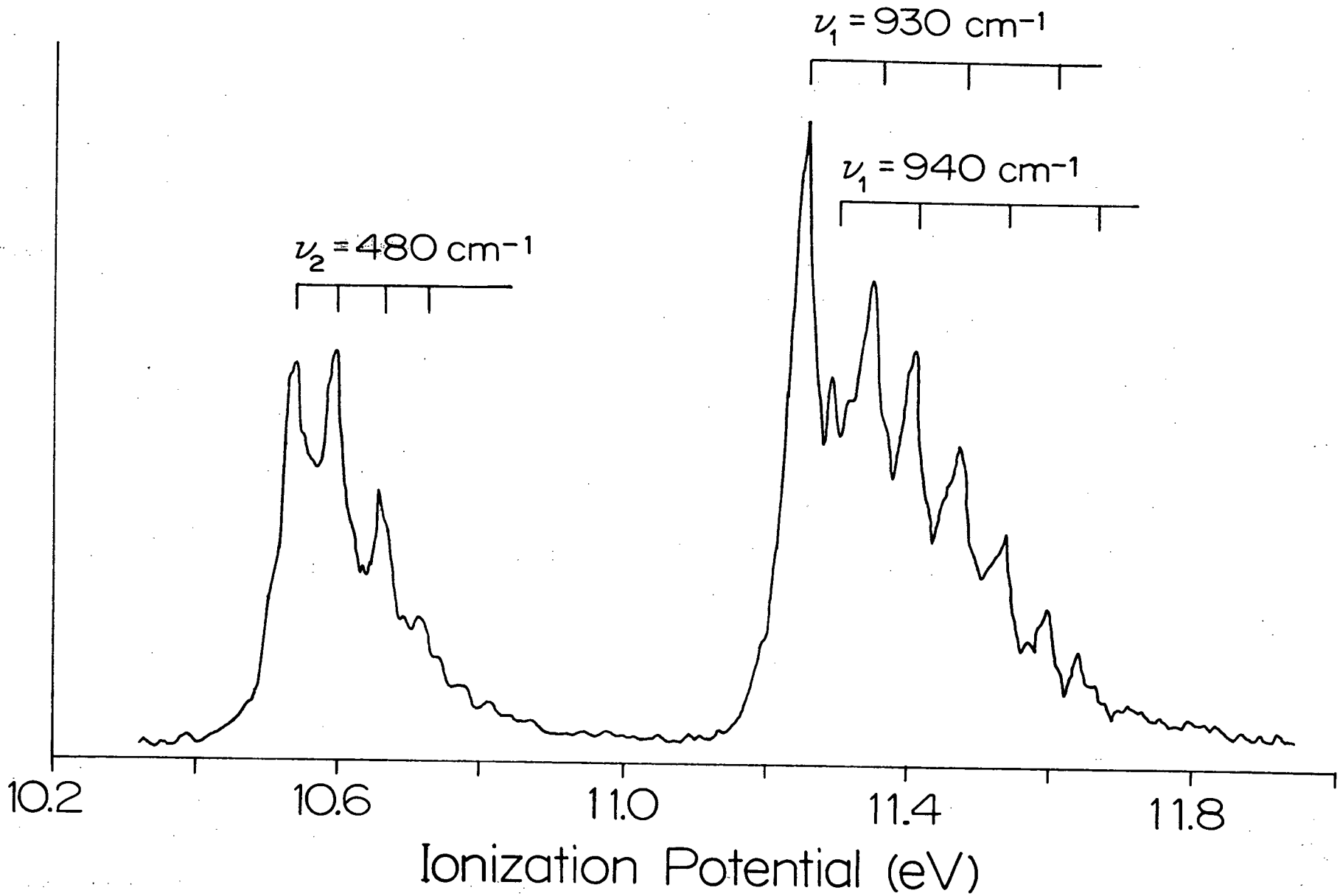
ν_1 = 930 cm^{-1}
ν_1 = 940 cm^{-1}
ν_2 = 480 cm^{-1}
10.2
10.6
11.0
11.4
11.8
Ionization Potential (eV)

FIGURE 25

both bands seems to be a simple series in ν_1, which is mainly S-O stretch, indicating a decrease in frequency in the ionic state. This is supported by the calculation, which predicts that the 6a' and 2a" orbitals are, respectively, bonding and slightly bonding between the central S and the O atoms, while they are both bonding between the S atoms.

The third and fourth bands are both broad and featureless. The former starts at 14.3 eV and has its maximum at 14.7 eV, while the corresponding values for the latter are 15.5 and 16.0 eV respectively. Hagemann[174] gave the appearance potential of SO from S_2O to be $\leq$ 14.5 ± 0.2 eV. This is consistent with the featureless character of the third band. Unequivocal assignment of these two bands is difficult. The CNDO/2 result is used for the tentative assignment, i.e. the third band arises from two IP's (MO's 5a' and 1a") and the fourth from one IP (MO 4a'). The shape of the third band (Fig. 23b) suggests a fourth IP at 14.3 eV and a fifth at 14.9 eV. This then leaves one IP (predicted by calculation) unaccounted for, which we suspect to be part of the fourth band or at ∿18.7 eV, where there is some indication of an additional band sitting on the rising background.

In the spectrum of S_2O obtained from the MW discharge of SO_2, in addition to the bands described above, we observed a clearly discernible vibrational series of three components with an averaging spacing of 920 cm^{-1}, corresponding to an

adiabatic and vertical IP at 14.95 eV. This band can be assigned unambiguously to be the third band of SO^+ because of the close agreement of IP and frequency values with those found by Jonathan et al[159] for SO^+ as well as the similar experimental conditions. Furthermore we wish to point out that the assignment of the weak band at 11.3 eV by Jonathan et al[159] to SO may not be certain. Considering that S_2O is invariably formed in the discharge of SO_2[163] and the intensity of the second band of SO[159] is seemingly incompatible with that of the other two bands, we would suggest that this is actually the second band of S_2O, which we find to have its origin at very nearly the same energy, i.e. 11.23 eV. The first band of S_2O may very well be buried underneath the first band of SO in the spectrum of Jonathan et al (see also section 4.2.3).

4.4 Diazene (HN=NH) And Diazene-d_2 (DN=ND)

4.4.1 Introduction

The short lived species HN=NH (or N_2H_2) has recently provoked a great deal of interest with regard to its chemistry[175-177] and its spectroscopic properties[178-185]. N_2H_2, as the first member of the azo series, has also attracted the attention of many theoreticians[186-189]. With this wealth of interest on the molecule, it thus seems surprising that N_2H_2 remains a spectroscopic enigma in many respects, e.g. the intensity alternation in the vacuum

ultraviolet spectrum[181], the uncertainty in the precise interpretation of near ultraviolet spectrum[184], the geometry of the excited states, and the possibility of cis/trans isomerism in the gas phase.

In view of these controversies and the potential of PES in providing information on the electronic structure of molecules, it therefore seemed appropriate to undertake a PE study of N_2H_2.

The properties of N_2H_2 which are relevant to our studies here may be summarized as follows. It is generally accepted that the molecule in its ground state assumes a trans form and is a singlet electronic state, although a triplet ground state has been suggested[181]. The molecule has a lifetime of the order of minutes in the vapor phase at low pressure, and decomposes rapidly to give N_2 and H_2 as major products.

4.4.2 Experimental

N_2H_2 was generated by two different methods.
(1) A very weak microwave discharge[177] in the equilibrium vapor of N_2H_4 (Eastman, 99% purity) at room temperature. The PE spectrum of N_2H_4 (Fig. 26a) was essentially that of previous workers[190]. Undissociated N_2H_4 and involatile products were trapped at -78°C, the only remaining species in the gas phase being N_2H_4, NH_3, N_2 and H_2 (Fig. 26b). Great trouble was experienced by other workers due to the

presence of the NH_3, which may confuse any spectroscopic measurement, and indeed partly obscures the PE spectrum of N_2H_2 (Fig. 26b). Distillation, or trapping and revolatilization of the NH_3/N_2H_2 mixture does not alleviate this problem. However, we have eliminated this problem by titrating the gas phase products with HCl after passage through the trap at -78°C.

(2) The second method involved preparation of sodium bis(trimethylsilyl)amide from hexamethyldisilazane[191,192]. This, in turn, was converted into sodium tosylhydrazide by reaction with tosylhydrazine[175]. The sodium tosylhydrazide was then pyrolyzed at 55-60°C (as recommended by Wiberg et al[175,176]) to give pure N_2H_2 plus N_2 and a little H_2 in the gas phase. However, we have found that by raising the temperature to 90-100°C and using faster differential pumping, the yield of N_2H_2 can be improved several fold with respect to N_2.

In both cases (1) and (2), the gas phase mixture of $N_2H_2/N_2/H_2$ was led directly into the ionization chamber, whcih was differentially pumped. The pressures registered at the ionization gauge were $2x10^{-5}$ and $0.3x10^{-5}$ mm Hg respectively in cases (1) and (2). Because of the much lower sample pressure in the latter, a long scanning time (∿1 hr) was necessary to record a decent spectrum. The PE spectra were identical in both cases except for a better N_2H_2/N_2 ratio in the 2nd method.

N_2D_2 was generated from N_2D_4 (Merck, Sharp and

Dohme) by method (1) above. ND_3 was eliminated by gas phase titration with DCl.

In the discharge method outlined above the efficiency of the discharge in selectively producing N_2H_2/N_2D_2 could be monitored by trapping all the products at -196°C, and observing the yellow color of the diazene. In this respect, we have confirmation of the production of the desired species, the alternative preparative method for N_2H_2 providing us with further evidence for correct identification.

The spectra were calibrated using the IP's of the N_2, H_2/D_2 or HCl/DCl, with an accuracy of ± 0.01 eV for the IP's of sharp peaks and ± 30 cm^{-1} for the vibrational spacings. Resolution in all cases was better than 30 meV.

4.4.3 Results

Fig. 26 depicts the spectra of N_2H_4 without (a) and with (b) the discharge, and, in addition, illustrates the effect of adding increasing amounts of HCl to the discharge products (c, d and e). Fig. 27 and 28 illustrate the analogous procedure for the deuterated system, except here the effect of DCl was monitored using only the first bands of ND_3 and N_2D_2 in Fig. 28. In both cases, it has been found that the gas phase reactions of HCl(DCl) with $NH_3(ND_3)$ is instantaneous, giving a white deposit of $NH_4Cl(ND_4Cl)$ on the walls, whereas the reaction of HCl(DCl) with $N_2H_2(N_2D_2)$ is very slow. We have done further experiments on the reaction of HCl with pure N_2H_2, generated by the 2nd method, and have

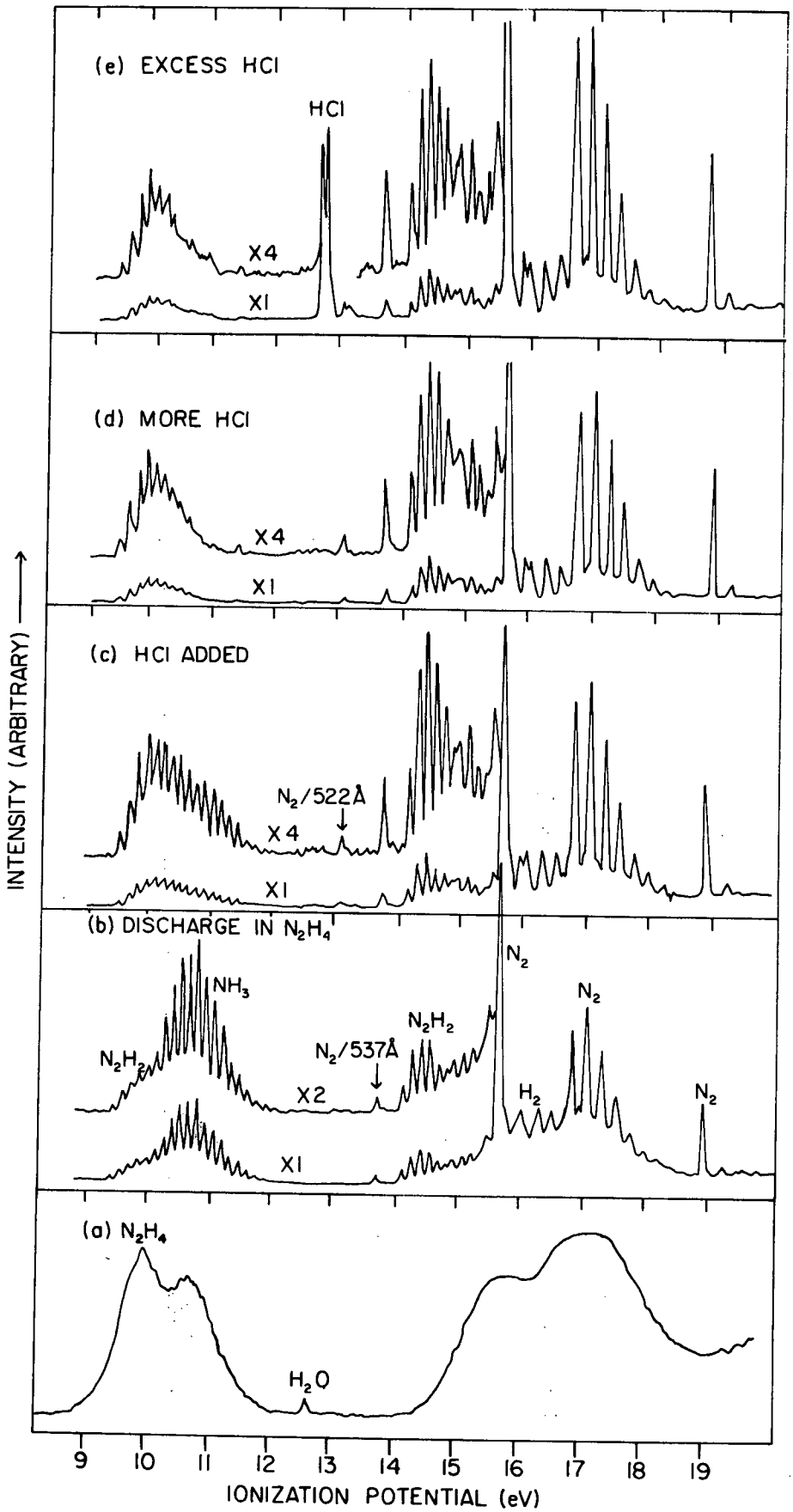
(e) EXCESS HCl
HCl
X4
X1
(d) MORE HCl
X4
X1
(c) HCl ADDED
N2/522Å
X4
X1
(b) DISCHARGE IN N2H4
NH3
N2H2
N2/537Å
X2
N2H2
N2
H2
N2
N2
X1
(a) N2H4
H2O
INTENSITY (ARBITRARY)
9
10
11
12
13
14
15
16
17
18
19
IONIZATION POTENTIAL (eV)

FIGURE 26

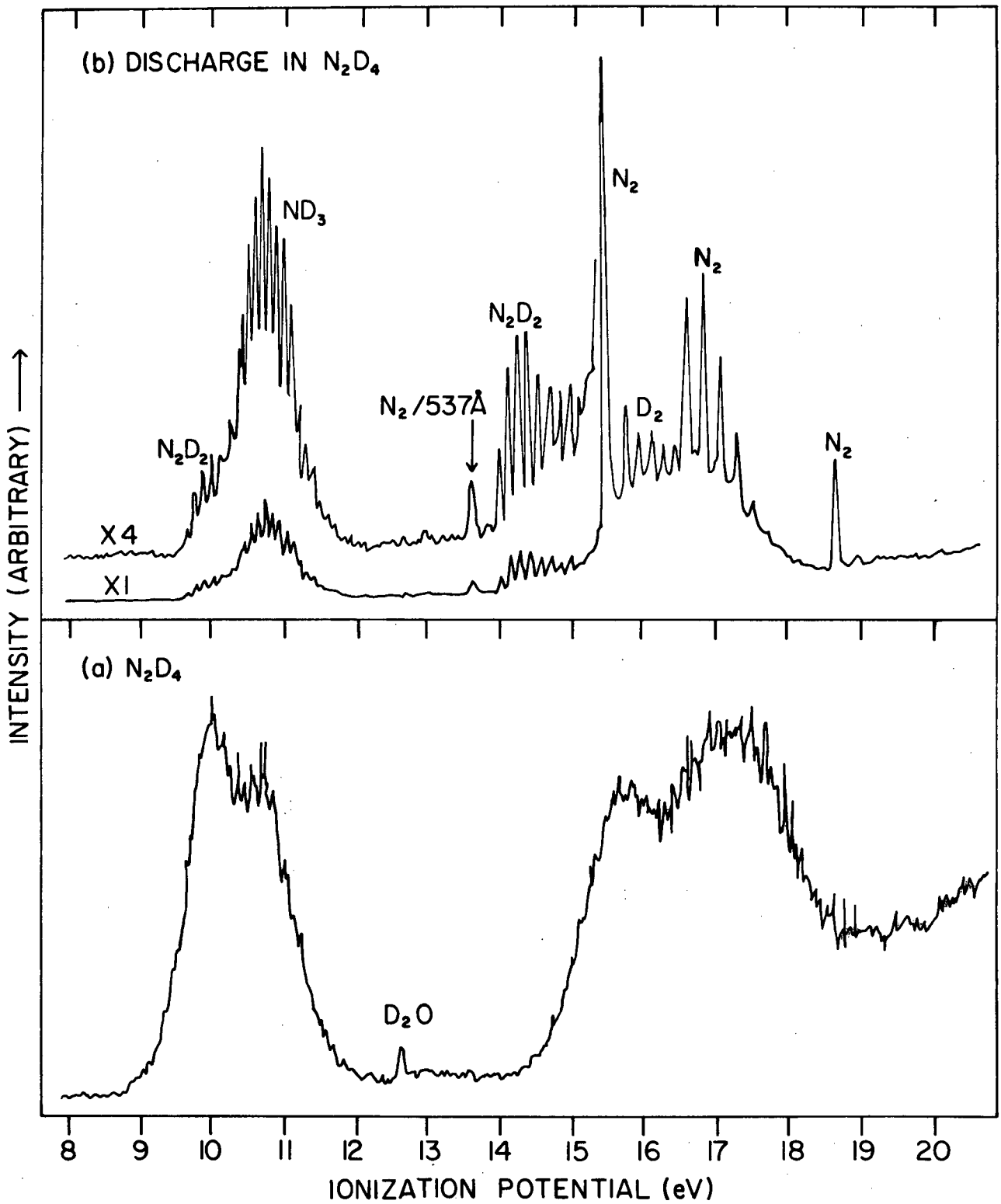
(b) DISCHARGE IN N_2D_4
ND_3
N_2
N_2
N_2D_2
$N_2/537Å$
D_2
N_2D_2
N_2
X4
X1
(a) N_2D_4
D_2O
INTENSITY (ARBITRARY) ⟶
8
9
10
11
12
13
14
15
16
17
18
19
20
IONIZATION POTENTIAL (eV)

FIGURE 27

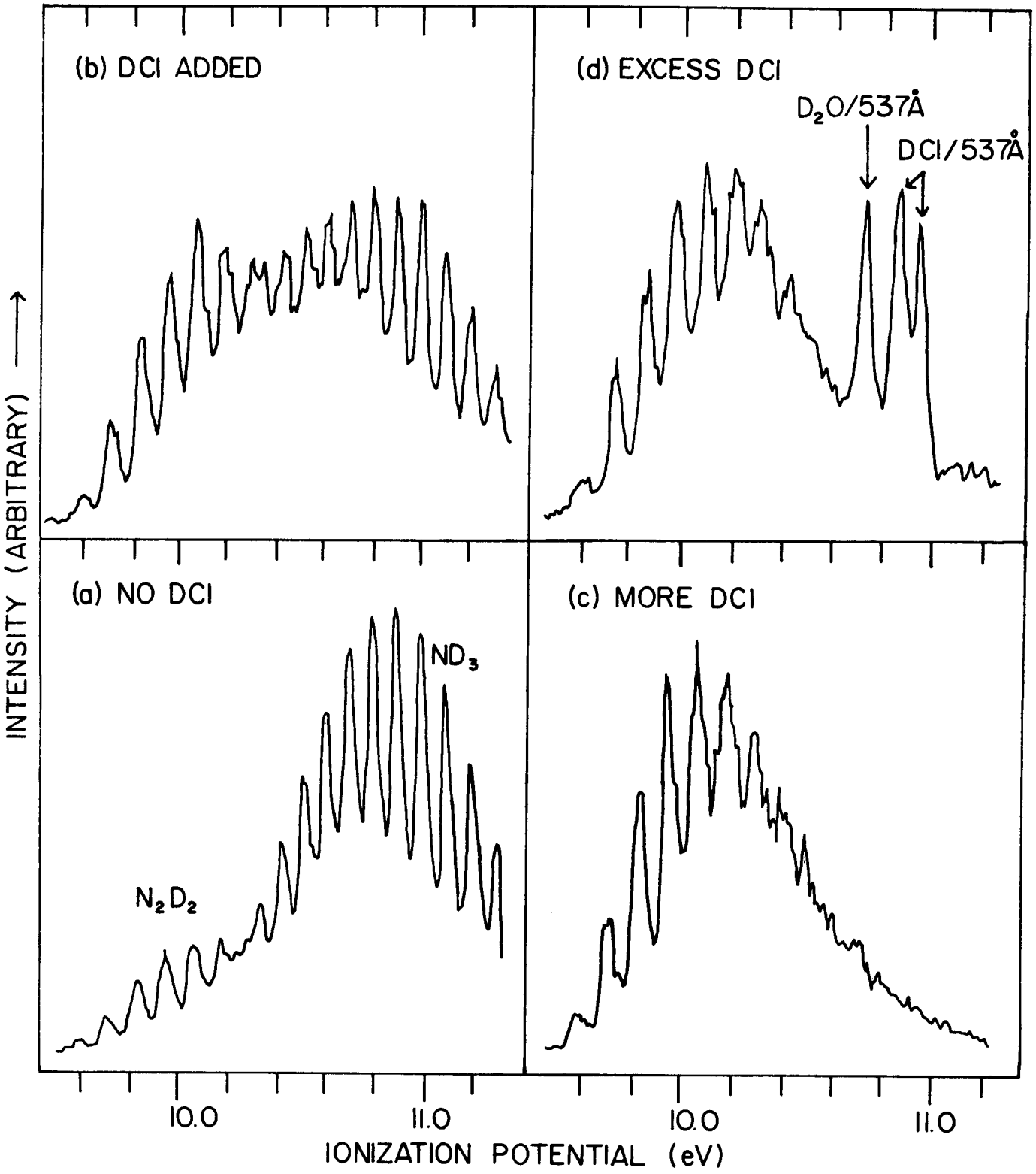
(b) DCl ADDED
(d) EXCESS DCl
D_2O/537Å
DCl/537Å
(a) NO DCl
ND_3
N_2D_2
(c) MORE DCl
INTENSITY (ARBITRARY)
10.0
11.0
10.0
11.0
IONIZATION POTENTIAL (eV)

FIGURE 28

observed the same behavior. By using the right amount of HCl(DCl), the resulting spectrum of $N_2H_2(N_2D_2)$ may then be obtained free from $NH_3(ND_3)$ interference (Fig. 26d and Fig. 28c), and, in some cases, contains additional bands due to HCl(DCl) (Fig. 26e and 28d), which prove useful for calibration purposes.

The experimentally determined IP's and vibrational frequencies are collected in Table 6, where the vibrational frequencies of the ground state molecules are also listed for comparison. The NH_3-free spectrum of N_2H_2 obtained by the second method, which because of its favorable N_2H_2/N_2 ratio gives a better presentation of the N_2H_2 bands, is shown in Fig. 29.

<u>HN=NH</u> The PE spectrum of N_2H_2 (Fig. 29) exhibits four distinguishable bands, with extensive vibrational structure on all of them. The first band (Fig. 30) has an adiabatic IP of 9.59 eV, and a vertical IP of 10.02 eV. This compares favorably with the only previously determined value of 9.85 ± 0.1 eV from mass spectrometry[178]. The band envelope extends over ca. 1.3 eV, with at least 12 components, the vertical transition occurring at v' = 3. The vibrational interval between the 0 and 1 vibrational quanta is 1180 cm^{-1} however, this tends to decrease towards high vibrational quanta, the value averaged over 0 to 9 being 1050 cm^{-1}. There is also the suggestion of another series, possibly starting at ∿1800 cm^{-1} above the v' = 0 peak between the v' = 1 and 2 vibrational components of the primary series. Here the vibrational spacing between members is a constant 1180 cm^{-1}.

TABLE 6 PES Data for HN=NH and DN=ND

Ionic state	N_2H_2 Vertical IP (adiabatic) (eV)	$\nu(cm^{-1})$ Ion	$\nu(cm^{-1})$ Molecule*	N_2D_2 Vertical IP (adiabatic) (eV)	$\nu(cm^{-1})$ Ion	$\nu(cm^{-1})$ Molecule*
X^2A_g	10.02 (9.59)	1180	1583	10.10 (9.61)	1020	1215
A^2A_u	14.39 (14.10)	1110	1529	14.39 (14.11)	1110	1539
B^2B_u	15.03 (14.71)	1170	1583	15.17 (14.69)	960	1215
C^2A_g	16.9 (16.19)	940	1529	----	----	----

* from ref. 182.

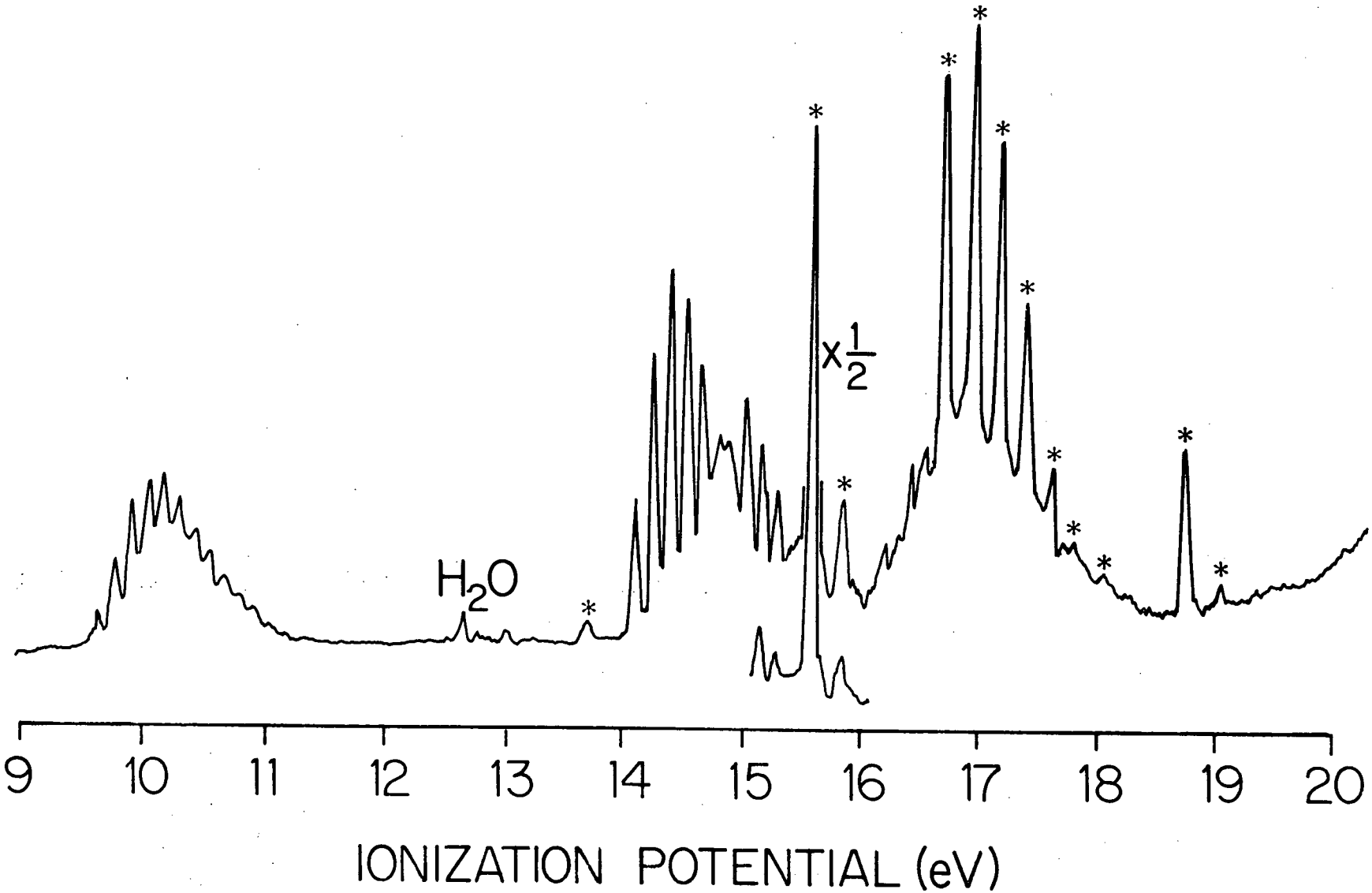
H_2O
$\times\frac{1}{2}$
9
10
11
12
13
14
15
16
17
18
19
20
IONIZATION POTENTIAL (eV)

FIGURE 29

Towards higher vibrational quantum numbers the two series appear to merge, making precise measurements difficult.

The second band (Fig. 30) has an adiabatic IP of 14.10 eV, and a vertical IP of 14.39 eV. Here the band envelope contains at least 7 members spreading over about 0.8 eV, with a fairly even vibrational spacing of 1110 cm^{-1}. The vertical transition occurs at v' = 2.

The third band (Fig. 30) is overlapped by the second band, but the adiabatic and vertical IP's can be confidently assigned at 14.71 eV and 15.03 eV, respectively. Here the band shows at least five discernible peaks with the vertical transition occuring at v' = 2.

The first five vibrational components of the fourth band are clearly distinguishable, but the higher energy side of the band is concealed by the intense second band of H_2(Fig. 30). Judging from the intensity under the latter, we expect the progression of the fourth band to be quite extensive, spreading over about 1.5 eV, and estimate the vertical IP at 16.9 eV. The adiabatic IP can be accurately assigned at 16.19 eV and the average vibrational spacing over the first five components is 940 cm^{-1}.

<u>DN=ND</u> The PE spectrum of N_2D_2 (Fig. 27) is in many respects similar to that of N_2H_2. Subtle differences induced by deuteration, however, enable us to be more confident about our assignments (see below).

The first band (Fig. 31) has an adiabatic IP of

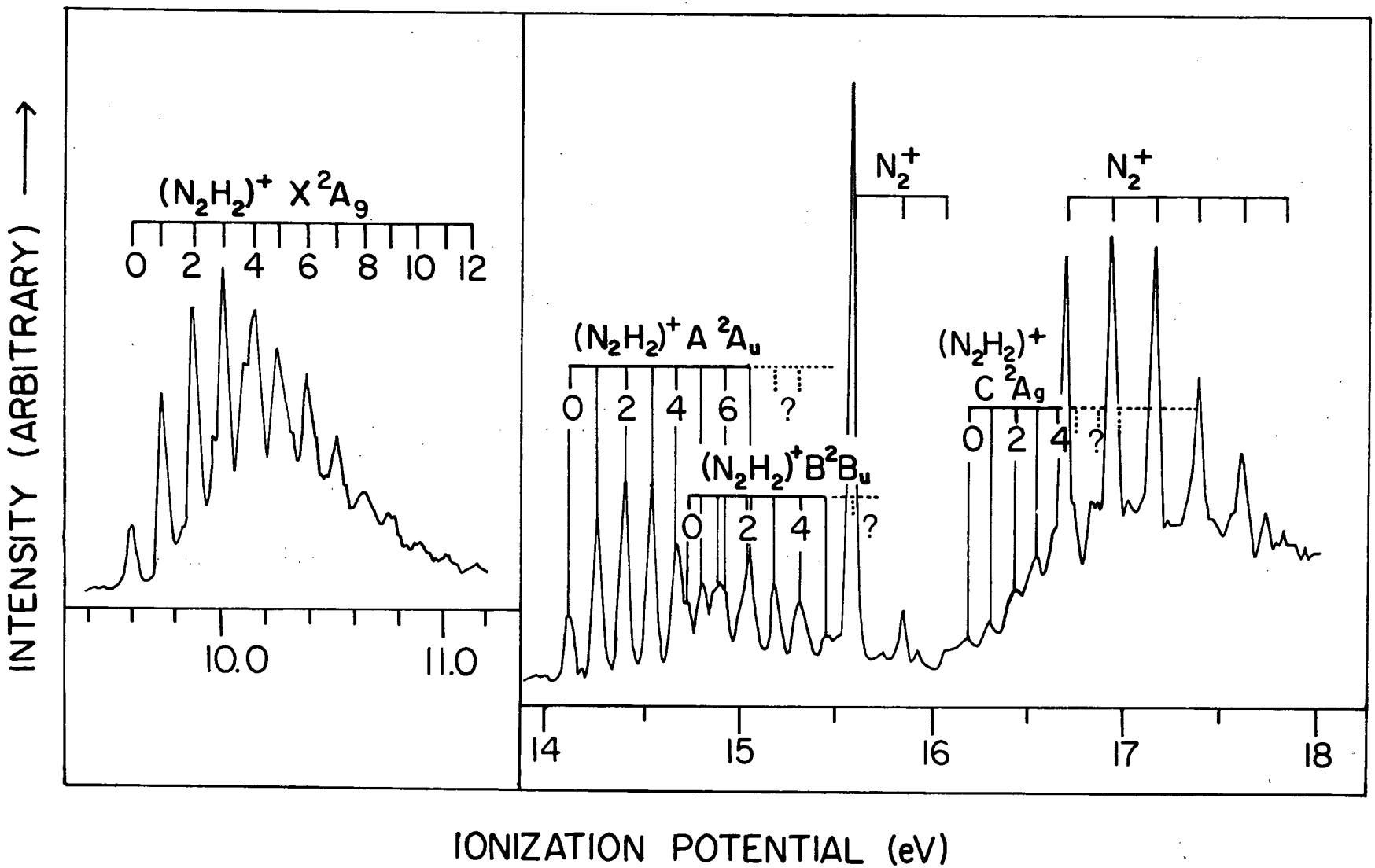
INTENSITY (ARBITRARY)
$(N_2H_2)^+ X^2A_g$
0 2 4 6 8 10 12
10.0
11.0
$(N_2H_2)^+ A^2A_u$
0 2 4 6 ?
$(N_2H_2)^+ B^2B_u$
0 2 4 ?
N_2^+
$(N_2H_2)^+$
C^2A_g
0 2 4 ?
N_2^+
14
15
16
17
18
IONIZATION POTENTIAL (eV)

FIGURE 30

9.61 eV, and a vertical IP of 10.10 eV. In this case, the vertical transition occurs at v' = 4, with the 0-0 transition having a much lower probability. The first vibrational spacing is 1020 cm^{-1}, this decreasing to an average of 980 cm^{-1} over the first 4 intervals, and to 880 cm^{-1} over the first 9 intervals. Again there is the suggestion of another vibrational series, but in view of the experimental difficulties, and narrower vibrational spacing it is impossible to be specific.

The second band (Fig. 31) has an adiabatic IP of 14.11 eV and a vertical IP of 14.39 eV. This occurs at v' = 2, the band envelope spreading over 8 distinguishable components. The vibrational spacing is fairly constant at 1110 cm^{-1}, and so in all respects it is identical to the second band of N_2H_2.

The third band (Fig. 31) again overlaps with the second band, but we are confident in assigning the adiabatic IP to 14.69 eV. (The agreement with the analogous value of N_2H_2 tends to support the correct assignment of the adiabatic transition). The vertical transition poses more of a problem, due to overlapping with the 537Å shadow of the second band of N_2. However, the general shape of the FC envelope, which extends over at least five vibrational components, suggests the vertical transition to occur around v' = 3 $\pm$ 1, i.e. at 15.17±0.12 eV. This assignment is consistent with the corresponding vertical IP of N_2H_2, (which

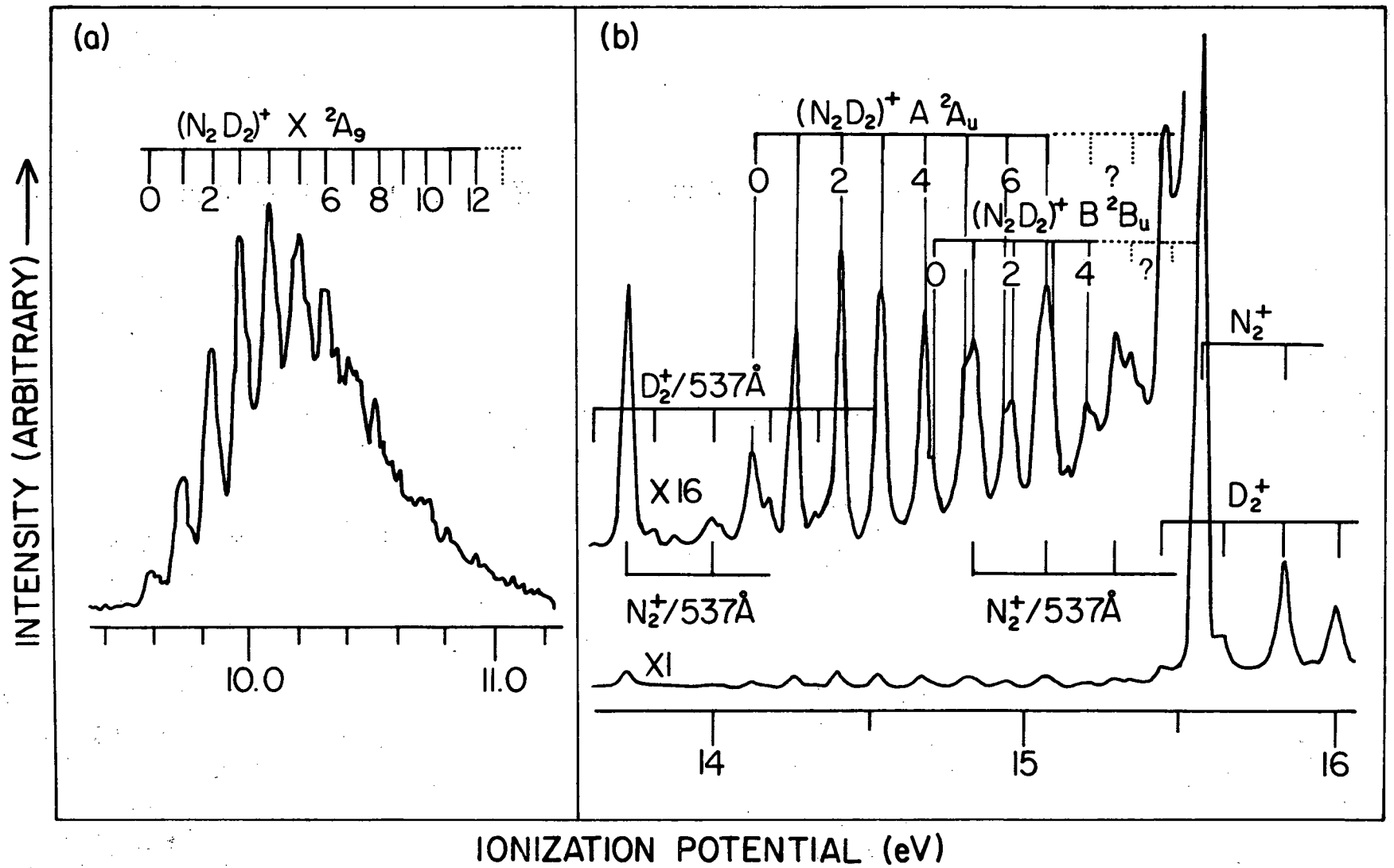
(a)
(b)
$(N_2D_2)^+$ X ^2A_g
0 2 6 8 10 12
10.0
11.0
$(N_2D_2)^+$ A ^2A_u
0 2 4 6 ?
$(N_2D_2)^+$ B ^2B_u
0 2 4 ?
$D_2^+/537Å$
X16
$N_2^+/537Å$
$N_2^+/537Å$
X1
N_2^+
D_2^+
14
15
16
INTENSITY (ARBITRARY)
IONIZATION POTENTIAL (eV)

FIGURE 31

occurs at v' = 2) since the vibrational spacing for N_2D_2, which averages 960 cm^{-1} (over the first 4 intervals), is 210 cm^{-1} smaller than that for N_2H_2, and thus a more extensive vibrational progression is expected for N_2D_2.

The fourth band is completely concealed by D_2^+ and the second band of N_2 (Fig. 27b), and thus cannot be observed.

4.4.4 Discussion

The assignments for the PE spectra are assisted by the analysis of the vibrational structure, the effect of deuteration, comparison with other azo compounds and with MO calculations.

By comparison with other azo compounds[193-195], the first band can be assigned to the $n_+(a_g)$ orbital (N_2H_2 assumes C_{2h} symmetry), i.e. the symmetric combination of N lone pairs. This assignment is corroborated by the vibrational structure which starts at 1180 cm^{-1} (for N_2H_2) and which steadily decreases to ca. 980 cm^{-1} around the 10th vibrational quantum number. For the neutral molecule ν_2 (δNNH) is 1583 cm^{-1}[182], and if this is the mode excited we observe a decrease of at least 400 cm^{-1}. This is to be anticipated if there is a large opening of the NNH angle, which is expected if an electron from the n_+ orbital is removed. The PE spectrum of the deuterated species confirms this assignment since here the vibrational structure on the first band decreases from 1020 cm^{-1} to ca. 800 cm^{-1} (at the 9th

vibrational quantum number). This compares with the value of 1215 cm^{-1} for ν_2 in the neutral molecule N_2D_2. The first components of both N_2H_2 and N_2D_2 are within the limits of the zero point energy giving us confidence regarding the value of the adiabatic IP.

The other vibrational structure with an average spacing of ca. 1800 cm^{-1}, which if genuine, may be assigned to the symmetric N-N stretch (ν_3), which is 1529 cm^{-1} in the neutral molecule.

The relative ordering of the bands corresponding to the $n_-(b_u)$ orbital, i.e. the antisymmetric combination of the N lone pairs, and the N-N π (a_u) orbital cannot be unequivocally assigned on the basis of the vibrational structure in N_2H_2 alone. Thus, both the second and third bands have vibrational structure in the range 1100 to 1200 cm^{-1}, and in the neutral molecule ν_2 and ν_3 are 1583 and 1529 cm^{-1} respectively. However, upon deuteration the vibrational structure on the second band remains exactly the same (1110 cm^{-1}), whereas that on the third band drops to 960 cm^{-1}. Thus we can confidently assign the second band to the π ionization and the third band to the n_- orbital.

The fourth band can be assigned to the strongly bonding N-N σ (a_g) orbital. This assignment is in line with the large decrease, i.e. ca. 600 cm^{-1}, in the ν_3 (N-N stretch) frequency of the ion.

The above assignments for the bands and vibrational structure are wholly supported by ab initio calculations[62,186-189].

In addition, these calculations consistently predicted that only four IP's are below 21.22 eV, thus suggesting that the HeI PE spectrum of N_2H_2 presented here is complete.

As the prototype of the azo compounds, N_2H_2 has by far the largest n_+-n_- separation (ΔE=5.1 eV) yet observed for adjacent nitrogen atoms. To date the largest observed value is to be found in 3,3 dimethyl diazirine[195] (ΔE=3.55 eV). The large splitting in N_2H_2 may be attributed to the dual facts that for this molecule the nitrogen 'lone' pairs have the largest contribution in n_+ and n_- orbitals. This, coupled with the 180° dihedral angle gives maximum overlap and thus interaction for the N lone pairs.

It is of interest to compare the PE spectrum of difluorodiazene, N_2F_2[62], with that of N_2H_2. Due to the uncertainty in the higher IP's, only the n_+ and π levels in N_2F_2 have been assigned, and are at 13.4 and 14.1 eV respectively. These compare with the n_+ and π ionizations of N_2H_2 at 10.0 and 14.4 eV respectively, indicating a positive perfluoro shift of 3.4 eV on the n_+ ionization and a negative perfluoro shift of 0.3 eV on the π level. Such a large positive shift for the n_+ level is indicative of the large contribution of the F atoms to this orbital in N_2F_2, and parallels the value of +3.6 eV obtained from the calculation[62]. The negative value for the π ionization is unusual, the only other negative value for such an ionization being observed on the C_2H_2 and C_2F_2 system (-0.14 eV)[62]. It is most

probable that this effect arises from a stabilization of the ionic state by delocalization over the F atoms. The overall result is thus in accord with the conclusions of the perfluoro effect, i.e. that the π ionization shift is small in comparison to the σ ionization shift. The Franck-Condon envelopes for the π ionization in N_2F_2 and N_2H_2 are similar, again illustrating the relatively small effect of the F atoms on the π ionization.

In comparing the vacuum ultraviolet (1700Å) absorption bands[181] of N_2H_2 and N_2D_2 with their respective first PE bands , we notice a number of similarities, which tend to suggest that the absorption band is probably a Rydberg transition leading to the first IP of the molecule. First, both the absorption and PE bands show an extensive progression in ν_2 (δNNH). Significantly, the vibrational frequencies are quite similar in the two cases, being 1192 and 1180 cm^{-1} (0-1 spacing) for the absorption and PE bands of N_2H_2, and 955 and 1020 cm^{-1} for the corresponding deuterated cases. Secondly, the single quantum excitation in N-N stretching mode in the absorption band also appears in the PE band and has similar frequencies, i.e. 1874 cm^{-1} and $\sim$1800 cm^{-1} for the absorption and ionization respectively. Thirdly, the FC envelopes of the two bands are similar. Although the vertical transitions in the absorption bands[181] of N_2H_2 and N_2D_2 appear to occur one quantum number lower than that in their respective PE bands, this difference

may not be certain in view of the overlap of the absorption band by the strong bands of NH_3, which inevitably causes difficulty in assigning the vertical transition. Furthermore, using the experimental FCF, we have estimated (section 2.2.3.c) an increase of 20° in the N-N-H angle, which, quite significantly, is also the angle increase estimated for the excited state[181]. Treating the absorption band as a Rydberg transition and using the experimentally determined IP value, the quantum defect is calculated to be 0.62 for the Rydberg state with a principal quantum number N=3. This value for the quantum defect is in the expected region[196] for N 3P Rydberg orbitals, and thus tends to support our assertion.

Recently, the near ultraviolet absorption spectra (3000-4300 Å, $\pi^* \leftarrow n_+$ transition) of the N_2H_2 and N_2D_2 have been studied in great detail by Back et al[185]. However, they could not rule out the possibility that a small fraction of the cis isomer, with an extinction coefficient 10 or 20 times that of the trans isomer, is responsible for the spectra. In the light of our results, it is of interest to investigate this possibility further. Both the absorption and the first ionization involve the highest occupied n_+ orbital, and consist of an extensive vibrational progression in ν_2. We note in particular, however, that the FC envelope is more extensive in the absorption case, in that for N_2H_2 the vertical transition in absorption occurs at v'=6 compared to v'=3 in ionization, and for N_2D_2 they are respectively at v'=8 and 4.

Moreover, the increase in the N-N-H angle is estimated to be 25°[185] in the excited state whereas it is only 20° in the ground ionic state. These trends in vibrational progression and angle increase appear to be in conflict with our expectation, since the opposite is to be anticipated in view of the larger perturbation caused by the ionization process, and the π^* orbital (involved in the absorption) has hardly any influence on the N-N-H angle. Therefore, on this basis we would not rule out the possibility of the cis isomer playing a role in the absorption spectrum.

From the PE spectra, it seems pertinent to make a comment regarding the possibility of the ground state of diazene being a triplet as suggested by Trombetti[181] based upon the analysis of the rotational structure in the 1700 Å absorption band. The simplicity of the PE spectrum of diazene and the fact that the spectrum can be convincingly assigned on the basis of a singlet ground state strongly argues against a triplet ground state.

4.5 Trans-methyldiazene ($CH_3N{=}NH$)

The monomethyl substituted derivative of N_2H_2, CH_3NNH, has also attracted a great deal of attention recently[198-204]. Despite its relative stability compared to N_2H_2, the study and understanding of CH_3NNH is far less complete than that of the former. In the following, preliminary results on the PE spectrum of this species are presented.

CH_3NNH was prepared in a weak microwave discharge in the equilibrium vapor of methylhydrazine at room temperature. Undischarged methylhydrazine and involatile products were trapped at -78°C leaving only $CH_3NNH/NH_3/N_2/CH_4$ in the gas phase. Elimination of NH_3 was achieved by trapping these gas phase products at -196°C, and holding the products at -126°C (methylcyclohexane slush bath). Pumping the products through the ionization chamber, we observed the spectra of NH_3 and CH_4, and traces of C_2H_6, until finally the spectrum of CH_3NNH was observed, free of any other species.

The efficiency of the discharge in selectively producing CH_3NNH was monitored by observing the yellow color[200] of CH_3NNH in the -196°C trap. In this respect, we also have confirmation of the production of the desired species. The resemblance of the PE spectrum of CH_3NNH (Fig. 32a) with that of CH_3NNCH_3 (Fig. 32b) and N_2H_2 (Fig. 29, neglecting the vibrational fine structure of the individual bands) provides further evidence for the correct spectrum. The identification of the spectrum is, moreover, substantiated by the observation of N_2 bands in the subsequent spectrum of CH_3NNH (Fig. 32a), which can only result from the decomposition of this species. An additional proof of its positive identification by preparing the species from an alternative route[200] is presently in progress.

The PE spectrum of CH_3NNH (Fig. 32a) consists of five distinct, featureless bands. The absence of vibrational structure on any of them is understandable in view of the low symmetry (C_s) of the molecule. The intensity and the

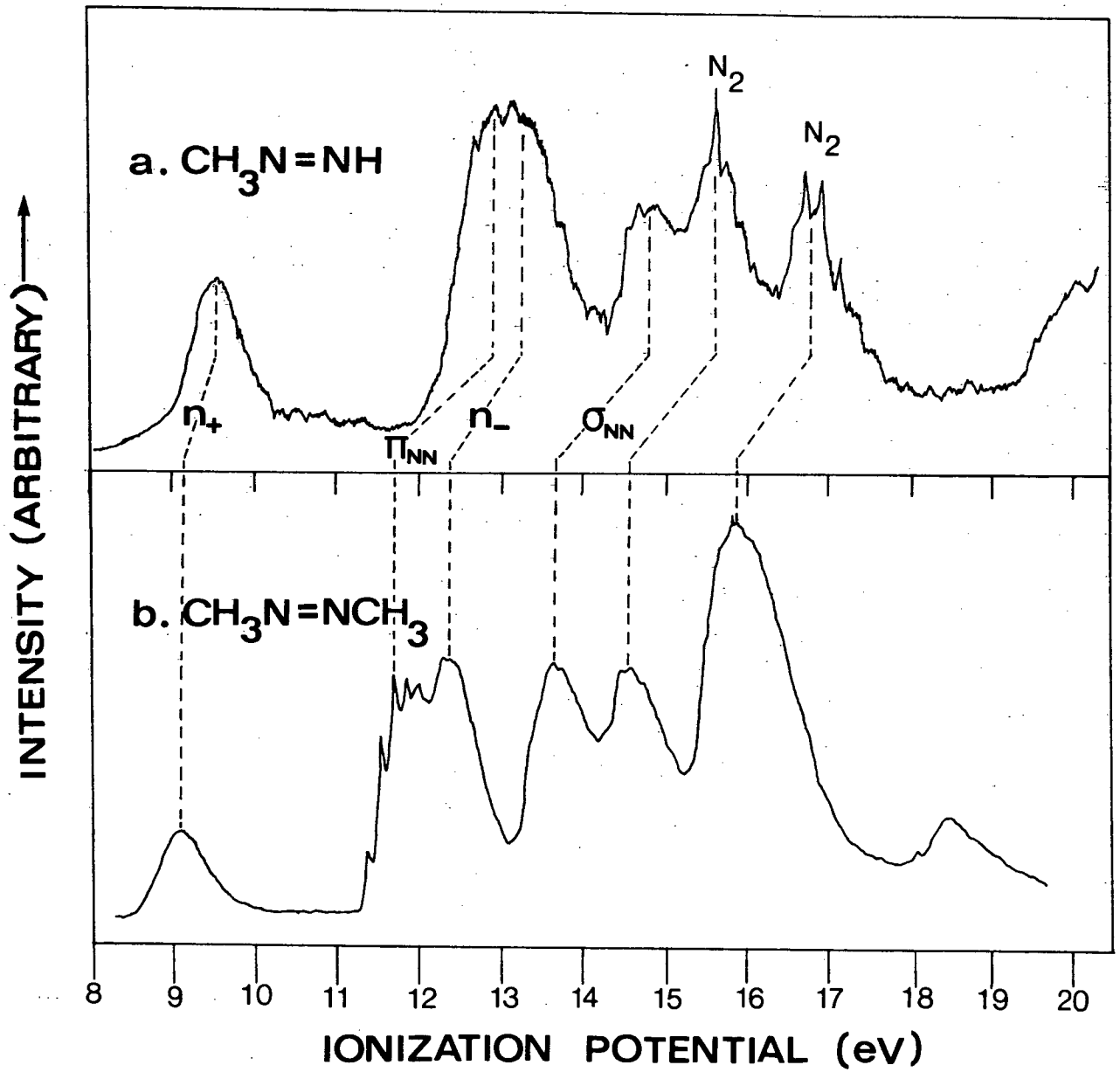
a. $CH_3N=NH$
b. $CH_3N=NCH_3$
N_2
N_2
n_+
π_{NN}
n_-
σ_{NN}
INTENSITY (ARBITRARY)
8
9
10
11
12
13
14
15
16
17
18
19
20
IONIZATION POTENTIAL (eV)

FIGURE 32

shape of the second band strongly suggest that it consists of two overlapping IP's, which is further supported by comparison with the spectra of N_2H_2 and CH_3NNCH_3 (see below). The experimental results are gathered in Table 7.

The assignment of the spectrum of CH_3NNH is fairly straightforward by comparison with the closely related molecules N_2H_2 and CH_3NNCH_3. Consideration of the effect of introducing a CH_3 group into N_2H_2 leads us to expect that the individual bands of CH_3NNH would be shifted to lower IP value compared to the corresponding bands of N_2H_2. This trend is expected to continue on going from CH_3NNH to CH_3NNCH_3. This is, indeed, what is observed (see Fig. 32 and Fig. 29), if the 2nd band of CH_3NNH is due to two IP's. Therefore, the same relative ordering n_+, π_{N-N}, n_- and σ_{N-N} can be assigned to CH_3NNH as in the case of N_2H_2 (section 4.4.4) and CH_3NNCH_3[195,196]. The two highest IP's are tentatively assigned on the basis of CNDO/2 and INDO calculations (Table 7).

TABLE 7 PES and Theoretical Ionization Potentials (in eV) of CH_3NNH

Ionic state	PES Vertical IP (adiabatic)		Theoretical Orbital	CNDO/$_2$*	INDO*
$^2A'$	9.57	(8.8)	7a'(n_+)	9.3	7.5
$^2A''$	12.9	(12.05)	2a"(π_{N-N})	11.4	11.3
$^2A'$	13.4		6a'(n_-)	16.3	14.8
$^2A'$	14.74	(14.4)	5a'(σ_{N-N})	12.9	12.5
$^2A''$	15.58	(15.2)	1a"(π_{C-H})	18.2	18.0
$^2A'$	16.72	(16.3)	4a'	20.3	19.3

* with 4 eV adjustment.

CHAPTER FIVE

PHOTOELECTRON SPECTROSCOPY OF SOME REACTIVE MOLECULES

5.1 Methiophosphide (HCP)

5.1.1 Introduction

The phosphorous analog of hydrogen cyanide (HCN), methiophosphide (HCP), is an unusual and interesting molecule in that it is the only isolated compound with a phosphorous atom bonded to only one neighboring atom, presumably through a carbon-to-phosphorous triple bond. Because of this unusual feature and its similarity to HCN, a photoelectron spectroscopic study of HCP was carried out. In addition, the results threw light on the as yet unresolved first PE band of HCN[205].

5.1.2 Experimental

HCP was first prepared in 1961 by Gier[206] and our method of synthesis followed his, in which phosphine was passed through a low intensity (70-80 amperes, 20 volts)

Carbon Arc Reactor

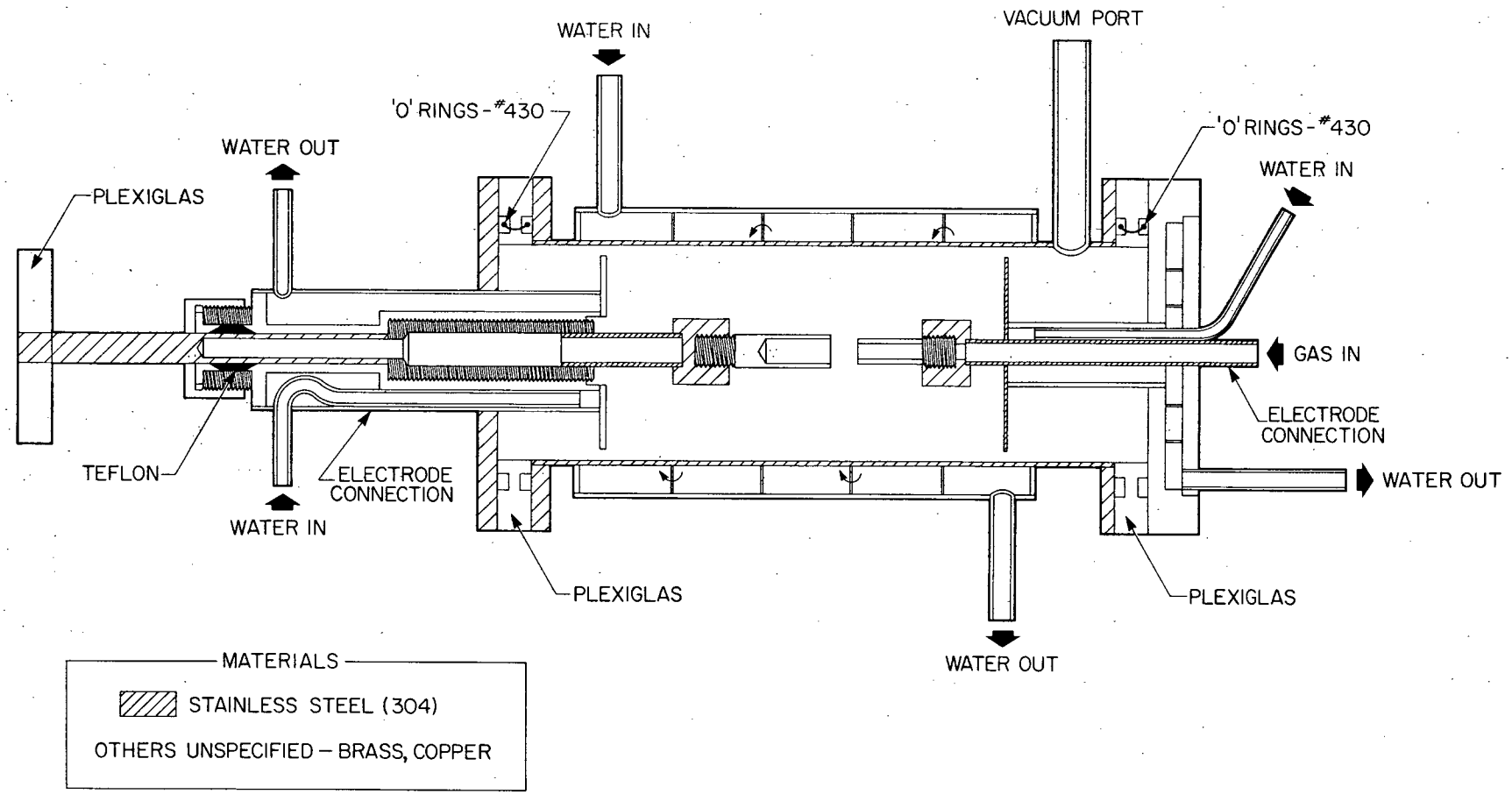

FIGURE 33

rotating arc struck between a pair of specially constructed carbon electrodes (Fig. 33). About four parts of acetylene to one of HCP[206] were formed in the reaction, but because of the very reactive[206] and unstable (stable for a few hours at room temperature[207]) character of HCP, no attempt was made to separate the two compounds.

The PE spectrum of HCP was recorded immediately after its synthesis and calibrated against the known ionization potentials (IP's) of xenon and acetylene. The sample was kept at -160°C (isopentene slush bath) in the Kel-F container (section 3.3.4.b) and the pressure was further controlled by the Kel-F valve.

5.1.3 Results And Discussion

Despite the presence of acetylene and traces of phosphine and ethylene it was possible to determine the first two of the three expected IP's of HCP under high resolution (Fig. 34). The third IP evaded detection, presumably because of its weak cross section as is the case for the corresponding IP of HCN, and we suspect it may very well be buried underneath the 2nd or 3rd bands from acetylene. The experimental results summarized in Table 8 compare favorably with a recent extensive ab initio MO calculation on HCP[208]. This agreement together with the experimental observation of the vibrational fine structure in each

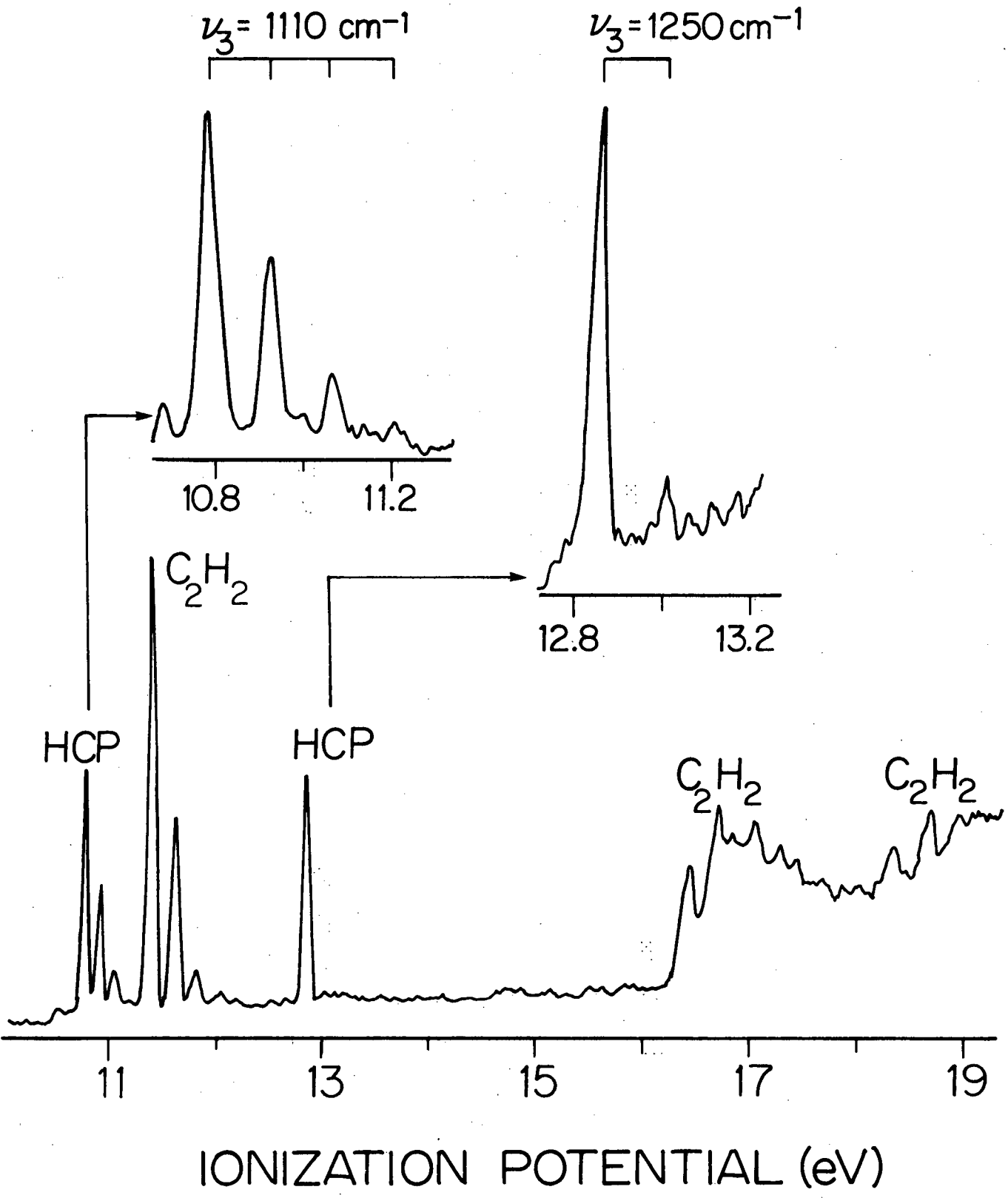
ν_3 = 1110 cm^{-1}
ν_3 = 1250 cm^{-1}
10.8
11.2
12.8
13.2
C_2H_2
HCP
HCP
C_2H_2
C_2H_2
11
13
15
17
19
IONIZATION POTENTIAL (eV)

FIGURE 34

TABLE 8 PES and Theoretical Data of HCP

Orbital assignment* and characteristics	Ionization potentials (eV)		Vibrational frequencies (cm^{-1})
	MO calculation*	PES	
1π (C-P bonding only)	10.0	10.793±0.005	ν_3 = 1110±30
3σ (lone pair electrons on P atom)	12.6	12.855±0.005	ν_3 = 1250±30
2σ (mainly C-H bonding)	20.0	--	--

* from Ref. 208.

band shows quite conclusively that the first and second IP's are from the π and σ MO's respectively, and the orbital configuration of HCP for the valence shell is $(1\sigma)^2(2\sigma)^2(3\sigma)^2(1\pi)^4$. The first band (Fig. 34) with a vibrational spacing of 1110 cm^{-1} (a decrease from 1276 cm^{-1} in the ground molecular state) comes from the C-P bonding π-orbital as predicted by the calculation[208]. The second band (Fig. 2) is typical of a non-bonding orbital, because of its sharpness and a vibrational frequency little changed from the neutral molecule.

5.2 CSe_2, OCSe And SCSe

5.2.1 Introduction

There are six triatomic linear molecules containing carbon and oxygen, sulfur or selenium, OCO, OCS, SCS, OCSe, SCSe and SeCSe. The first three have been studied extensively both by optical[209] and photoelectron[3,172] spectroscopy; however, the spectroscopic data for the other three is very limited. The toxicity, unpleasant odors (even in very low concentrations), other adverse physiological effects, instability and the difficulty of obtaining them in pure form make these molecules unappealing to spectroscopists. In this section, the PE spectra of these selenium compounds are presented and discussed, and the spectra of CO_2, OCS

and CS_2 have been included for the sake of comparison and completeness.

PES has in recent years stimulated a growing interest in the quantitative formulation and application of Franck-Condon principle to polyatomic molecules[210]. The major motive behind these studies has been to determine the geometry of ionized molecules from experimentally determined relative vibrational transition probabilities. The general approach in all these studies has been to assume a constant electronic transition moment, thus reducing the problem to an evaluation of vibrational overlap integrals, i.e. the Franck-Condon overlaps, and to use the harmonic oscillator approximation to simplify the integration. Although the theoretical Franck-Condon factor (FCF) may not reproduce the experimental one quantitatively, qualitative agreement is always obtained[210]. From past experience, it is reasonable to expect that the best geometry will give a set of FCF's in best agreement with experiment. We have checked this expectation by determining the geometry of the ionic states of the molecules studied here employing the procedure outlined in section 2.2.3.c, and comparing them, where possible, with experimental data, in the hope that a systematic and reliable way of determining ionic geometry can be established. An attractive feature of these structurally and chemically similar compounds is that several "analogous" series are available for study.

5.2.2 Experimental

CO_2, OCS and CS_2 were obtained commercially (Matheson) and were used without further purification. CSe_2 was prepared by passing methylene chloride vapor over molten selenium at about 500°C[211]. Selenium was removed by steam distillation and the majority of methylene chloride by simple distillation. The residue from simple distillation was subjected to repeated processes of freezing (-78°, dry ice-acetone bath), thawing and pumping at -78°C. The spectrum of CSe_2 was finally recorded when the PE bands of methylene chloride were no longer in evidence. OCSe was obtained in low yield by passing carbon monoxide gas over molten selenium at about 500°C[212]. The reaction vessels were kept scrupulously dry. Traces of carbon monoxide were removed by pumping. SCSe was synthesized by mixing CS_2 vapor with selenium vapor at about 500°C and heating the mixture at about 750°C[213]. Selenium was removed by simple distillation and the bulk of CS_2 by fractional distillation. The SCSe enriched solution of CS_2 was then subject to trap (-78°C) to trap (-195°C) distillation. The last trace of CS_2 was pumped away at -78°C.

The IR spectra of the prepared selenium compounds agreed very well with previously reported work[214] and showed little impurity. All the selenium compounds were found to decompose readily in contact with metal, OCSe being the most serious. The deposition of selenium inside the ionization

chamber caused severe deterioration in the instrumental resolution. To alleviate this problem, two procedures were taken; (1) The ionization chamber was differentially pumped to shorten the time of contact between the sample and the metallic surfaces, (2) A glass sample inlet system (section 3.3.4.b) was adopted (for OCSe), because the CO formed by decomposition interfered strongly with the PE spectrum of OCSe. The pressure of the sample was controlled by an appropriate slush bath (isopentane for OCSe) and a teflon stop cock. With these precautions taken, it was still necessary to clean the vacuum chamber frequently, especially the ionization chamber. Procedure (2) was not adopted for CSe_2 and SCSe, where the decomposition products did not interfere with the spectra of the parent compounds.

The spectra were recorded with a resolution between 20-30 meV (measured by FWHM of the argon doublet) and calibrated against appropriate noble gases. The ionization potentials (IP's) were accurate to 0.01 eV and vibrational frequencies to 30 cm^{-1}, unless specified otherwise.

5.2.3 Results

The PE spectrum of each compound is shown in Fig. 35. The experimental results are tabulated in Table 9, where the vibrational frequency for the ground state of each neutral molecule is also included for comparison.

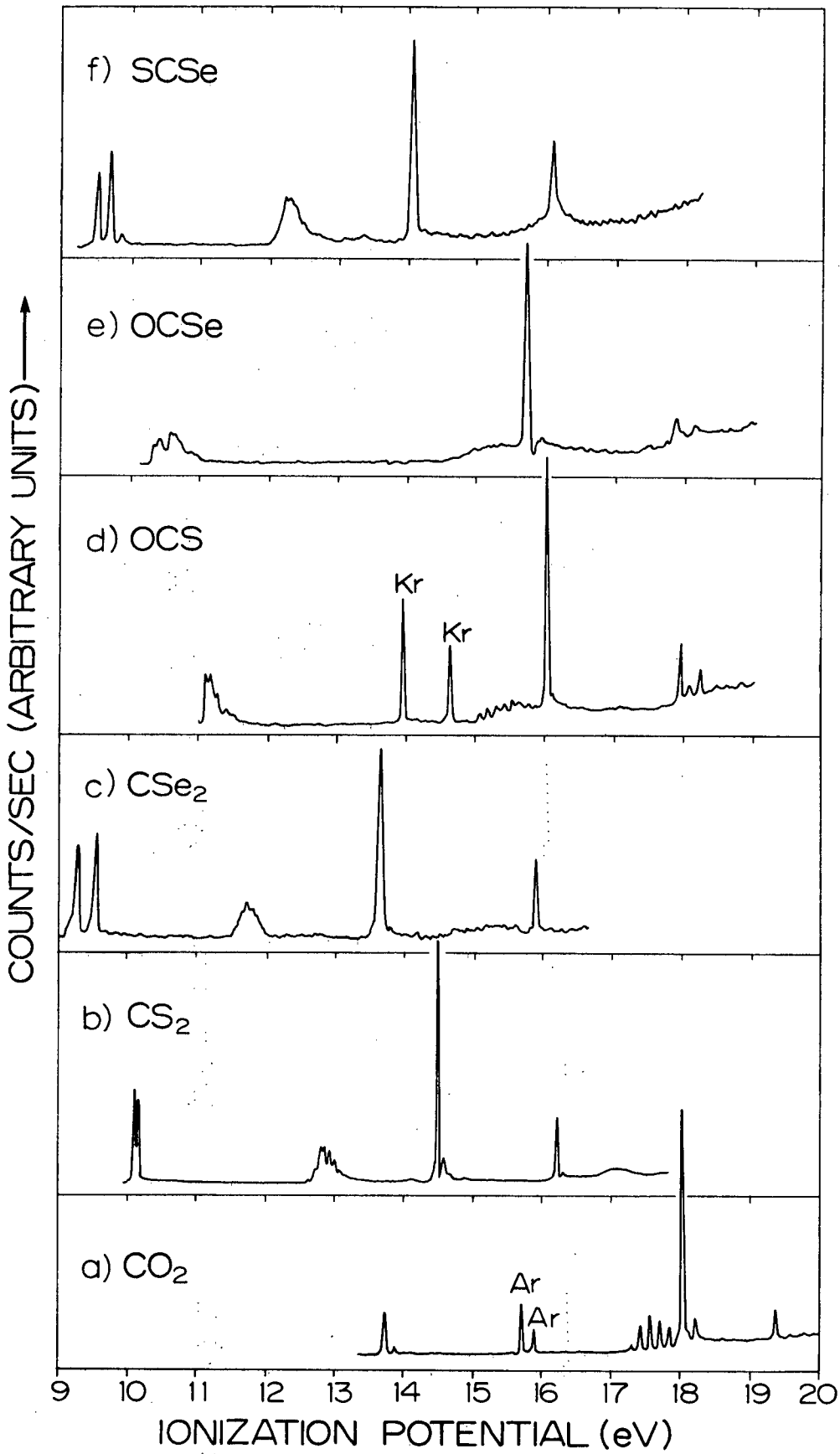
f) SCSe
e) OCSe
d) OCS
Kr
Kr
c) CSe2
b) CS2
a) CO2
Ar
Ar
COUNTS/SEC (ARBITRARY UNITS)
9
10
11
12
13
14
15
16
17
18
19
20
IONIZATION POTENTIAL (eV)

FIGURE 35

TABLE 9 PES Data for CO_2, CS_2, CSe_2, OCS, OCSe and SCSe

Molecule	Electronic state	Adiabatic IP's[a] (eV)	Vibrational frequencies (cm^{-1}) ν_1	ν_2	ν_3	spin-orbit splitting d) (eV)
CO_2	$X^1\Sigma_g^+$	--	1388[b]	667[b]	2349[b]	--
CO_2^+	$X^2\Pi_g$	13.80	1270	--	1440	0.020[b]
	$A^2\Pi_u$	17.34(17.60)	1100	--	--	--
	$B^2\Sigma_u^+$	18.08	1310	--	--	--
	$C^2\Sigma_g^+$	19.39	1340	--	1470	--
CS_2	$X^1\Sigma_g^+$	--	658[b]	397[b]	1533[b]	--
CS_2^+	$X^2\Pi_g$	10.06	--	--	--	0.055
	$A^2\Pi_u$	12.67(12.81)	570	--	--	--
	$B^2\Sigma_u^+$	14.47	640	--	--	--
	$C^2\Sigma_g^+$	16.18	660	--	810	--
	CI state	16.70(17.08)	--	--	--	--
CSe_2	$X^1\Sigma_g^+$	--	368[c]	308[c]	1303[c]	--
CSe_2^+	$X^2\Pi_g$	9.27	--	--	--	0.265
	$A^2\Pi_u$	11.49(11.69)	320	--	--	--
	$B^2\Sigma_u^+$	13.63	310	--	--	--
	$C^2\Sigma_g^+$	15.90	--	--	--	--

TABLE 9 (cont'd) PES Data for CO_2, CS_2, CSe_2, OCS, OCSe and SCSe

Molecule	Electronic state	Adiabatic IP's (eV)	Vibrational frequencies (cm^{-1})			spin-orbit splitting (eV)
			ν_1	ν_2	ν_3	
OCS	$X^1\Sigma^+$	--	2062[b)]	520[b)]	859[b)]	--
OCS^+	$X^2\Pi$	11.18	2080	--	700	0.046
	$A^2\Pi$	15.09	1990	--	790	--
	$B^2\Sigma^+$	16.05	--	--	--	--
	$C^2\Sigma^+$	17.96	2150	--	960	--
OCSe	$X^1\Sigma^+$	--	2021[c)]	466[c)]	642[c)]	--
$OCSe^+$	$X^2\Pi$	10.36(10.43)	2100±50	--	500	0.207
	$A^2\Pi$	14.58(14.73)	2000±100	--	590	--
	$B^2\Sigma^+$	15.75	1930±100	--	--	--
	$C^2\Sigma^+$	17.90	2100	--	720±50	--
SCSe	$X^1\Sigma^+$	--	1435[c)]	355[c)]	506[c)]	--
$SCSe^+$	$X^2\Pi$	9.58	1220±50	--	490±50	0.185
	$A^2\Pi$	12.13(12.35)	--	--	440	--
	$B^2\Sigma^+$	14.07	--	--	460	--
	$C^2\Sigma^+$	16.06	980±50	--	430±50	--

TABLE 9 (cont'd) PES Data for CO_2, CS_2, CSe_2, OCS, OCSe and SCSe

a) values in parentheses are vertical IP's

b) from ref. 209

c) from ref. 214

d) experimental error ± 0.004 eV

CO_2, CS_2 and OCS

Our results and interpretation of the PE spectra for these compounds are in complete agreement with the previous studies (see discussion below), accordingly no further discussion will be given here.

CSe_2

The spectrum of CSe_2 (Fig. 35c) exhibits four distinguishable bands, and vibrational structure is resolved on two of them. The adiabatic IP of the first band is 9.27 eV. This band consists of two equally intense peaks which are the doublet components $^2\Pi_{3/2}$, $^2\Pi_{1/2}$, with a spin-orbit splitting of 0.265 eV. The second band (Fig. 36a) shows an extensive, simple vibrational progression in ν_1. It spreads over approximately 0.5 eV and consists of at least 12 components with an average spacing 320 cm^{-1}. The adiabatic and vertical IP's are 11.49 and 11.69 eV respectively. The third band (Fig. 36b) has an identical adiabatic and vertical IP at 13.63 eV. It shows two levels of vibrational excitation in ν_1 with a spacing of 310 cm^{-1}. The fourth band is a single peak with an IP at 15.90 eV.

OCSe

Four bands are distinguishable in the spectrum (Fig. 35e), and vibrational fine structure is seen on all four. The second and third bands overlap (as in OCS) and

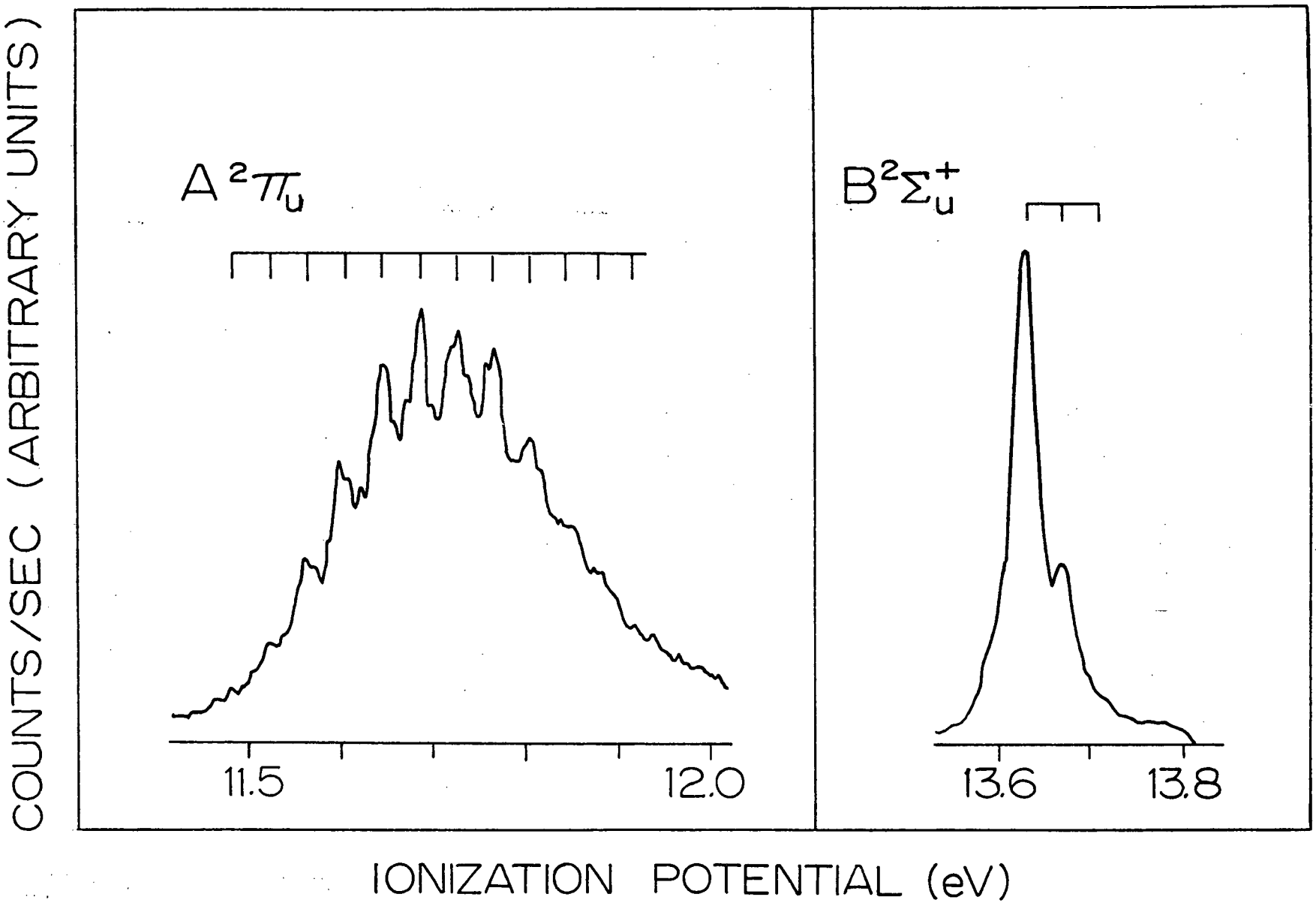
COUNTS/SEC (ARBITRARY UNITS)
A ²Πu
11.5
12.0
B²Σu+
13.6
13.8
IONIZATION POTENTIAL (eV)

FIGURE 36

the overall form of the spectrum is very similar to that of OCS, with the bands of the latter being slightly higher in energy.

Considerable overlap occurs in the first band (Fig. 37a). The band, however, can be satisfactorily analyzed if the first and fourth peaks are treated respectively as the origins of the doublet components $^2\Pi_{3/2}$, $^2\Pi_{1/2}$. This assignment is strongly supported by the experimental fact that the appearance of the first three peaks is reflected in the next three, except for a difference in intensity (see below). This gives a $^2\Pi_{3/2}$ - $^2\Pi_{1/2}$ splitting of 0.207 eV and the adiabatic and vertical IP's at 10.36 and 10.43 eV respectively. A vibrational progression in ν_3 with an average spacing of 500 cm^{-1} is clearly discernible in each of the doublet components. Judging from the intensity distribution of the progression, at least four levels of excitation are expected for ν_3. This means the (003) and (004) components of the $^2\Pi_{3/2}$ state are buried underneath the $^2\Pi_{1/2}$ band. A single level excitation in ν_1 is also observed with an average spacing of 2100 cm^{-1}. The progression ($10n_3$) of the $^2\Pi_{1/2}$ state can be distinguished, with n_3 = 0,1,2, and 3, while the corresponding progression of the $^2\Pi_{3/2}$ state is completely overlapped by the ($00n_3$) progression of the former state. This explains the greater intensity of the $^2\Pi_{1/2}$ band.

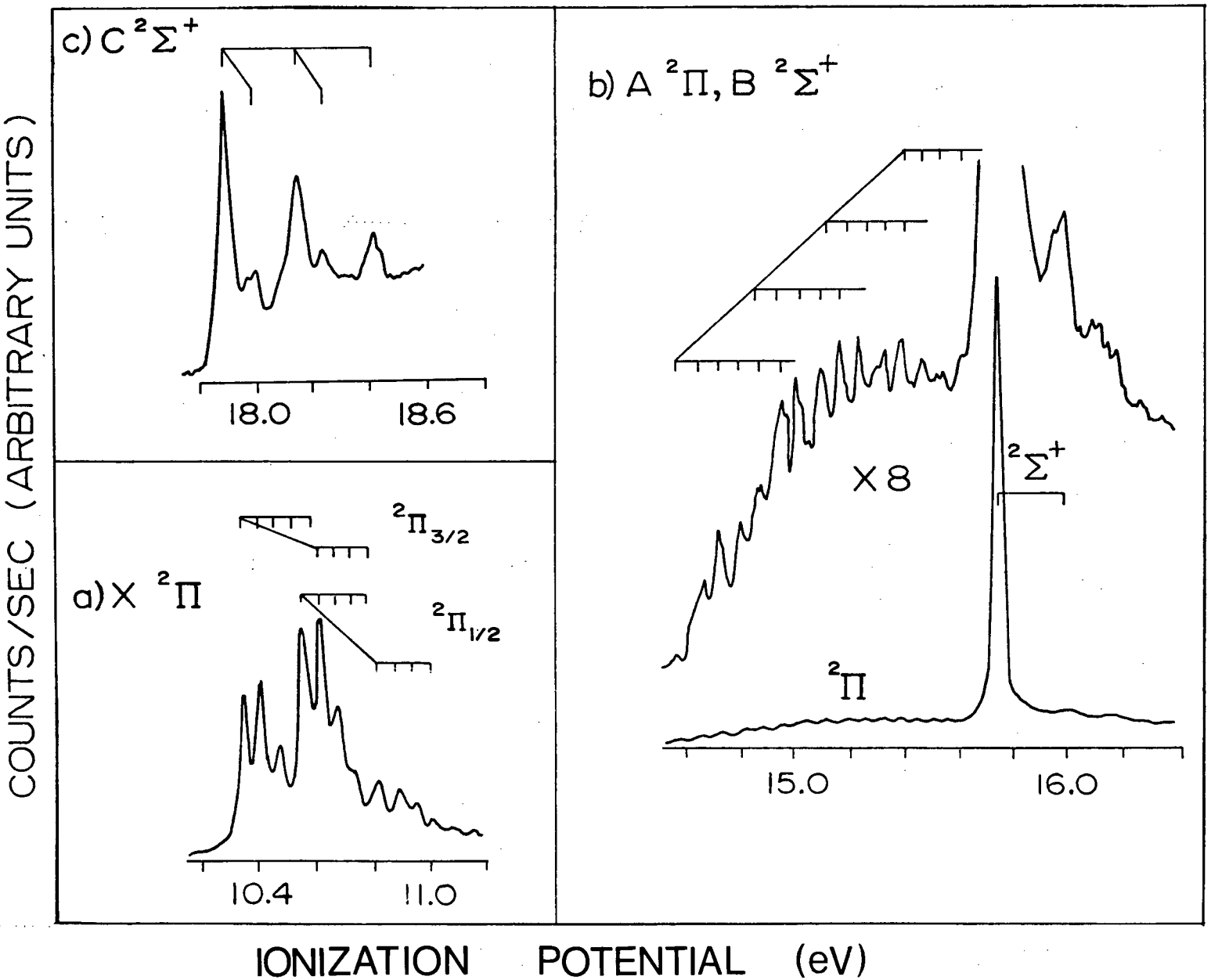
c) C ²Σ⁺
18.0
18.6
b) A ²Π, B ²Σ⁺
X 8
²Σ⁺
²Π
15.0
16.0
a) X ²Π
²Π3/2
²Π1/2
10.4
11.0
COUNTS/SEC (ARBITRARY UNITS)
IONIZATION POTENTIAL (eV)

FIGURE 37

The second band (Fig. 37b), with adiabatic IP at 14.58 eV consists of at least 15 peaks spreading over about 1 eV. The regular spacing of 590 cm^{-1} suggests a progression in ν_3, yet the complexity and the irregular intensity distribution of the band tend to suggest more than one vibrational progression. As in OCS, the additional excitation of ν_1 is most likely. Judging from the intensity variation profile of the band, a spacing of ca. 2000 cm^{-1} is assigned to ν_1. The third peak at 14.73 eV is then taken as the vertical transition. This uncertainty arises because of the overlap with the much more intense third band. The third band (Fig. 37b, adiabatic IP 15.75 eV) is a very intense sharp peak with perhaps another peak at 1930 cm^{-1} to higher energy, assigned to ν_1 by comparison with the ground-state frequency. The fourth band (Fig. 37c, adiabatic IP 17.90 eV) shows two ionic frequencies to be involved, as in OCS. They are assigned to ν_1 and ν_3 respectively, by comparison with the molecular ground-state frequencies.

SCSe

Four bands can be distinguished in the spectrum (Fig. 35f), each showing vibrational fine structure.

The adiabatic IP for the first band is 9.58 eV (Fig. 38a). The peaks occur in pairs indicating the splitting of the state into doublet components $^2\Pi_{3/2}$, $^2\Pi_{1/2}$ with a spin-orbit splitting of 0.185 eV. Analysis of the vibrational fine structure indicates single quantum level excitation of

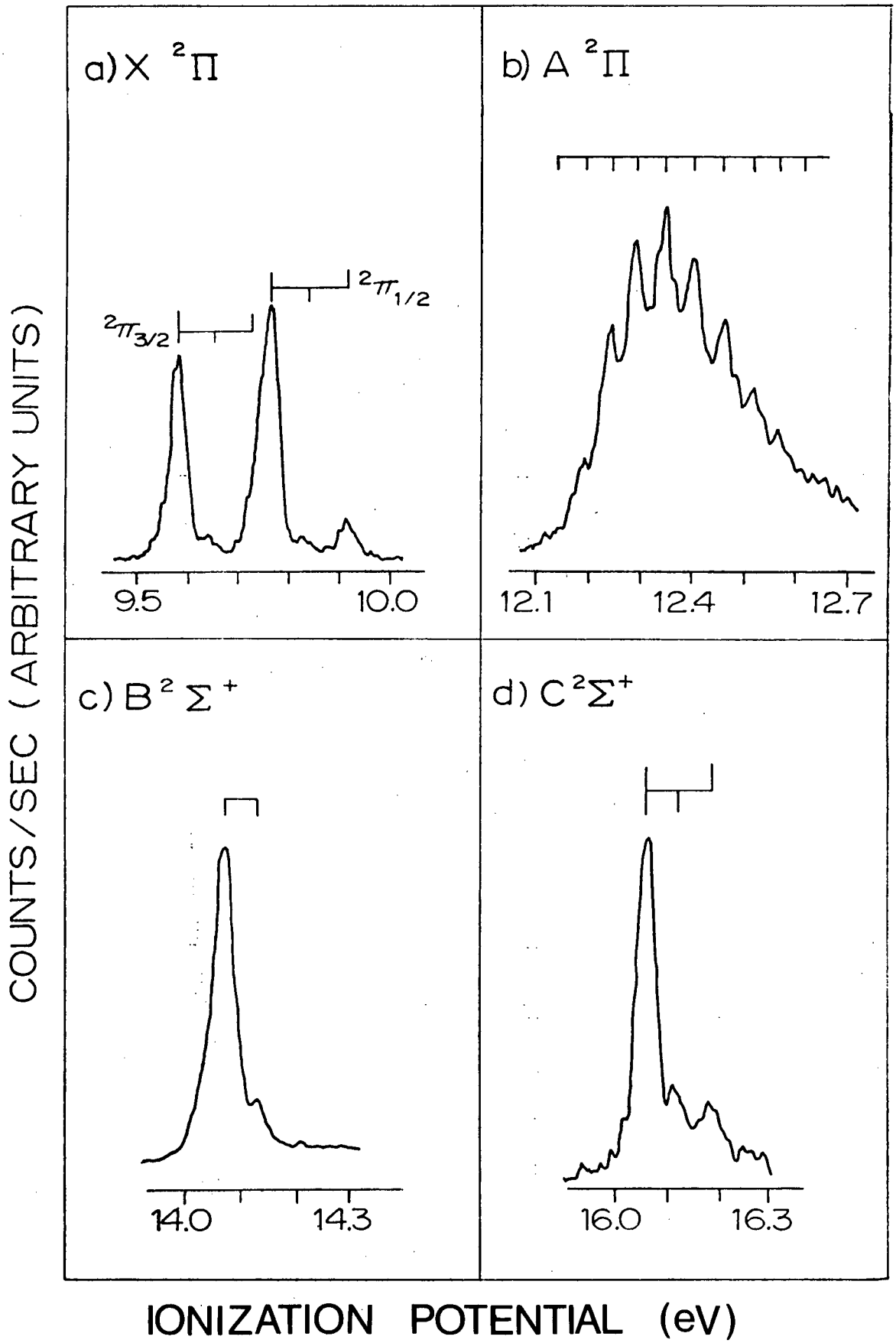
a) X ²Π
²π3/2
²π1/2
9.5
10.0
b) A ²Π
12.1
12.4
12.7
c) B ² Σ +
14.0
14.3
d) C ²Σ+
16.0
16.3
COUNTS/SEC (ARBITRARY UNITS)
IONIZATION POTENTIAL (eV)

FIGURE 38

two ionic frequencies to be involved. One is ν_3, and the other ν_1. The (100) peak of the $^2\Pi_{3/2}$ state overlaps with the (000) peak of the $^2\Pi_{1/2}$ state. The second band (Fig. 38b, adiabatic IP 12.13 eV, vertical IP 12.35 eV) consists of a long series of peaks, spreading over approximately 0.6 eV. At least ten peaks are resolved with an average spacing of 440 cm^{-1}, which is assigned to ν_3. The third band (Fig. 38c, adiabatic IP 14.07 eV) consists of a single quantum of excitation in ν_3. The fourth band (Fig. 38d, adiabatic IP 16.06 eV) indicates a single quantum of excitation in both ν_1 and ν_3.

5.2.4 Discussion

Assignment Of The PE Spectra

The assignment of the PE spectra of the selenium compounds studied here can easily be accomplished by a simple correlation with the known ionic states of CO_2, OCS and CS_2[3,172]. The identification of vibrational fine structure of each band can be facilitated by comparison with the molecular ground-state frequencies and by considering the following selection rules for vibrational excitation (section 2.2.4.b); (1) Totally symmetric vibrations may assume any quantum number in the ionic state; (2) vibrations antisymmetric with a symmetry species can only assume zero or even quantum number.

An examination of Fig. 35 shows the general resemblance of all the PE spectra. Typically, the second band of

each molecule shows an extensive vibrational progression indicating a considerable change in geometry from the molecule to ion and the ionized electron must therefore have come from a strongly bonding or antibonding MO. The other three bands show less or little vibrational fine structure, indicating little change in geometry and the involvement of a more or less nonbonding electron in each case. In addition, the first PE band of each molecule shows a resolvable spin-orbit splitting (except CO_2). Considering these resemblances and the chemical similarity between the compounds, we conclude that the order of ionic states is the same throughout the series.

A correlation diagram of ionic states is shown in Fig. 39, and it shows several interesting trends. The energy of each ionic state is lowered if one end atom is substituted by a heavier one. The effect of substitution of S by Se is much smaller than that of O by S or Se. The latter substitutions result in an energy lowering greater than 1eV, while the former produce far less than 1 eV. This reflects a well established fact that the resemblance between two successive elements in a periodic group is closer as one proceeds down the group. The trend in the magnitude of spin-orbit splitting A of the ground ionic state is as expected except perhaps where that of $OCSe^+$ is larger than that of $SCSe^+$. A closer analysis of A values will explain this paradox and give a deeper insight into the bonding character

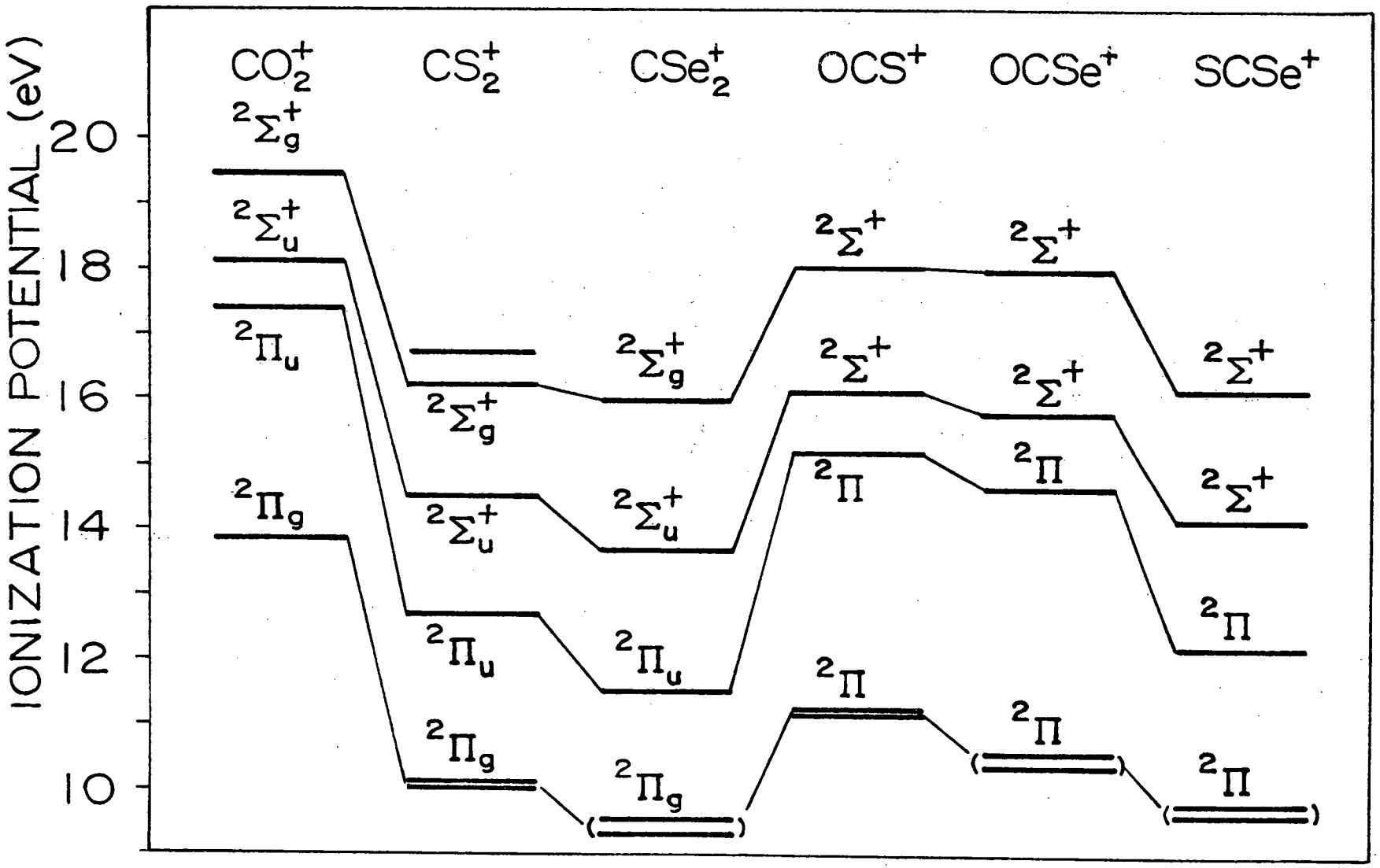
IONIZATION POTENTIAL (eV)
20
18
16
14
12
10
CO_2^+
CS_2^+
CSe_2^+
OCS^+
$OCSe^+$
$SCSe^+$
$^2\Sigma_g^+$
$^2\Sigma_u^+$
$^2\Pi_u$
$^2\Pi_g$
$^2\Sigma_g^+$
$^2\Sigma_u^+$
$^2\Pi_u$
$^2\Pi_g$
$^2\Sigma_g^+$
$^2\Sigma_u^+$
$^2\Pi_u$
$^2\Pi_g$
$^2\Sigma^+$
$^2\Sigma^+$
$^2\Pi$
$^2\Pi$
$^2\Sigma^+$
$^2\Sigma^+$
$^2\Pi$
$^2\Pi$
$^2\Sigma^+$
$^2\Sigma^+$
$^2\Pi$
$^2\Pi$

FIGURE 39

of the highest occupied $\Pi_{(g)}$MO. A semiempirical method by Ishiguro and Kobori[215] gave a very close estimate of A values for simple diatomic molecules. Their method should apply equally well to our linear molecules, especially in the $^2\Pi_{(g)}$ ionic state, because the half filled MO of the ion is nonbonding (or nearly so) and has little contribution from the central carbon atom to make the two center contribution negligible[215]. The spin-orbit coupling constant can then be approximated[215] by: $A = C_c^2\zeta_c + C_x^2\zeta_x + C_y^2\zeta_y$; where C's are the coefficients of the corresponding p_π atomic orbital in the highest occupied $\Pi_{(g)}$MO and ζ's are the corresponding atomic spin-orbit coupling constants. Because $C_c \cong \zeta_c \cong 0$, we can write $A = C_x^2\zeta_x + C_y^2\zeta_y$. Using the observed A values we obtained ζ_O = 0.020 eV, ζ_S = 0.055 eV and ζ_{Se} = 0.265 eV. With these ζ and appropriate A values, we obtain the following approximate wave function for the $\Pi_{(g)}$MO;

$$\psi_\Pi \begin{Bmatrix} OCS \\ OCSe \\ SCSe \end{Bmatrix} = \begin{Bmatrix} -0.51\ p_{\pi,O} + 0.86\ p_{\pi,\ S} \\ -0.49\ p_{\pi,O} + 0.87\ p_{\pi,\ Se} \\ -0.62\ p_{\pi,S} + 0.79\ p_{\pi,\ Se} \end{Bmatrix}$$

The greater contribution of the $p_{\pi,Se}$ orbital, as indicated by the MO coefficients, in OCSe than SCSe can be inferred directly from the larger difference in the orbital energies between O and Se than between S and Se and is the explanation for the larger A value of the $X^2\Pi$ state of $OCSe^+$.

In view of the existence of the fifth band in the PE spectrum of CS_2, an effort has been made to find a similar band for the selenium compounds. If the photoionization cross section is not too small to evade the detection of the fifth band, as is most likely true, we then are led to the conclusion that the fifth band of CS_2 is not formed by an one-electron process, but by a two-electron one. This results in an ionic state whose electron configuration differs from that of the ground state of the neutral molecule by two (or more) MO's. This normally forbidden transition to a doubly-excited state of the molecular ion is allowed as a result of configuration interaction (section 2.2.4.a). The further clarification of this state must await future theoretical work.

Franck-Condon Factors and The Geometry of the Molecular Ion.

The vibrational Franck-Condon factors (FCF) for each ionic state have been measured and are listed in Table 10. The FCF's in the $X^2\Pi$ and $A^2\Pi$ states of $OCSe^+$ have not been measured because of severe overlap. The errors in these experimental FCF's vary considerably, and increase with the extent of overlap in the band. However, the qualitative feature, i.e., the intensity distribution, is not expected to change.

The measured FCF's have been used to estimate the geometry of each state of the molecular ion using the method

TABLE 10(a) Experimental and Calculated Franck-Condon Factors in the Individual States of CO_2^+, CS_2^+ and CSe_2^+

Ionic state	Vibrational level	Franck-Condon factor					
		CO_2^+		CS_2^+		CSe_2^+	
	n_1 n_2 n_3	Experimental	Calculated	Experimental	Calculated	Experimental	Calculated
$X^2\Pi_g$	000	0.80	0.81	1.0	1.0	1.0	1.0
	100	0.15	0.16				
	200	~0.02	0.01				
	002	~0.03	0.02				
$A^2\Pi_u$	000	0.08	0.06	0.10	0.07	0.01	0.002
	100	0.20	0.19	0.20	0.20	0.03	0.013
	200	0.23	0.27	0.24	0.27	0.06	0.043
	300	0.21	0.24	0.19	0.23	0.09	0.092
	400	0.13	0.15	0.13	0.14	0.13	0.143
	500	0.08	0.07	0.09	0.06	0.15	0.173
	600	0.04	0.02	0.05	0.02	0.14	0.171
	700	0.03	0.01	0.02	0.01	0.13	0.142
	800	0.01	0.001			0.10	0.100

TABLE 10(a) (cont'd) Experimental and Calculated Franck-Condon Factors in the Individual States of CO_2^+, CS_2^+ and CSe_2^+

Ionic state	Vibrational level	Franck-Condon factor					
		CO_2^+		CS_2^+		CSe_2^+	
	n_1 n_2 n_3	Experimental	Calculated	Experimental	Calculated	Experimental	Calculated
	900					0.07	0.061
	1000					0.05	0.033
	1100					0.03	0.015
	1200					0.02	0.006
	1300					0.01	0.002
$B^2\Sigma_u^+$	000	0.89	0.90	0.87	0.89	0.71	0.73
	100	0.10	0.10	0.10	0.10	0.24	0.25
	200	∿0.01	<0.01	∿0,02	<0.01	∿0.05	0.02
$C^2\Sigma_g^+$	000	0.88	0.91	0.87	0.85	1.0	1.0
	100	0.06	0.06	0.11	0.11		
	002	0.06	0.03	∿0.02	0.04		

TABLE 10(b) Experimental and Calculated Franck-Condon Factors in the Individual States of OCS^+, $OCSe^+$ and $SCSe^+$

Ionic state	Vibrational level	Franck-Condon factor					
		OCS^+		$OCSe^+$		$SCSe^+$	
	n_1 n_2 n_3	Experimental	Calculated	Experimental	Calculated	Experimental	Calculated
$X^2\Pi$	000	0.45	0.41	a)		0.78	0.76
	001	0.27	0.27			0.09	0.09
	002	~0.09	0.07				0.004
	003		<0.01				
	100	0.13	0.12			0.13	0.13
	101	0.07	0.08				0.02
	102		0.02				
	200		0.02				
	201		0.01				
$A^2\Pi$	000	0.05	0.048	0.03[b)]	0	0.01	0.01
	001	0.08	0.105	0.04	0.004	0.05	0.05
	002	0.10	0.110	0.05	0.02	0.13	0.11
	003	0.07	0.074	0.07	0.04	0.17	0.18

TABLE 10(b)(cont'd) Experimental and Calculated Franck-Condon Factors in the Individual States of OCS^+, $OCSe^+$ and $SCSe^+$

Ionic state	Vibrational level	Franck-Condon factor					
		OCS^+		$OCSe^+$		$SCSe^+$	
	n_1 n_2 n_3	Experimental	Calculated	Experimental	Calculated	Experimental	Calculated
	004	0.04	0.036	0.10	0.08	0.19	0.20
	005	Overlap with 200	0.013	0.10	0.12	0.16	0.18
	006		0.004	0.11	0.15	0.13	0.13
	007			0.11	0.16	0.08	0.08
	008			0.11	0.14	0.06	0.04
	009			0.10	0.11	0.03	0.02
	0010			0.08	0.08		
	0011			0.07	0.05		
	0012			0.05	0.03		
	0013				0.015		
	100	0.05	0.047				
	101	0.10	0.102				
	102	0.10	0.107				

TABLE 10(b)(cont'd) Experimental and Calculated Franck-Condon Factors in the Individual States of OCS^+, $OCSe^+$ and $SCSe^+$

Ionic state	Vibrational level $n_1\ n_2\ n_3$	Franck-Condon factor					
		OCS^+		$OCSe^+$		$SCSe^+$	
		Experimental	Calculated	Experimental	Calculated	Experimental	Calculated
	103	0.09	0.072				
	104	0.05	0.035				
	105	0.02	0.013				
	106	~0.01	0.004				
	005 + 200	(0.06)	0.022				
	201	0.06	0.048				
	202	0.07	0.050				
	203	0.05	0.034				
	204		0.016				
	300	Overlap with $B^2\Sigma^+$ state.	0.002				
	301		0.014				
	302		0.015				
	303		0.010				
	304		0.005				

TABLE 10(b)(cont'd) Experimental and Calculated Franck-Condon Factors in the Individual States of OCS^+, $OCSe^+$ and $SCSe^+$

Ionic state	Vibrational level n_1 n_2 n_3	Franck-Condon factor					
		OCS^+		$OCSe^+$		$SCSe^+$	
		Experimental	Calculated	Experimental	Calculated	Experimental	Calculated
$B^2\Sigma^+$	000	1.0		0.96	0.96	0.83	0.83
	001			~0.04	0.04	0.14	0.14
	002					~0.03	0.03
$C^2\Sigma^+$	000	0.48	0.43	0.44	0.42	0.70	0.67
	001	0.16	0.15	0.12	0.12	0.17	0.17
	002		0.03		0.02		0.01
	100	0.24	0.22	0.25	0.25	0.13	0.12
	101	~0.03	0 07	0.10	0.07		0.03
	102		0.02		0.01		
	200	0.07	0.05	0.09	0.08		
	201	0	0.02		0.02		
	300	~0.02	0.01		0.02		

a) FCF was not measured because of severe overlap.

b) a single vibrational progression in ν_3 was assumed.

outlined in section 2.2.3.c, the results are collected in Table 11. For comparison the geometries of two ionic states of N_2O have also been estimated using the FCF's reported by Turner et al[3], and compared with the measured bond lengths. The estimated ionic geometries turned out to agree reasonably well with the available experimental ones, with a maximum deviation of 0.006 Å (Table 11). Unfortunately, the comparison is limited by available experimental data on ionic geometry. Guided by the initial success stated above, we might expect the results for the types of molecules studied here, i.e. linear triatomic molecules, would be reliable. The method used here together with the PES technique might provide a very general and convenient way of estimating ionic geometries. The test for the reliability of this method if applied to molecules of other symmetry species has to await future experimental data.

Several instructive conclusions can be drawn from the series of calculations: (1) Because of the criteria (section 2.2.3.c) used in determining the d values, we do not expect the calculated ionic geometry to be very much dependent on the accuracy of ionic vibrational frequencies. This means the frequencies determined by PES are accurate enough for the purpose although they normally have an error limit of 30 cm^{-1}; (2) The method outlined in section 2.2.3.c assumes no mixing of normal coordinates of the same symmetry in going from the neutral to the ionic state, i.e., $A_{ij} = \delta_{ij}$

TABLE 11 Estimated Bond Lengths of the Individual States of CO_2^+, CS_2^+, CSe_2^+, OCS^+, $SCSe^+$, and N_2O^+.

Molecule XCY	Electronic State	$d_1 X10^{20}$ $g^{\frac{1}{2}}cm$	$d_3 X10^{20}$ $g^{\frac{1}{2}}cm$	$\Delta r(C-X)$ Å	$\Delta r(C-Y)$ Å	$r(C-X)^{a)}$ Å	$r(C-Y)^{a)}$ Å
OCO	$X^1\Sigma_g^+$					$1.162^{b)}$	$1.162^{b)}$
OCO^+	$X^2\Pi_g$	0.124	0.124	0.017	0.017	1.179(1.177)	1.179(1.177)
	$A^2\Pi_u$	0.503	0.503	0.069	0.069	1.231(1.228)	1.231(1.228)
	$B^2\Sigma_u^+$	0.095	0.095	0.013	0.013	1.175(1.180)	1.175(1.180)
	$C^2\Sigma_g^+$	0.073	0.073	0.010	0.010	1.172	1.172
SCS	$X^1\Sigma_g^+$					$1.555^{b)}$	$1.555^{b)}$
SCS^+	$X^2\Pi_g$	0	0	0	0	1.555(1.554)	1.555(1.554)
	$A^2\Pi_u$	0.702	0.702	0.068	0.068	1.623	1.623
	$B^2\Sigma_u^+$	0.144	0.144	0.014	0.014	1.569(1.564)	1.569(1.564)
	$C^2\Sigma_g^+$	0.144	0.144	0.014	0.014	1.569	1.569
SeCSe	$X^1\Sigma_g^+$					$1.711^{c)}$	$1.711^{c)}$
	$X^2\Pi_g$	0	0	0	0	1.711	1.711
	$A^2\Pi_u$	1.425	1.425	0.088	0.088	1.799	1.799

TABLE 11 (cont'd) Estimated Bond Lengths of the Individual States of CO_2^+, CS_2^+, CSe_2^+, OCS^+, $SCSe^+$, and N_2O^+.

Molecule XCY	Electronic State	$d_1 X 10^{20}$ $g^{\frac{1}{2}}cm$	$d_3 X 10^{20}$ $g^{\frac{1}{2}}cm$	$\Delta r(C-X)$ Å	$\Delta r(C-Y)$ Å	$r(C-X)^{a)}$ Å	$r(C-Y)^{a)}$ Å
$SeCSe^+$	$B^2\Sigma_u^+$	0.324	0.324	0.020	0.020	1.731	1.731
	$C^2\Sigma_g^+$	0	0	0	0	1.711	1.711
OCS	$X^1\Sigma^+$					$1.160^{b)}$	$1.560^{b)}$
OCS^+	$X^2\Pi$	0.126	0.281	-0.024	0.074	1.136	1.634
	$A^2\Pi$	0.230	0.534	0.092	0.046	1.252	1.606
	$B^2\Sigma^+$	0	0	0	0	1.160	1.560
	$C^2\Sigma^+$	0.166	0.211	-0.039	0.069	1.121	1.629
OCSe	$X^1\Sigma^+$					$1.159^{c)}$	$1.709^{c)}$
$OCSe^+$	$X^2\Pi$						
	$A^2\Pi$ d)	0	1.170	0.031	0.181	1.190	1.890
	$B^2\Sigma^+$	0.048	0	-0.014	0.009	1.145	1.718
	$C^2\Sigma^+$	0.181	0.219	-0.048	0.067	1.111	1.776
SCSe	$X^1\Sigma^+$					$1.557^{c)}$	$1.709^{c)}$

TABLE 11 (cont'd) Estimated Bond Lengths of the Individual States of CO_2^+, CS_2^+, CSe_2^+, OCS^+, $SCSe^+$ and N_2O^+.

Molecule XCY	Electronic State	$d_1 X 10^{20}$ $g^{1/2}cm$	$d_3 X 10^{20}$ $g^{1/2}cm$	$\Delta r(C-X)$ Å	$\Delta r(C-Y)$ Å	$r(C-X)^{a)}$ Å	$r(C-Y)^{a)}$ Å
$SCSe^+$	$X^2\Pi$	0.115	0.161	-0.020	0.041	1.537	1.750
	$A^2\Pi$	0	1.054	0.063	0.104	1.620	1.813
	$B^2\Sigma^+$	0	0.119	-0.007	-0.012	1.550	1.738
	$C^2\Sigma^+$	0.122	0.234	-0.017	0.050	1.540	1.759
NNO	$X^1\Sigma^+$					$1.128^{b)}$	$1.184^{b)}$
NNO^+	$X^2\Pi$	0.046	0.078	0.022	0.007	1.150(1.155)	1.191(1.185)
	$A^2\Sigma^+$	0.063	0.131	0.011	-0.041	1.139(1.140)	1.143(1.141)

a) values in ( ) are experimental bond lengths from ref. 209

b) from ref. 209

c) from ref. 214

d) a single vibrational progression in ν_3 was assumed.

in the exact expression $Q_i' = \Sigma A_{ij} Q_j'' + d_i$. For molecules of $D_{\infty h}(CX_2)$ symmetry, no such assumption is necessary. Therefore, we expect the results for these molecules to be more reliable than those for molecules of $C_{\infty v}$ symmetry. This argument can further be extended to triatomic molecules of other symmetries. The reliability of the results would then be in this order $D_{\infty h} > C_{2v} > C_{\infty v} > C_s$, because the extent of coupling between normal vibrations of the totally symmetric species would normally increase in the same order; (3) In comparing the experimental and calculated FCF's (evaluated at the estimated geometry) in Table 10, we notice the agreement is much less satisfactory for the second bands where higher levels of vibrational excitation are involved. In particular, the calculated FCF's indicate a much narrower intensity distribution envelope. These discrepancies are understandable in view of the harmonic oscillator assumption. The unsatisfactory agreement is due to a poorer description of the vibrational function by harmonic wave functions at higher vibrational quantum numbers, whereas the more 'peaked' intensity distribution is due to the steeper slope of the harmonic potential compared to the true potential. An improvement in the method would be the inclusion of anharmonicity in the vibrational wave functions. (4) If the second band of OCSe were treated as a single progression in ν_3 only, the estimated geometry would give an increase of 0.181 Å in r (C-Se), which would be rather large. A smaller increase in r (C-Se) would mean a less extensive progression. This result is consistent with

our assignment that more than one progression is involved in the band.

5.3 Ozone (O_3)

5.3.1 Introduction

The PE spectrum of O_3 has previously been recorded by Radwan and Turner[216] using a low resolution, retarding grid analyzer. Our study differs from theirs in that it is of much higher resolution and the measurements were made on a very pure O_3 sample (> 98%). Vibrational fine structure is now resolved in some bands and spurious bands due to the presence of residual oxygen can be unambiguously identified, thus enabling a more accurate determination of ionization potentials for O_3.

5.3.2 Experimental

The PE spectra were recorded with a nominal resolution of 20-25 meV (measured at FWHM of the argon doublet), and calibration was effected using both argon and oxygen peaks as markers. About 8 ml of ozonized oxygen (∿ 4% O_3) produced in a laboratory ozonizer was condensed, and the condensate pumped at -196°C down to a volume of about 1 ml which was then transferred to the Kel-F inlet system (section 3.3.4.b). The spectrometer was then pumped from

atmospheric pressure while keeping the O_3 sample at -196°C with the valve completely open. The operating vacuum was achieved in about an hour, by which time the amount of the residual oxygen should be negligible since at -196°C oxygen has a vapour pressure of ∿ 130 mm Hg. The PE spectrum of ozone was then recorded with the sample held in an isopentane slush bath (-160°C) after regulating the pressure with the Kel-F valve.

The handling of O_3 adopted here involved the least disturbance of the sample and hence greatly reduced the hazard of an explosion. Furthermore, with the use of the direct inlet system, the decomposition of O_3 was found to be negligible and thus a study of pure O_3 was possible. The purity of the O_3 sample was checked by focussing on the first band of oxygen for at least 5 minutes and noting no detectable signal above the background. By repeating this process several times, we finally estimated the oxygen impurity to be less than 2% and we expect it to decrease as the experiment proceeded.

5.3.3 Results and Discussion

The HeI PE spectrum of O_3 is shown in Fig. 40. The first band has a peculiar contour which consistently showed up in two independent measurements separated in time by several days, with both the HeI (Fig. 41a) and NeI (Fig. 41b) light sources. The persistence of the band structure

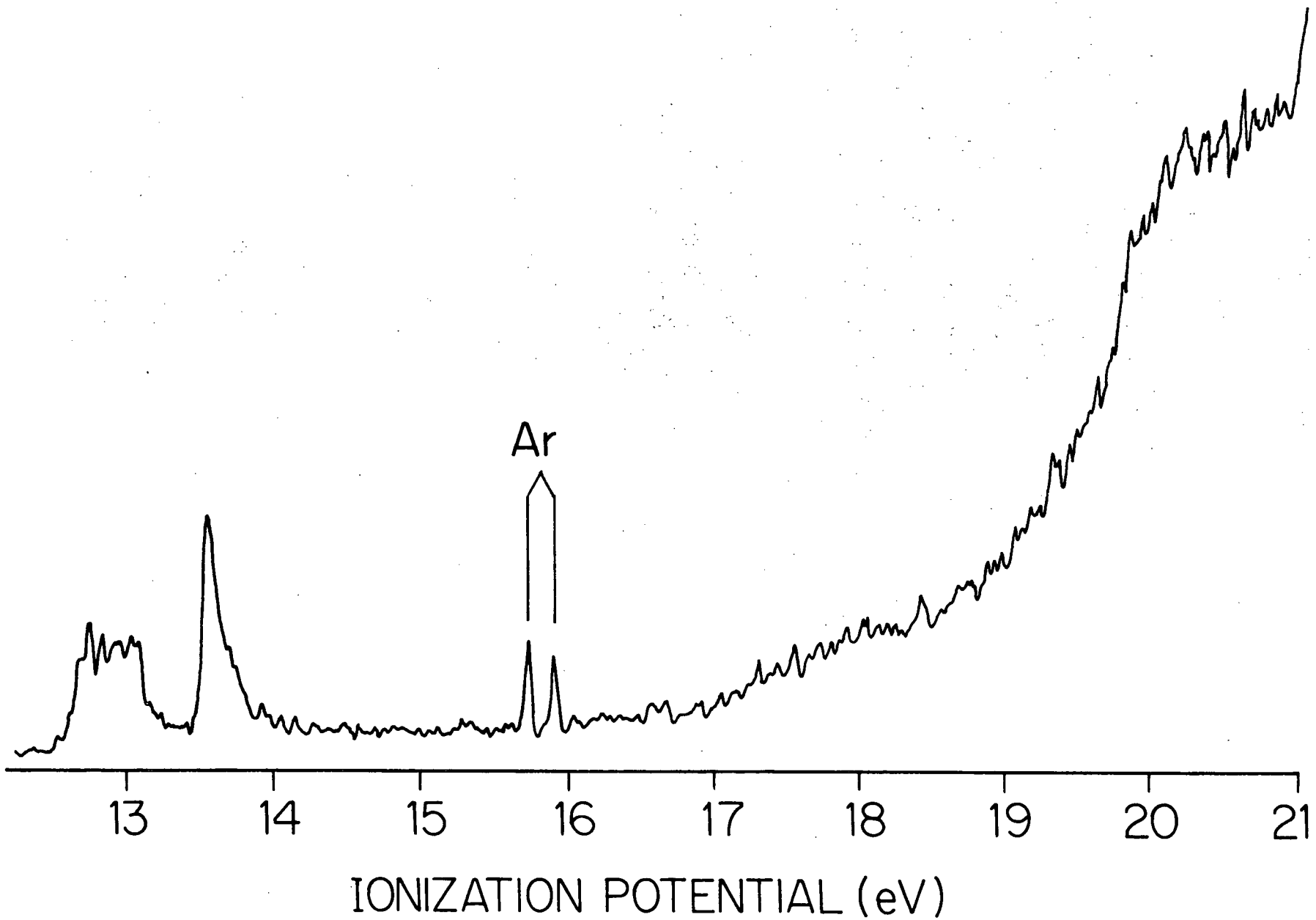

FIGURE 40

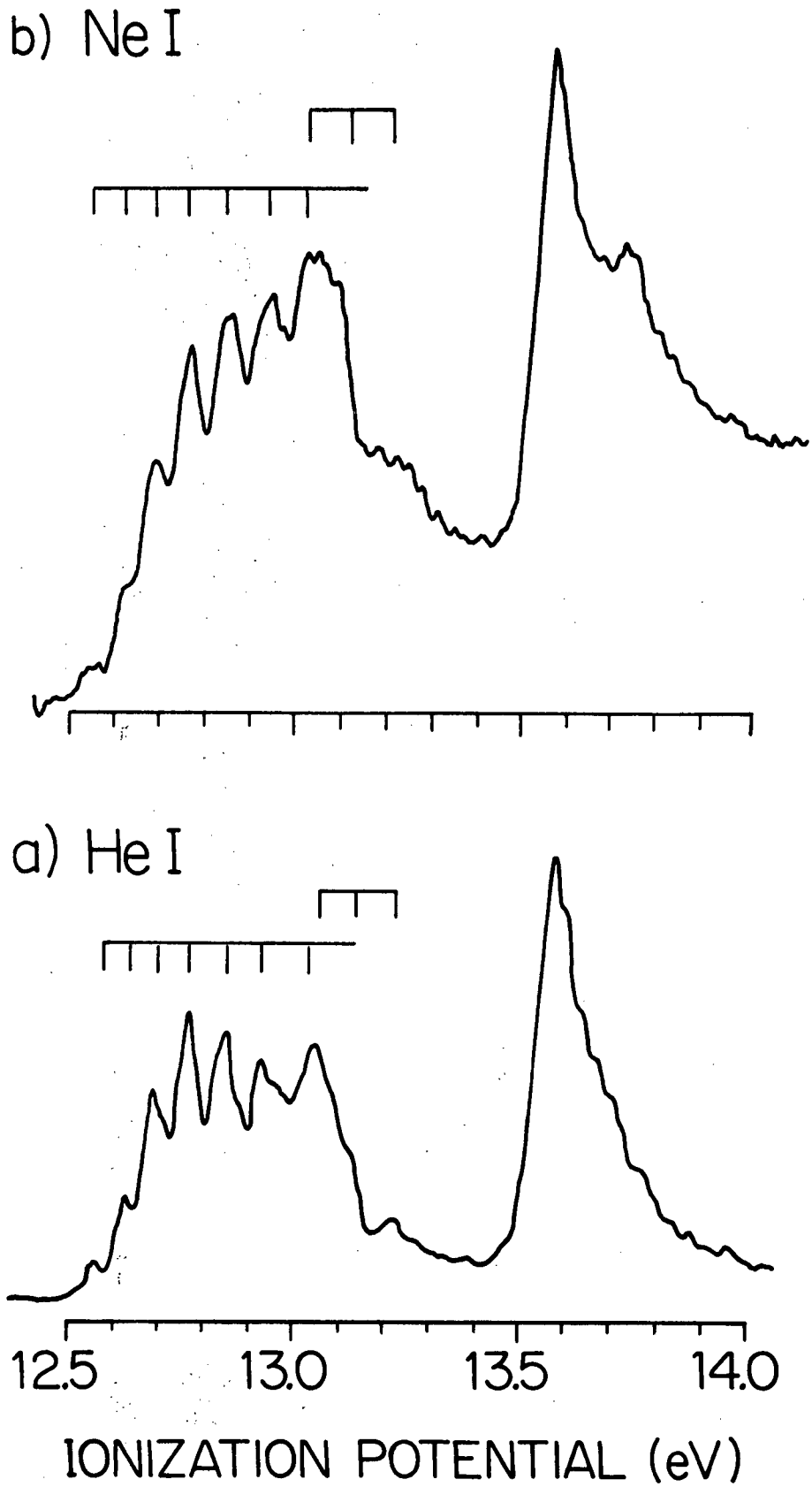

FIGURE 41

rules out the possibility of either an autoionization process or an experimental artifact. In fact, upon close examination two bands can be identified and assigned to two independent ionization processes. The first IP has adiabatic and vertical values of 12.53 ± 0.01 and 12.75 ± 0.01 eV respectively, while the second IP appears to have an identical adiabatic and vertical value at 13.03 ± 0.02 eV. The first band exhibits six clearly resolved vibrational peaks, and beyond the sixth peak ($\nu' = 5$) overlaps strongly with the second band. The vibrational spacing, unlike most cases, increases towards higher vibrational levels indicating a positive anharmonicity constant. With extensive averaging, the average vibrational spacing is found to be 630 cm^{-1} with the first being 520 ± 30 cm^{-1}. This vibrational progression is assigned to the bending mode, ν_2, which is 705 cm^{-1}[209] in the molecular ground state, since the symmetric stretch ν_1, the other possible mode, is 1110 cm^{-1} in the neutral molecule and would be expected to be much larger. Two additional peaks associated with the second IP can be identified (Fig. 41a) with an averaging spacing of 700 ± 50 cm^{-1} which again can be assigned to the bending vibration. The third band is sharp and intense with an IP at 13.57 ± 0.01 eV, and definitely involves a rather extensive progression. It was, however, only possible to resolve some vibrational structure in some of the scans, thus rendering the vibrational analy-

sis of the band inconclusive. In favourable cases, a weak progression of ∿ 500 cm^{-1} appeared, which, if real, would then probably correspond to the bending vibration. The fourth and fifth bands are both weak, broad and featureless centering at 17.8 eV and 20.3 eV respectively. Because of the fast rising background in the low electron kinetic energy region, the existence of these bands may not be entirely certain.

Contrasting our results with those of Radwan and Turner[216] (Table 12), we note that the additional IP's given by them at 12.3, ∿ 17 eV and ∿ 19.3 eV are most probably due to oxygen while the other IP values agree very closely with ours. The first IP from PES is in accord with the value 12.8 ± 0.1 eV obtained by electron impact[217] considering that the vertical IP is usually obtained from the latter technique. A recent photoionization study of ozone with mass anlysis[218] gave the first IP at 12.67 ± 0.02 eV which is 0.14 eV higher than our adiabatic value. This large difference, which is far beyond the experimental error limit claimed, is perplexing since photoionization is a threshold phenomenon. In view of the experimental difficulty[218], we would be inclined to resolve this apparent discrepancy by suggesting that the transition to the first two cationic vibronic levels may be too weak to be detected in the photoionization study and the value 12.67 eV actually

TABLE 12 PES and Theoretical Data for O_3

	Vertical IP (eV) from PES		IP (eV) from ab initio SCF MO		
Ionic	This work	Ref. 216	Orbital	Ref. 219	Ref. 221
$^2A_1$	12.75 ± 0.01 (12.53)*	12.52 ± 0.05	$6a_1$	15.00	15.39
$^2A_2$	13.03 ± 0.02	12.3 ± 0.1 ?	$1a_2$	13.22	13.35
$^2B_2$	13.57 ± 0.01	13.52 ± 0.05	$4b_2$	15.31	15.80
$^2B_1$	17.8 ± 0.1	16.4 - 17.4 ?	$1b_1$	21.19	20.69
$^2B_2$		19.24 ± 0.1	$3b_2$	21.67	21.25
$^2A_1$	20.3 ± 0.1		$5a_1$	22.57	22.23

* adiabatic IP

corresponds to the $\nu_2' = 2$ peak in the PE spectrum. For the first PE band, we further notice that the peaks beyond the $\nu_2' = 2$ level broaden considerably. The broadening can be explained as due to the short lifetime of the ion in the higher vibronic levels as supported by Cook's[218] measurement that the appearance potentials of the O_2^+ and O_5^+ ions are both at 12.67 eV, which, as pointed out above, corresponds to the $\nu'_2 = 2$ peak.

There are a number of accurate SCF MO calculations[219-221] for the ground state of O_3 and the agreement among them is excellent. It is interesting to see what useful information these calculations provide. According to Rothenberg and Schaefer[219], who employed the most extensive basis set and obtained the lowest total energy, the orbital configuration of O_3 is:

$$\ldots\ldots (2b_2)^2(4a_1)^2(5a_1)^2(3b_2)^2(1b_1)^2(4b_2)^2(6a_1)^2(1a_2)^2,\ {}^1A_1$$

They also studied the effect of d-orbital contribution and found that the ordering of MO energies is the same with and without them. Assuming Koopmans' theorem (KT),[49] the IP's are calculated from the results of reference 219 and 221 and are collected in Table 12 for comparison. Considering that the calculated IP's are usually higher than the corresponding experimental values, we expect from the calculations five to six IP's accessible with HeI excitation. It seems then reasonable to assign three IP's to the PE bands between 12 and 14 eV and the rest to the fourth and

fifth bands. Direct application of KT to the MO results[219,221] gives the ordering of the observed ionic states as X^2A_2, A^2A_1, B^2B_2, C^2B_1, D^2B_2 and E^2A_1. The long vibrational progression in the first band, however, indicates substantial geometry change, and is not likely to be associated with the non-bonding $1a_2$ MO which is the antisymmetric combination of the end atom p_π functions. This is clearly manifested in Peyerimhoff and Buenker's work[221] in which the angular dependence of orbital energies was studied and the energy of the $1a_2$ orbital was found to have little angular dependence. In fact, by fitting the calculated Franck-Condon factors to the experimental ones (section 2.2.3.c), the bond angle and bond length of this ionic state were estimated to be 12° and 0.024 Å greater than that of the molecular ground state. Considering further that the failure of KT in predicting the correct ordering of states is more frequent when these states are close together, it would seem reasonable to believe KT is inapplicable in the present case and we would provisionally propose an interchange of cationic states relative to the KT ordering, i.e. the three lowest ionic states would be X^2A_1, A^2A_2 and B^2B_2. The assignment proposed here is consistent with the predictions drawn from comparing the PE spectrum of O_3 with that of NO_2[109,222] and SO_2[3,172]; all of these molecules have similar electronic structure. The bands associated with the corresponding

states in the three molecules show similar behaviour, namely, the length of the vibrational progression in each band is comparable from molecule to molecule, and decreases in the order of $^2A_1 > {}^2B_2 > {}^2A_2$, as expected from the respective bonding character of the orbitals involved. The long vibrational progression associated with the second ($^2B_2$) and third ($^2A_2$) IP's in SO_2[3,172] is understandable in view of the far more important d-orbital participation[219,223] in SO_2 than in O_3 or NO_2.

The band separations in the PE spectrum of a neutral molecule should correlate with the electronic spectrum of its ion if due care is given to the fact that two-electron processes are normally forbidden in PES. Consequently, some of the ionic states observed in the electronic spectrum may not be accessible in photoionization and hence there may not always be a one-to-one correspondence between the corresponding PE and electron spectra. With this provision, it would be instructive to compare the electronic spectrum of NO_2, an isoelectronic species to O_3^+, with the PE spectrum of O_3^+. Comparisons of this type have been attempted for CP and CS^+ (section 4.1), NH_2 and H_2O^+[3] as well as PH_2 and H_2S^+[224]. In these cases, the spectra for each pair of molecules are identical with respect to the ordering of electronic states, and are remarkably similar in the order of magnitude of the corresponding excitation energies. It seems, therefore, reasonable to expect a similar resemblance

between O_3^+ and NO_2. We note that the orbital configuration of NO_2[219] is:

$$\ldots\ldots (3b_2)^2(1b_1)^2(4b_2)^2(1a_2)^2(6a_1)^1,\ ^2A_1$$

with the three highest occupied MO's arranged in the same order as the three lowest states of O_3^+ and that the ground state of NO_2 is X^2A_1[109,222]. One $^2B_2$ state of NO_2 has recently been observed by Brand et al.[225] to lie at 1.48 eV above the ground state and has been assigned as the lowest excited state. Unfortunately, no $^2A_2$ state has been identified for NO_2, probably because a forbidden transition is involved. A straightforward comparison between O_3^+ and NO_2 is thus impossible since the position of the unobserved $^2A_2$ state of NO_2 with respect to that of the $^2B_2$ state is not known. Yet some interesting inferences can be drawn by comparing the corresponding excitation energies if they can be assumed to be comparable. The first and second excitation energies (adiabatic) of O_3^+ are 0.50 and 1.04 eV respectively. Comparing these two values to 1.48 eV, we tend to believe that the new $^2B_2$ state of NO_2 is likely to correspond to the second excited state of O_3^+ rather than the first one. If this is the case, the second excited state of O_3^+ would be the $^2B_2$ state, and further, if the ordering of their respective electronic states is assumed to be the same, then the first excited state of NO_2 would be the $^2A_2$ state instead of the $^2B_2$ state as is the case proposed for O_3^+.

In view of the apparent failure of KT in assigning the first IP of O_3, the validity of KT when applied to higher IP's is even more doubtful. Therefore, the assignment of the PE band at 17.8 eV to $1b_1$ and $3b_2$ ionizations, and that 20.3 eV to $5a_1$, based purely on MO results, is only tentative. Preliminary calculations by Herring et al.[226] has suggested that the band at 17.8 eV may be due to CI states. If such is the case, the band at 20.3 eV would then be most likely due to ionizations from the orbitals $1b_1$, $3b_2$ and $5a_1$.

5.4 Nitrosyl Halides (XNO, X = F, Cl, Br)

5.4.1 Introduction

In spite of the fact that these are simple molecules, there is only a meager understanding of the electronic structure of the nitrosyl halides. This is presumably due to their instability and high reactivity, as exemplified by the fact that they are highly oxidizing. These molecules are increasingly unstable towards decomposition in the series FNO, ClNO, BrNO, such that BrNO is very difficult to obtain in pure form (e.g. it is ∿ 7% decomposed in the gas phase at room temperature). All of them attack many metals with FNO being the most reactive.

This series of molecules is, moreover, of additional interest in view of the weak bonding between the halogen

atom and the NO radical, as reflected in their abnormally long N-X bond lengths[227]. This aspect has, in fact, been extensively discussed by Peyerimhoff and Buenker[228] for the case of FNO.

5.4.2 Experimental

All three molecules were run using the stainless steel direct inlet (section 3.3.4.b) with the sample cooled and held in an appropriate temperature bath (FNO at -112°, ClNO at -78° and BrNO at -63°C). It was found necessary in all cases to use the differential pump to alleviate the problem of decomposition. Calibration of the spectra was effected using the argon doublet.

BrNO was prepared by reacting liquid Br_2 with an excess of NO, which was finally pumped away. ClNO and FNO were both commercial products (Matheson and Ozark Mahoning respectively).

5.4.3 Results

The PE spectra of these molecules are shown in Fig. 42 and the IP's are gathered in Table 13.

FNO The PE spectrum of FNO (Fig. 42a) consists of three featureless bands. The first band starts at 12.66 eV and has its vertical IP at 12.94 eV. It is relatively sharp compared to the other two bands. The second band is broad extending over 2.4 eV, and has an intensity almost twice

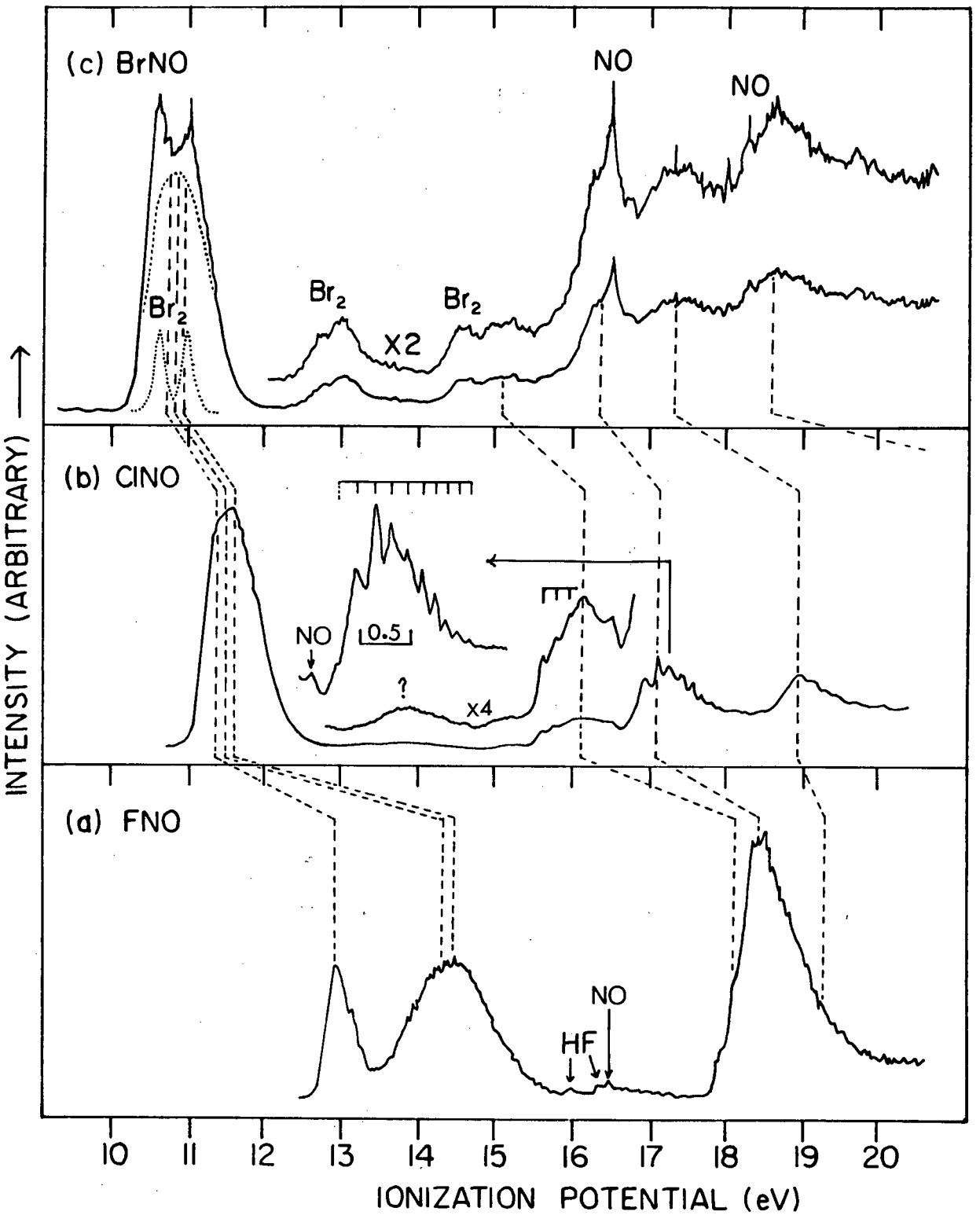
(c) BrNO
NO
NO
Br2
Br2
Br2
X2
(b) ClNO
NO
0.5
?
X4
(a) FNO
NO
HF
INTENSITY (ARBITRARY)
10
11
12
13
14
15
16
17
18
19
20
IONIZATION POTENTIAL (eV)

FIGURE 42

TABLE 13 PES Data for the Nitrosyl Halides (XNO)

	FNO	ClNO	BrNO
	Vertical IP (adiabatic) (eV)	Vertical IP (adiabatic) (eV)	Vertical IP (adiabatic) (eV)
1.	12.94(12.66)	11.5 (10.94)	10.9 (10.7)
2.	14.5 (13.5)	11.5	10.9
3.	14.5	11.5	10.9
4.	18.5 (17.85)	16.15(15.63)	15.12(14.7)
5.	19.0	17.13(16.95)	16.42(15.8)
6.	19.5 (?)	18.97(18.59)	17.41(16.8)
7.	--	--	18.66(18.0)

that of the first band. It commences at 13.5 eV and reaches its maximum at 14.5 eV. The third band is also broad and intense, with a spread of ca. 2 eV. The threshold and maximum of this band are at 17.85 and 18.5 eV respectively.

ClNO The PE spectrum of ClNO (Fig. 42b) shows four distinct bands with vibrational structure resolved on two of them. The first band is by far the most intense, with adiabatic and vertical IP's of 10.94 and 11.47 eV respectively. The second distinct band shows some vibrational fine structure, which disappears beyond the third component peak. The vibrational spacing averages 1380 ± 100 cm^{-1}. The adiabatic IP is at 15.63 eV while the vertical occurs at 16.15 eV. The third band extending from ca. 16.7 to 18.3 eV shows at least nine vibrational components, the spacing between them decreasing rapidly from 1370 to 930 cm^{-1}. The vertical IP is at 17.13 eV but the exact position of adiabatic IP at 16.95 eV is tentative because of a possible peak at 16.76 eV. The fourth band is featureless, with adiabatic and vertical IP's at 18.59 and 18.97 eV respectively. There is, in addition, a suggestion of an additional broad band at 13.8 eV, which is extremely weak relative to the other bands.

BrNO Although the PE spectrum of BrNO (Fig. 42c) is complicated by the presence of the bands due to Br_2 and NO, five bands of BrNO, all structureless, can be distinctly identified. The first band in the spectrum is due to a superimposition

of the bands of Br_2 and BrNO, which upon manual deconvolution gives the first band of BrNO (Fig. 42c) having adiabatic and vertical IP's at 10.17 and 10.9 eV respectively. In all respects, this band of BrNO is similar to the corresponding band of ClNO. The second band of BrNO is partially overlapped by the third band of Br_2, but its vertical IP can be confidently placed at 15.12 eV. The third band which is partly concealed by the intense peak of NO at 16.54 eV is estimated to have its vertical at 16.42 eV. The vertical IP's of the fourth and fifth bands are 17.41 and 18.66 eV respectively.

5.4.4 Discussion

To assist the assignment of the PE spectra, we have carried out CNDO type MO calculations for the nitrosyl halides. The results are collected in Table 14, which lists the symmetry, bonding character and energy of the individual MO. In addition, the ab initio calculations[228,229] on FNO are also included. All these calculations consistently indicate that the individual nitrosyl halides can be described quite concisely as a loosely bound combination of a halogen atom and a NO radical. More specifically, the XNO molecule can be treated as a collection of unperturbed doubly occupied halogen atomic orbitals and NO MO's with one true MO, i.e. 7a', formed from an almost equal admixture of halogen np and NO 2π orbital character.

ABLE 14 SCF-MO Results for the Nitrosyl Halides (XNO)

ymmetry	Bonding Character	IP(eV) =-MO energy						
		FNO				ClNO		BrNO
		Perturbation[a]	Ab-initio[b]	CNDO/2[c]	CNDO[d]	CNDO/2[c]	CNDO[d]	CNDO[d]
7a'	2π-NO(out of phase)+p_x-X	13.1	14.6	11.3	14.0	8.7	12.4	11.7
2a"	p_y-X	15.6	17.6	15.3	15.6	10.5	13.4	12.4
6a'	p_z-X	15.6	17.8	15.4	15.6	10.5	13.4	12.4
1a"	1π-NO(in phase)	19.1	21.4	19.2	16.7	18.3	15.7	15.2
5a'	5σ-NO(in phase)	19.7	21.6	19.4	16.9	18.4	16.1	15.6
4a'	1π-NO(in phase)	20.3	23.0	21.7	17.7	20.4	16.9	16.4
3a'	4σ-NO(out of phase)	23.5	27.8	24.8	26.9	23.7	24.2	23.3

) ref. 229. b) ref. 228. c) ref. 76; all IP's with 4 eV adjustment. d) ref. 232

In addition to the correlations with these theoretical results, the assignment of the PE spectra should also invoke the following considerations:

(1) In view of the localization of the halogen lone pairs, the reorganization energy is expected to be appreciable upon ionization. This is especially true for the fluorine lone pairs since a positively charged fluorine atom is particularly unstable, and thus tends to draw electrons from the NO moiety. Consequently, allowance for such an effect should be made when applying Koopmans' theorem to the theoretical results.

(2) Since the electronic structures of the three molecules are closely related, qualitative considerations lead one to expect that bands in the spectrum of BrNO should be shifted to lower IP's relative to the corresponding bands in the spectrum of ClNO, which should, in turn, be lower than those of FNO.

Based upon these considerations and, in addition, the relative band intensities, the spectra of the nitrosyl halides can be satisfactorily assigned as follows:

<u>FNO</u> The first band is to be associated with the 7a' orbital (the only true MO), whereas the second band is due to the almost degenerate, highly relaxed F lone pairs, 2a" and 6a'. While it is difficult to decide whether two or three IP's are to be associated with the third band, the band shape and

relative intensity tend to suggest that three IP's (1a", 5a' and 4a') are occurring here. This conclusion is also supported by the ab initio calculation with perturbation corrections to Koopmans' theorem[229] (Table 14).

<u>ClNO</u> The intense, first band is assigned to three IP's, the 7a' and the two Cl lone pairs, 2a" and 6a'. The second, third and fourth bands are respectively due to 1a", 5a' and 4a'. The vibrational structure observed in the second and third bands (1380 and 1200 cm^{-1} respectively) is a simple progression of ν_{NO} (1800 cm^{-1} in the neutral molecule[230]). The excitation of ν_{NO} and the decrease in frequency are to be expected in view of the bonding character of the respective MO's (Table 14). The sudden loss of the vibrational structure beyond $\nu' = 2$ in the second band is indicative of a dissociation process. The assignment of the weak band at 13.8 eV poses a problem. At the moment, we can only suggest several alternatives to explain this feature: - (1) The possibility of impurities is unlikely since the band exists with the same relative intensity in spectra obtained with different samples and its intensity appears to follow that of the other bands. (2) In view of the extremely weak intensity of the band and by comparing the individual spectra of the three nitrosyl halides, we do not expect a band arising from an 'allowed' single-step one-electron ionization to appear in this region. (3) Its

abnormal intensity and position tends to suggest that the band may be associated with a CI state.

BrNO Except for an additional band, the spectrum of BrNO is very similar to that of ClNO, and indeed it can be analyzed in a similar fashion. The first band is again due to three IP's, one from 7a' and two from the Br lone pairs, 2a" and 6a', while other bands are successively assigned to 1a", 5a', 4a' and 3a' orbitals.

The assignment of the bands due to the two halogen lone pairs to be part of the first band in the cases of ClNO and BrNO is supported by the following observations. (1) The region 12-14 eV in both cases is free of any bands that may be associated with Cl or Br lone pair IP's. As they are not anticipated to fall at an IP greater than 14 eV, they must have merged with the first (7a') band.(2) This is corroborated by the relative intensity of the first band in ClNO and BrNO, suggesting that this band is associated with more than one IP. (3) In addition the trend of all the IP's from the F through the Cl to the Br substituted compounds (see correlation lines in Fig. 42) is what is anticipated for the halogen series on electronegativity grounds.

Comparing the IP's of the halogen lone pairs in these molecules (F = 14.5 eV, Cl = 11.5 eV and Br = 10.9 eV) to their respective valence orbital ionization potentials

(F = 18.7 eV, Cl = 13.7 eV and Br = 12.4 eV)[231], one notes the large effect of reorganization upon ionization. The magnitude of this reorganization which is in the order, Br < Cl < F, is understandable on the basis of the difference of their electronegativities (Br < Cl < F), since the more electronegative halogen will tend to withdraw more electrons from the NO moiety, and thus gives rise to more reorganization upon ionization. In this respect, one has the case of FNO approaching the situation of F^-NO^+[227], thus resulting in an abnormally low IP (14.5 eV) for the F lone pairs, which are generally around 16 eV or higher (e.g. HF, the fluorine substituted methanes[3], SiF_4).

5.5 Nitric Acid (HNO_3) And Nitryl Halides (XNO_2, X = F, Cl)

5.5.1 Introduction

HNO_3 and its halogen substituted derivatives FNO_2 and $ClNO_2$ are extremely corrosive compounds and strong oxidants. They attack many metals and decompose readily. Hence, they appear to be appropriate contenders for the present spectrometer.

In view of the remoteness of the hydrogen atom from the NO_2 group in HNO_3 and the free rotation of the N-O(H) bond, the OH group may be quite concisely treated as a pseudo-halogen atom when the interaction between the OH and

NO_2 groups is considered. Thus, HNO_3 may be assumed to have C_{2v} symmetry in order to facilitate a comparison with the nitryl halides. In addition, these molecules are all of the same valence electronic structure, and thus are conveniently dealt with together.

5.5.2 Experimental

HNO_3 and $ClNO_2$ were run using the pyrex direct inlet, while the stainless steel inlet was used for FNO_2. All samples were immersed in an appropriate temperature bath (HNO_3 and $ClNO_2$ at -78°C, FNO_2 at -112°C) and had to be differentially pumped to reduce decomposition.

Pure HNO_3 was prepared by the reaction of dry sodium nitrate and ~ 100% sulfuric acid[233]. $ClNO_2$ was prepared by reacting chlorosulfonic acid with anhydrous HNO_3[234] available from the above procedure. FNO_2 was of commercial origin (Ozark Mahoning).

All spectra were recorded at least twice on separate days using fresh samples to ensure reproducibility of the spectra. Calibration was effected using the argon doublet.

5.5.3 Results

The PE spectra of the three molecules are shown in Figure 43, and the experimental results are tabulated in

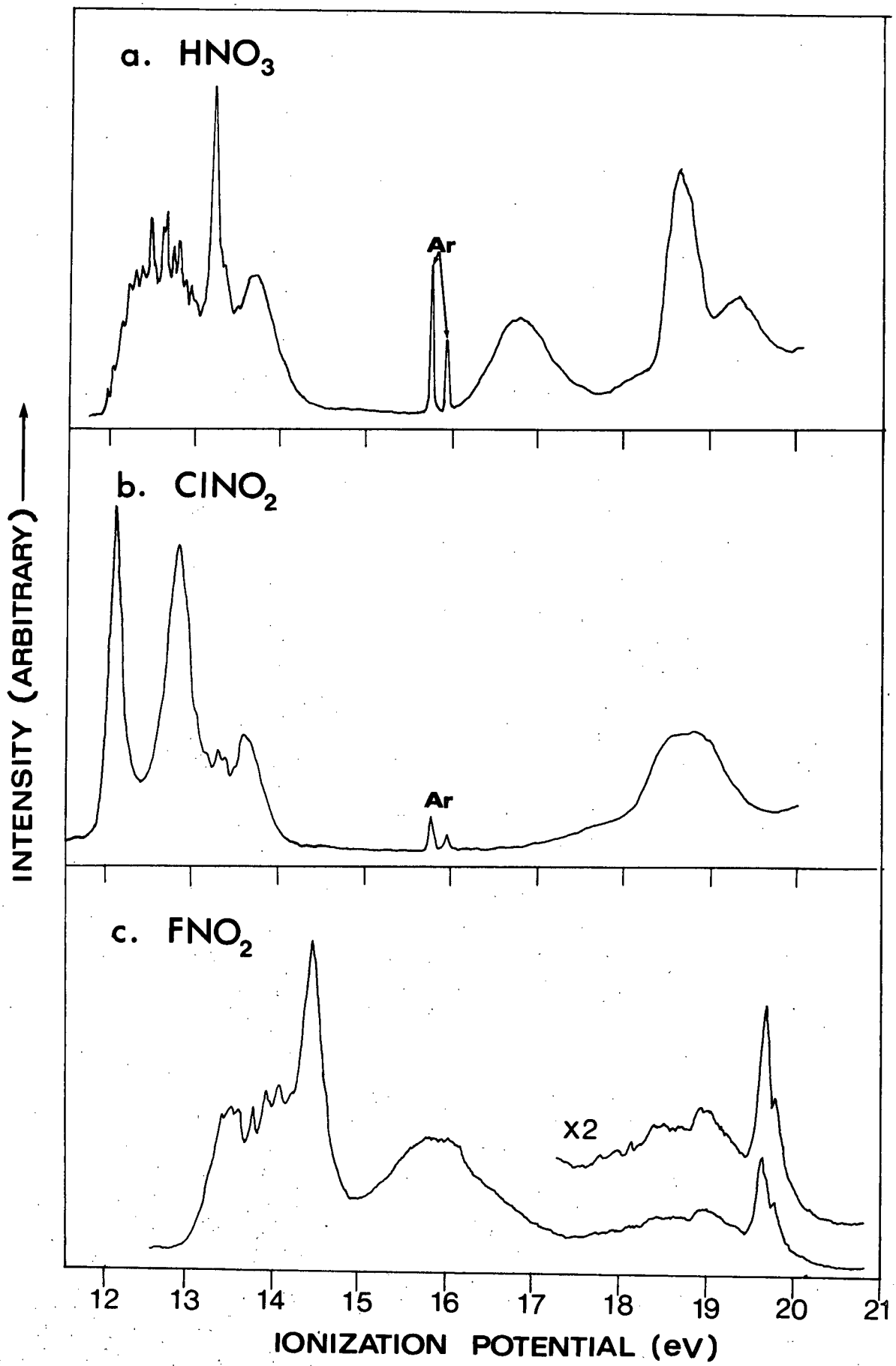
a. HNO3
Ar
b. ClNO2
Ar
c. FNO2
X2
INTENSITY (ARBITRARY)
12
13
14
15
16
17
18
19
20
21
IONIZATION POTENTIAL (eV)

FIGURE 43

Table 15.

<u>HNO_3</u> The PE spectrum of HNO_3 (Fig. 43a) shows evidence for at least eight IP's. There is extensive vibrational structure in the region between 12.0 and 13.1 eV (Fig. 44a), which can be identified as arising from three bands. The first band has an adiabatic IP of 11.96 eV and a vertical IP of 12.39 eV corresponding to the seventh peak. The extensive vibrational progression with an average spacing of 560 cm^{-1} probably corresponds to the ionization of a strongly bonding or antibonding electron. There is also strong evidence for another series starting at 1370 cm^{-1}. Here the vibrational spacing is again $\sim$ 560 cm^{-1}. Towards higher vibrational quantum number, the two series merge, and are then overlapped by the second and third bands. The second band (Fig. 44a) has an identical adiabatic and vertical IP of 12.49 eV and shows a simple progression with a fairly even spacing of 1060 cm^{-1}. The third band (Fig. 44a) resembles the second, with coincident adiabatic and vertical IP's at 12.63 eV. Here the vibrational series shows four discernible peaks, with once again a fairly even spacing of 1160 cm^{-1}. The fourth band with a coincident adiabatic and vertical IP at 13.23 eV is sharp and intense, most likely corresponding to the ionization of a nonbonding electron. This band shows a weak vibrational series with an average spacing of 840 cm^{-1}. The fifth band with a vertical

TABLE 15 PES and Theoretical Data for HNO_3, $ClNO_2$ and FNO_2

	PES		CNDO/2	
	Vertical IP (adiabatic) (eV)	Vibrational frequency (cm-1)	Orbital symmetry	Orbital energy* (eV)
HNO_3				
$^2A_1$	12.39(11.96)	560,1370(?)	$1a_2$	10.6(10.3)
$^2A_2$	12.49	1060	$5a_1$	11.7(11.0)
$^2B_2$	12.63	1160	$4b_2$	12.8(11.9)
$^2B_1$	13.23	840	$2b_1(O_H\text{-}P\pi)$	15.2(13.9)
$^2B_2$	13.70(13.4)		$3b_2(\sigma_{OH})$	16.5(15.2)
$^2B_1$	16.78(16.10)		$1b_1$	21.9(21.4)
$^2A_1$	18.63(18.36)		$4a_1$	21.3(19.9)
$^2B_2$	19.24(19.0)		$2b_2$	20.5(18.7)
			$3a_1$	24.1(23.3)
$ClNO_2$				
$^2B_2$, $^2B_1$	12.08(11.84)	420	$4b_2(Cl\text{-}P\sigma)$	12.5
			$2b_1(Cl\text{-}P\pi)$	12.6

TABLE 15 (cont'd) PES and Theoretical Data for HNO_3, $ClNO_2$ and FNO_2

	PES		CNDO/2	
	Vertical IP (adiabatic) (eV)	Vibrational frequency (cm^{-1})	Orbital symmetry	Orbital* energy (eV)
$^2A_2$	12.81(12.40)		$1a_2$	11.0
$^2A_1$	13.25(13.01?)	850	$5a_1$	10.3
$^2B_2$	13.62		$3b_2$	13.3
$^2B_1$, $^2A_1$, $^2B_2$	18.1 - 19.6		$1b_1$	21.0
			$4a_1$	20.9
			$2b_2$	19.2
			$3a_1$	23.0
FNO_2				
$^2A_2$	13.51(13.09)		$1a_2$	11.5(11.3)
$^2A_1$	13.91	1170	$5a_1$	13.2(12.7)
$^2B_2$	14.40(14.2)		$4b_2$	13.8(12.9)

TABLE 15 (cont'd) PES and Theoretical Data for HNO_3, $ClNO_2$ and FNO_2

	PES		CNDO/2	
	Vertical IP (adiabatic) (eV)	Vibrational frequency (cm^{-1})	Orbital symmetry	Orbital energy* (eV)
$^2B_2$	15.0 - 17.1		$3b_2$(F-Pσ)	17.6(16.3)
$^2B_1$			$2b_1$(F-Pπ)	17.8(16.9)
$^2B_1$	18.5(18.0)		$1b_1$	23.4(23.0)
$^2A_1$	18.9		$4a_1$	22.5(21.0)
$^2B_2$	19.60	1000	$2b_2$	21.6(20.0)
			$3a_1$	25.9(24.7)

* Values in brackets are INDO results; all IP's with 4 eV adjustment.

IP at 13.70 eV is broad and structureless. The next three bands with vertical IP's at 16.78, 18.63 and 19.24 eV respectively are again structureless.

<u>$ClNO_2$</u> The PE spectrum of $ClNO_2$ (Fig. 43b) shows five distinct bands. The first band (Fig. 44b) with a vertical IP at 12.08 eV is sharp, suggesting that the ionization of nonbonding electrons is involved. There is, however, some weak vibrational structure on this band, the average spacing between peaks being 420 cm^{-1}. The second band (Fig. 44b) with a vertical IP at 12.81 eV partially overlaps the third band and appears to have no structure. Because of this overlap, the adiabatic IP of the third band cannot be determined accurately, but is estimated at 13.01 eV. The vertical transition of the third band occurs at 13.25 eV, and the vibrational progression appears to be a simple series with an average spacing of 850 cm^{-1}. The fourth band at 13.62 eV, which partly overlaps with the third, appears to be structureless. The fifth band (Fig. 43b) at 18.7 eV separated by $\sim$ 4 eV from the first four bands, is fairly broad and intense, and thus probably corresponds to more than one IP.

<u>FNO_2</u> The PE spectrum of FNO_2 (Fig. 43c) exhibits six distinct bands. The first three bands overlap one another, and are shown at higher resolution in Fig. 44c. The vertical transitions of these three bands are at 13.51, 13.91 and

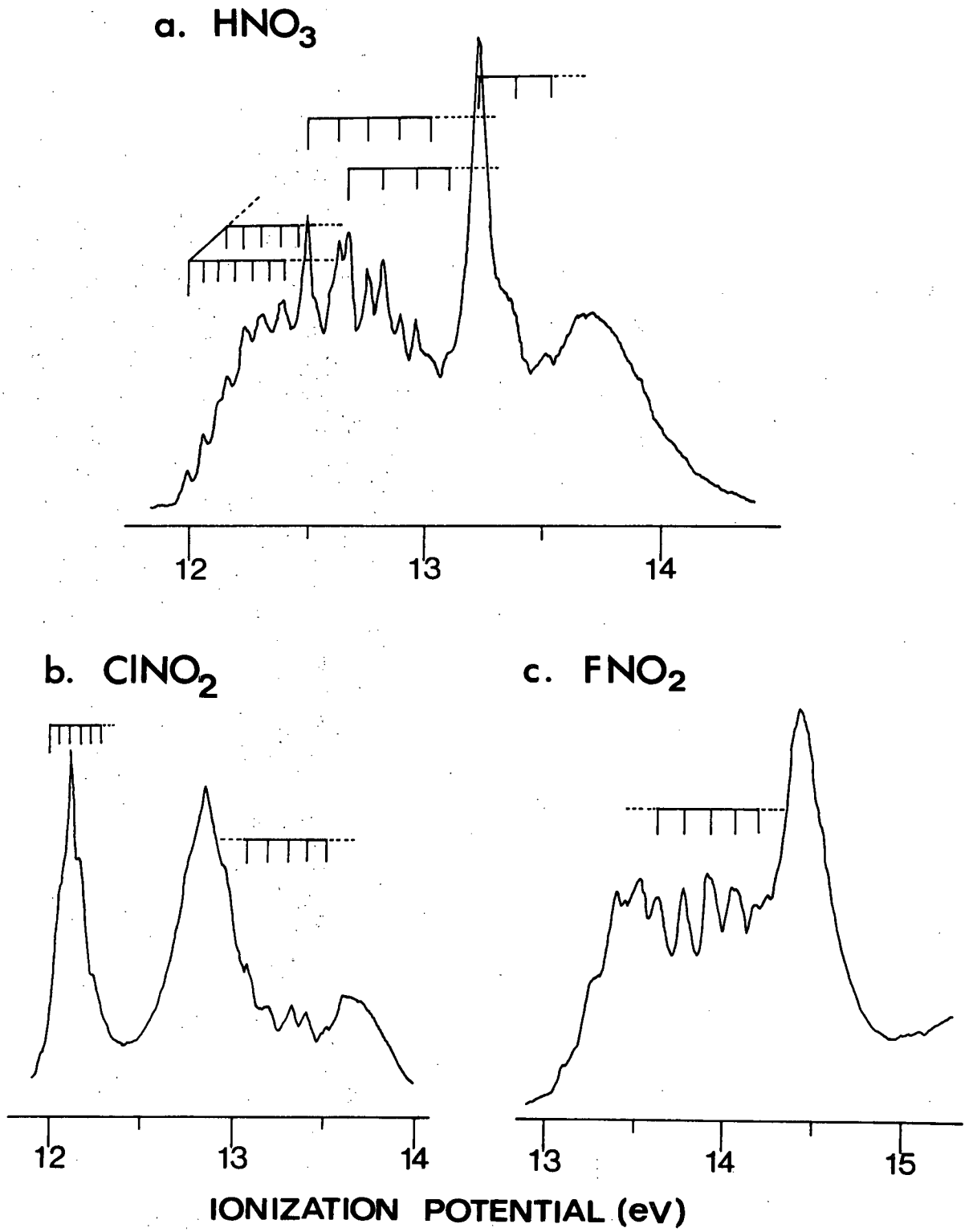
a. HNO3
12
13
14
b. ClNO2
12
13
14
c. FNO2
13
14
15
IONIZATION POTENTIAL (eV)

FIGURE 44

14.40 eV respectively. The overall shape of the first band definitely suggests the existence of some vibrational structure. However, because of the overlap from the second band, and the severe deterioration of resolution (presumably resulting from sample poisoning), it is impossible to be specific about the nature of this vibrational structure. Around the maximum of the second band a vibrational spacing of 1170 cm^{-1} is observed, but due to the overlap the 0-0 transition for this band cannot be measured. Judging from the FC envelope, this band appears to be fairly extensive, corresponding to the ionization of a fairly bonding or anti-bonding electron. The third band is quite sharp yet shows no structure. The fourth and fifth bands are both broad and featureless. The shape of the fifth band suggests that is may actually consist of two bands having vertical IP's of 18.5 and 18.9 eV respectively. The sixth band has an identical adiabatic and vertical IP of 19.60 eV and two higher vibrational peaks with an average spacing of 1000 cm^{-1}.

5.5.4. Discussion

The assignments for the PE spectra of these molecules are assisted by correlation with the known levels of NO_2[109,222], by consideration of the electronic effects of the X substituent, by using information from vibrational analysis, and by reference to the MO calculations.

The PE spectra of HNO_3, $ClNO_2$ and FNO_2 (Fig. 43)

can be conveniently divided into two regions. The first region refers to bands lying between 12-16 eV, while the other region considers bands above 16 eV. If the NO_2 group and the X substituent may be considered as separate moieties as in the case of XNO (section 5.4), then from a qualitative point of view we expect to find in the HeI spectra of XNO_2 approximately eight IP's. They correspond roughly to the six IP's from the NO_2 group and the two IP's from the X substituent, which are respectively the number of MO's capable of being ionized by HeI radiation (21.22 eV) in the individual moieties. The actual number of IP's observed may differ from the expected eight if interactions between the NO_2 and X moieties results in a lowering or raising of some of the originally accessible IP's. Furthermore, using the same kind of qualitative consideration it seems safe to expect that in the first region of the spectra there will be three IP's resulting from the ionization of the highest occupied (a_1, a_2 and b_2) MO's of NO_2, and two further IP's from the X substituent, i.e. a total of five IP's below ca. 16 eV. The two IP's coming from the halogen group correspond to the nearly degenerate $p_\sigma(b_2)$ and $p_\pi(b_1)$ lone pairs, and those for the OH group correspond to the single O lone pair and OH σ orbital.

The above expectations are corroborated by the CNDO/2 MO results (Table 15), in that the calculations

consistently predict that the individual spectra indeed separate into two regions with the first region having exactly five IP's. Furthermore, two of the first five IP's are mainly localized on X and the other three are predominantly from the NO_2 contribution.

Considering that the IP of the Cl lone pair in other Cl substituted compounds (Cl_2, CH_3Cl, ClNO etc.) normally falls between 11-12 eV, we may assign the first band (12.1 eV) of $ClNO_2$ to the essentially degenerate Cl lone pairs ($4b_2$ and $2b_1$). The sharpness of the band is consistent with the nonbonding character of the lone pair orbitals, and the general shape suggests the almost complete superimposition of two IP's. The weak vibrational excitation of 420 cm^{-1} may be assigned to the symmetric NO_2 bending mode, which is 411 cm^{-1} in the neutral molecule[235]. Similar considerations lead us to assign the broad band at 15.8 eV in FNO_2 to the two almost degenerate F lone pairs. The width of this band compared to that of the corresponding band of $ClNO_2$ may be accounted for by the dual facts that the two F lone pairs may have slightly different energies, and that appreciable reorganization occurs upon ionization. In the case of HNO_3, the sharp band at 13.23 eV is most likely due to the O lone pair ($2b_1$), while comparative energy considerations lead us to assign the featureless band at 13.70 eV to the OH σ orbital ($3b_2$). The energy separation (0.5 eV)

between these two IP's is surprisingly small compared to that of other OH containing compounds (e.g. 2.1 eV for H_2O). The low value for the σ OH ionization may be explained by the fact that the bond between O and H is highly ionic as reflected in the strong acidity of HNO_3, and thus less energy is required to remove an electron dwelling mainly on the O atom. On the other hand, the high IP for the O lone pair may be accounted for by the strong electron withdrawing ability of the NO_2 group. The vibrational structure (840 cm^{-1}) on the fourth band is most likely ν_2 (The N-OH stretch), which is 886 cm^{-1} in the neutral molecule[236].

As discussed above, the three other bands in the first region correspond to the three lowest occupied orbitals (a_1, a_2 and b_2) of NO_2. In NO_2 itself, the relative ordering of these orbitals is $a_1 < a_2 \sim b_2$. The orbital a_1 is strongly bonding all over the NO_2 group, a_2 is the non-bonding, antisymmetric combination of O p_π orbitals, and b_2 is antibonding. As a result, the PE band corresponding to the ionization of an electron from the a_1 orbital usually shows extensive vibrational structure. Taking this into account we are led to assign the first band (12.39 eV) of HNO_3, the third band (13.25 eV) of $ClNO_2$ and the second band (13.91 eV) of FNO_2 to the a_1 ionization, since all of them show extensive vibrational structure. In view of the bonding character of the a_1 orbital, the 560 and 1370 cm^{-1}

vibrational intervals on the first band of HNO_3 are then assigned to ν_3 (symmetric NO_2 bend) and ν_1 (symmetric N-O stretch), the corresponding frequencies in the neutral molecule being 675 and 1320 cm^{-1}[236]. Similarly, the 850 cm^{-1} vibrational interval on the third band of $ClNO_2$ and the 1170 cm^{-1} on the second band of FNO_2 are identified as ν_1, which is 1293[235] and 1312[237] cm^{-1} in the neutral states of $ClNO_2$ and FNO_2 respectively.

The relative ordering of the two remaining NO_2 type levels a_2 and b_2 presents somewhat of a problem, since in these cases vibrational analysis is not helpful. However, by reference to the calculations (Table 15), and by comparison with NO_2 itself, the a_2 level probably lies lower in energy than b_2. Consequently, the relative ordering of the NO_2 type levels is $a_1 < a_2 < b_2$ for HNO_3 and $a_2 < a_1 < b_2$ for $ClNO_2$ and FNO_2. In HNO_3 the vibrational structure associated with the second (a_2) and third (b_2) bands may be assigned to ν_1 (1320 cm^{-1} in the neutral molecule). The reverse ordering of the a_1 and a_2 levels in going from HNO_3 to $ClNO_2$ and FNO_2 is understandable in view of the electronic effects of the X substituents. Considering the bonding character of the a_1 and a_2 orbitals, we then expect the a_2 orbital (with no X character) to be the least perturbed, and the a_1 orbital to be appreciably affected. As a result, the a_1 orbital is more stable than the a_2 orbital in $ClNO_2$ and FNO_2.

Definitive assignments for the bands in the second region (> 16 eV) of the PE spectra are difficult. By analogy with NO_2[109,222], the tentative assignments are given in Table 15. In the second region, there are three bands in the spectra of HNO_3 and FNO_2, while only one broad band is observed for $ClNO_2$. Considering that the inductive effect of Cl is somewhere between that of OH and F, we should expect the same number of bands for $ClNO_2$. This expectation is well satisfied if the band of $ClNO_2$ lying between 18.1 - 19.6 eV is actually due to three overlapping bands. The vibrational excitation (1000 cm^{-1}) on the last band (19.6 eV) of FNO_2 is identified as ν_1 (1312 cm^{-1} in the neutral molecule), and is thus consistent with the strongly bonding character of the b_1 orbital.

Qualitative considerations of the ordering of the inductive effects of the substituents, i.e. OH < Cl < F, lead us to expect that the bands corresponding to the removal of electrons from orbitals mainly of NO_2 character should be shifted to higher IP's in the order HNO_3 < $ClNO_2$ < FNO_2. That this condition is satisfied is illustrated in the correlation diagram shown in Fig. 45, which lends further support to the assignments proposed here.

In the light of the present study, it seems pertinent to make a few comments on the PE spectra of CH_3NO_2[238], which has similar electronic structure to the

XNO_2 molecules. First, in drawing an analogy between NO_2 and CH_3NO_2, Rabalais[238] makes no mention of the bands that may be due to the CH_3 group. If this is done, then the six IP's observed would be all that should be expected in the PE spectrum of CH_3NO_2. However, by considering the smaller inductive effect of the CH_3 group compared to that of the OH group, and further, assuming the above considerations for the band positions to hold, we are tempted to suggest that two IP's have not been identified in the HeI PE spectrum of CH_3NO_2 (Fig. 45). Moreover, the existence of two additional IP's are further suggested by the INDO MO calculations[238], which predicts eight IP's below 21 eV for CH_3NO_2. Secondly, the assignment[238] of the third band in the spectrum of CH_3NO_2 at 14.73 eV as due to the $4b_2$ ionization conflicts with our qualitative picture, and thus appears to be unrealistic since the $^2B_2$ state of $CH_3NO_2^+$ lies higher in energy than in any other related XNO_2 molecule as shown in Fig. 45. In this respect, we also note that the calculations (Table 15 and ref. 238) predict the NO_2 type b_2 orbital in CH_3NO_2 has the smallest absolute energy in the XNO_2 series. In view of these apparent discrepancies, the following amendments may be proposed:- In order for the spectrum of CH_3NO_2 to correlate well with those of the other XNO_2 molecules (Fig. 45), two additional IP's are required. Inspection of Rabalais' spectrum suggests one additional band may be

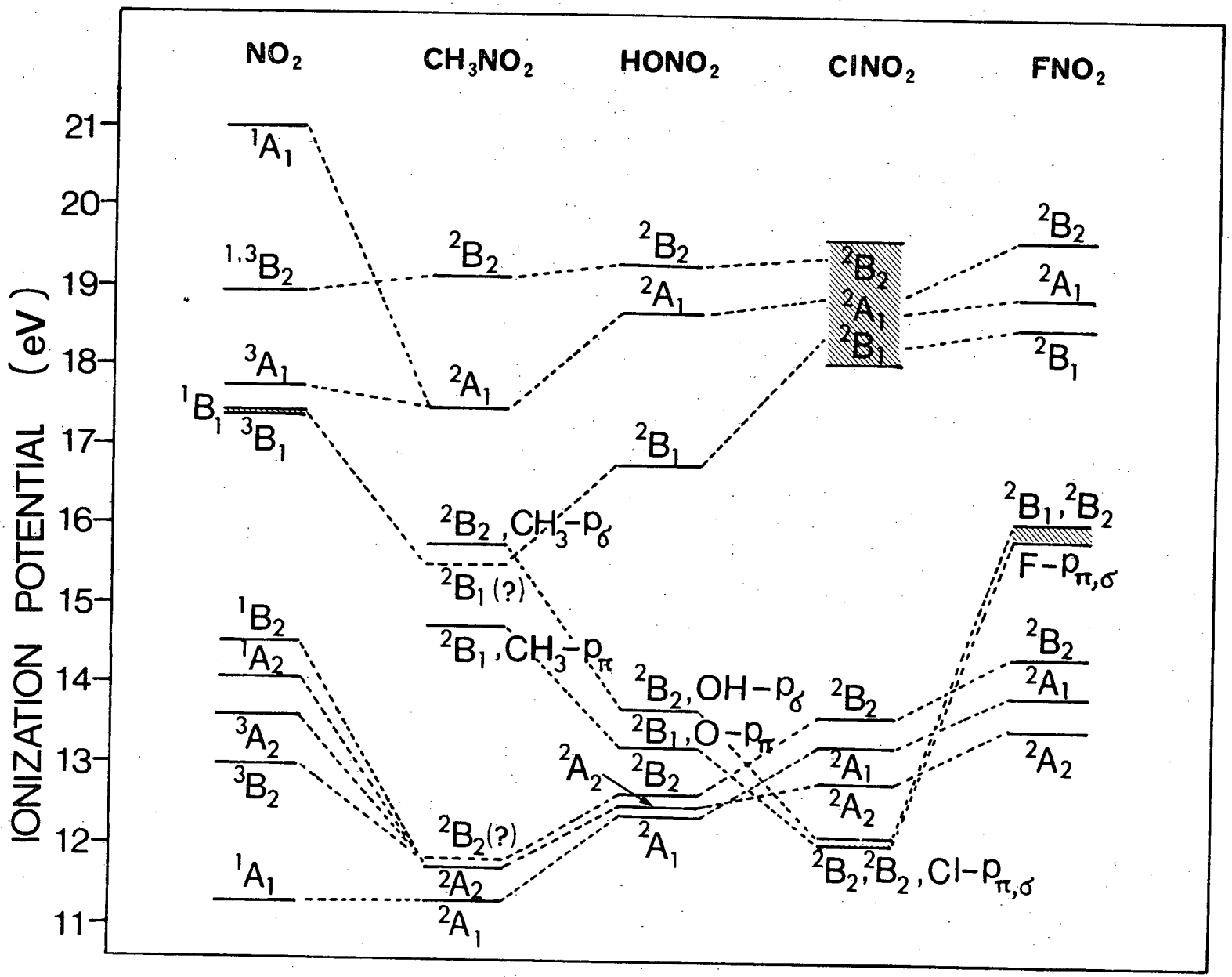
NO2
CH3NO2
HONO2
ClNO2
FNO2
IONIZATION POTENTIAL (eV)
21
20
19
18
17
16
15
14
13
12
11
1A1
1,3B2
3A1
1B1
3B1
1B2
1A2
3A2
3B2
1A1
2B2
2A1
2B2, CH3-pσ
2B1 (?)
2B1, CH3-pπ
2B2(?)
2A2
2A1
2B2
2A1
2B1
2B2, OH-pσ
2B1, O-pπ
2A2
2B2
2A1
2B2
2A1
2A2
2B2, 2B2, Cl-pπ,σ
2B2
2A1
2B1
2B1, 2B2
F-pπ,σ
2B2
2A1
2A2

FIGURE 45

found underneath the first or second band, and another under the strong third or fourth band. The first of these two new bands would then be identified as due to the $4b_2$ level. The assignments for the five bands above 14 eV would be facilitated by the identification of bands due to the CH_3 group as in the case of other XNO_2. By comparison with CH_4[3] and the methyl halides[3], the bands corresponding to ionization from the CH_3 group probably lie between 14-16 eV. With these amendments the resulting assignments for the spectrum of CH_3NO_2 are shown in Fig. 45, and indicate satisfactory correlation with the other molecules. It is further noted that the proposed assignments are also in complete agreement with the calculations[238].

CHAPTER SIX

CONCLUSION

The results presented in this study have shown that the PE spectrometer can be successfully used to study transient species and reactive molecules, and that PES provides invaluable information on the molecular electronic structure of these systems, information that is difficult to obtain by any other spectroscopic techniques. Work is in progress to extend the range of transient species that can be studied by this technique. In this respect, we note that the principal requirement for a successful study is the formation of a sufficient concentration of the species of interest in the ionization region. The ultimate concentration of the species is mainly limited by its lifetime and the efficiency with which the species is produced. The limitation imposed by the lifetime can usually be alleviated by fast pumping, forming the species into a molecular beam, or by producing the species right in the ionization region. This leaves the efficiency of producing the species as the crucial factor for a successful study. Thus, the spectra

of the atomic species O, N, H and F (section 3.4) have been obtained whereas, those of BF and HNO, which have longer lifetimes, have so far evaded our detection. In addition to the sensitivity of the PE spectrometer, the lowest limit of the necessary concentration for detection is further determined by the photoionization cross section of the species, and by the extent of overlap in the PE spectrum. This latter point may be serious in systems in which we are trying to produce modifications by, say, discharge or pyrolysis, and where the products and reactants have IP's of similar energies. However under favorable conditions, concentrations as low as a few per cent (as in the case of N atoms) may be detected.

Work is also in progress to use the high temperature pyrolysis unit (section 3.3.4.d) and the variable temperature unit (section 3.3.4.e), which have so far been only tested, to study some practical systems. For the high temperature unit, the following projects are presently underway.

(1) $S_8 \xrightarrow{800°C} S_2$ (ref. 239)

(2) $CCl_4 \xrightarrow{800°C} CCl_3$ (ref. 240)

(3) $CBr_4 \xrightarrow{800°C} CBr_3$ (ref. 240)

$\xrightarrow{1200°C} CBr_2$ (ref. 241)

(4) $CH_3NH_2 \xrightarrow{1200°C} CH_2{=}NH$ (ref. 242)

(5) 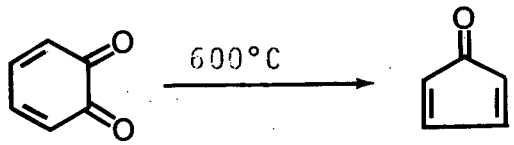

(ref. 243)

The study of the equilibrium between NO_2 and N_2O_4 at variable temperature is proceeding, as well as work on the conformational analysis of oxalyl halides[244] by the use of the variable temperature unit.

The present study has also revealed a further aspect of PES which merits immediate attention, i.e. the use of PES for in-situ analysis of dynamic chemical systems. The potential of PES for such studies has been exemplified in the study of the systems of SO-S_2O-SO_2 (section 4.2) and N_2H_2-NH_3-HCl (section 4.4). With a knowledge of the (relative) photoionization cross sections of molecules (which may also be available by specific PE studies), such analysis by PES can be quantitative as well as qualitative. The capability of continuously monitoring the system of interest, together with the simplicity and speed of the operation is a great advantage, and PES promises to be a potential tool for analysis of such dynamic systems.

In the study of transient species, the positive identification of the bands due to species of interest is usually a problem, since other species are also present by virtue of the methods of production. The techniques that can be applied in this respect involve comparison

with molecules of similar electronic structure (e.g. SO), with MO calculations, the judicial use of the chemical properties of the species (e.g. N_2H_2), and methods of producing the species by alternative routes to be certain of identification (e.g. S_2O, N_2H_2). Even so, unequivocal identification of the molecule is very often difficult. A further advance would be the use of the mass spectrometer in conjunction with the PE spectrometer to detect the molecular ions in coincidence with the photoelectrons. This would greatly simplify the procedure, and enable one to be certain of the origin of an electron of a particular energy.

REFERENCES

1. K. Siegbahn, C. Nordling, A. Fahlman, R. Nordberg, K. Harmin, J. Hedman, G. Johansson, T. Bergmark, S. Karlsson, I. Lindgren, and B. Lindgren, Electron Spectroscopy for Chemical Analysis. Nova Acta Regiae Socientatis Scientiorum Uppsaliensis Ser. IV, Vol. 20, 1967.

2. K. Siegbahn, C. Nordling, G. Johansson, J. Hedman, P. F. Heden, K. Harmin, U. Gelius, A. T. Bergmark, L. O. Werme, R. Manne and Y. Baer, ESCA Applied to Free Molecules. North-Holland, Armsterdam, 1970.

3. D. W. Turner, A. D. Baker, C. Baker and C. R. Brundle, High Resolution Molecular Photoelectron Spectroscopy. John Wiley, New York, 1970.

4. K. Siegbahn, in Electron Spectroscopy (D. A. Shirley, ed.), P. 17, North-Holland, Armsterdam, 1972.

5. G. R. Parr and J. W. Taylor, Analy. Chem. 44, 1578 (1973).

6. W. L. Stebbing and J. W. Taylor, Int. J. Mass Spectrum. Ion Phys. 9, 471 (1972).

7. M. O. Krause, Chem. Phys. Lett. 10, 65 (1971).

8. A. Einstein, Ann. d. Physik 17, 132 (1905); 20, 199 (1906).

9. F. I. Vilesov, B. L. Kurbatov and A. N. Terenin, Sov. Phys.-Dokl. 6, 490 (1961); 6, 883 (1962).

10. M. E. Akopyan, F. I. Vilesov and A. N. Terenin, Sov. Phys.-Dokl. 6, 890 (1962).

11. B. L. Kurbatov and F. I. Vilesov, Sov. Phys.-Dokl. 6 1091 (1962).

12. M. I. Al-Joboury and D. W. Turner, J. Chem. Phys. 37, 3007 (1962); J. Chem. Soc., 5141 (1963); 4434 (1964).

13. A. D. Baker and D. Betteridge, Photoelectron Spectroscopy: Chemical and Analytical Aspects. Pergamon Press, Oxford, 1972

14. A. D. Baker and C. R. Brundle, Ionizing Photon Impact Phenomena. Academic Press, in preparation.

15. D. W. Turner, in Molecular Spectroscopy (P. Hepple, ed.), p. 209. Institute of Petroleum, London, 1968

16. W. C. Price, in Molecular Spectroscopy (P. Hepple, ed.), p. 221, Institute of Petroleum, London, 1968.

17. C. R. Brundle and M. B. Robin, in Determination of Org. Struct. by Phys. Methods (F. A. Nachod and J. J. Juckerman, eds.), p. 1. Academic Press, N. Y., 1971.

18. D. A. Shirley, Adv. Chem. Phys. 23, 85 (1973).

19. D. W. Turner, Adv. Mass Spectrom. 4, 755 (1968).

20. D. W. Turner, Adv. Phys. Org. Chem. 4, 31 (1966).

21. D. W. Turner, in Phys. Methods in Adv. Inorg. Chem. (H. A. O. Hill and P. Day, eds.), p.74. John Wiley, New York, 1968.

22. D. W. Turner, Chem. Brit. 4, 435 (1968).

23. W. C. Price, Endeavour 26, 78 (1967).

24. R. S. Berry, Ann, Rev. Phys. Chem. 20, 357 (1969).

25. D. Betteridge and A. D. Baker, Analy. Chem. 42, 43A (1970).

26. A. D. Baker, Acc. Chem. Res. 3, 17 (1970).

27. D. M. Hercules, Analy. Chem. 42, 20 (1970).

28. S. D. Worley, Chem. Rev. 71, 295 (1971).

29. J. Hollander and W. L. Jolly, Acc. Chem. Res. 3, 193 (1970).

30. C. E. Brion, in MTP Int. Rev. of Sci., Phys. Chem. (A. Maccol, ed.) Ser. 1, Vol. 5. Butterworth, London, 1972.

31. H. Bock and B. G. Ramsay, Angew. Chem. (internat. edit.) 12, 734 (1973).

32. W. E. Swartz, Jr., Analy. Chem. 45, 788A (1973).

33. C. S. Fadley, "Theoretical Aspects of X-ray Photoelectron Spectroscopy", N.A.T.O. Adv. Study Institute on Electron Spectroscopy, Ghent University, Ghent, Belgium, Aug. 28-Sept. 8, 1972.

34. A. D. Baker, C. R. Brundle and M. Thompson, Quarterly Rev. p.355, The Chem. Soc., London, 1972.

35. A. Hamnett and A. F. Orchard, in Electronic Structure and Magnetism of Inorganic Compounds, p.1. The Chem. Soc., London, 1970.

36. S. Evans and A. F. Orchard, in Electronic Structure and Magnetism of Inorganic Compounds, p.1. The Chem. Soc., London, 1971.

37. C. Nordling, Angew. Chem. (internat. ed.) 11, 83 (1972).

38. "A Discussion on Photoelectron Spectroscopy" in Phil. Trans. of the Roy. Soc. London, 268, 1 (1970).

39. "General Discussion on the Photoelectron Spectroscopy of Molecules" in Fara. Dis. 54, 1 (1972).

40. D. A. Shirley, ed., Electron Spectroscopy. North-Holland, Armsterdam, 1972.

41. International Conference on Electron Spectroscopy, Namur, Belgium, April 16-19, 1974.

42. T. A. Carlson, in Electron Spectroscopy (D. A. Shirley, ed.), p.53. North-Holland, Armsterdam, 1972.

43. Commercial spectrometers are manufactured in U.S.A. by McPherson Instrument Corp. and Hewlett-Packard Co.; in Britain by Perkin-Elmer Corp., A.E.I. Ltd. and Vacuum Generators Ltd.; and in Japan by Japan Applied Spectroscopy Co..

44. N. Jonathan, A. Morris, D. J. Smith and K. J. Ross, Chem. Phys. Lett. 7, 497 (1970).

45. N. Jonathan, D. J. Smith and K. J. Ross, J. Chem. Phys. 53, 3758 (1970).

46. N. Jonathan, A. Morris, K. J. Ross and D. J. Smith, J. Chem. Phys. 54, 4954 (1971).

47. N. Jonathan, A. Morris, K. J. Ross and D. J. Smith, Chem. Phys. Lett. 9, 317 (1971).

48. A. B. Cornford, D. C. Frost, F. G. Herring and C. A. McDowell, J. Chem. Phys. 54, 1872 (1971).

49. T. Koopmans, Physica 1, 104 (1933).

50. J. Franck, Faraday Soc. 21, 536 (1926).

51. E. U. Condon, Phys. Rev. 28, 1182 (1926); 32, 858 (1928).

52. R. N. Dixon, J. N. Murrel and B. Narayan, Mol. Phys. 4, 611 (1971).

53. J. L. Berkosky, F. O. Ellision, T. H. Lee and J. W. Rabalais, J. Chem. Phys. 59, 5342 (1973).

54. J. W. Rabalais and A. Katrib, Mol. Phys. 27, 923 (1974).

55. G. W. Mines and R. K. Thomas, Proc. Roy. Soc. A336, 355 (1974).

56. J. W. Rabalais, L. Karlsson, L. O. Werme, T. Bergmark and K. Siegbahn, J. Chem. Phys. 58, 3370 (1973).

57. J. W. Rabalais, T. Bergmark, L. O. Werme, L. Karlsson and K. Siegbahn, Physica Scripts 3, 13 (1971).

58. D. C. Frost, A. Katrib, C. A. McDowell and R. A. N. Mclean, Int. J. Mass Spectrom. Ion Phys. 7, 485 (1971).

59. R. N. Dixon, G. Dusbury, M. Horani and J. Rostas, Mol. Phys. 22, 977 (1971).

60. D. Chadwick, A. B. Cornford, D. C. Frost, F. G. Herring, A Katrib, C. A. McDowell and R. A. N. Mclean, in Electron Spectroscopy (D. A. Shirley, ed.), p. 453. North-Holland, Armsterdam, 1972.

61. A. D. Baker, D. Betteridge, N. R. Kemp and R. E. Kirby, Analy. Chem. 43, 375 (1971).

62. C. R. Brundle, M. B. Robin, N. A. Kuebler and H. Basch, J. Am. Chem. Soc. 94, 1451 (1972).

63. C. R. Brundle, M. B. Robin and N. A. Kuebler, J. Am. Chem. Soc. 94, 1466 (1972).

64. W. C. Price. A. W. Potts and D. G. Streets, in Electron Spectroscopy (D. A. Shirley, ed.), p. 187. North-Holland, Armsterdam, 1972.

65. M. B. Robin, N. A. Kuebler and C. R. Brundle, in Electron Spectroscopy (D. A. Shirley, ed.), p. 351. North-Holland, Armsterdam, 1972.

66. A. Schweig and W. Thiel, J. Chem. Phys. 60, 951 (1974).

67. W. Thiel and A. Schweig. Chem. Phys. Lett. 16, 409 (1972).

68. W. Thiel and A. Schweig, Chem. Phys. Lett. 12, 49 (1971).

69. L. L. Lohr and M. B. Robin, J. Am. Chem. Soc. 92, 7241 (1970).

70. T. A. Carlson, G. E. McGuire, A. E. Jonas, K. L. Cheng, C. P. Anderson, C. C. Lu and B. P. Pullen, in Electron Spectroscopy (D. A. Shirley, ed.), p. 207. North-Holland, Armsterdam, 1972.

71. T. A. Carlson and C. P. Anderson, Chem. Phys. Lett. 10, 561 (1971).

72. R. G. Parr. Quantum Theory of Molecular Electronic Structure. Benjamin, New York, 1974.

73. P. O. Löwdin, Adv. Chem. Phys. 2, 207 (1959).

74. H. Basch, M. B. Robin, N. A. Kuebler, C. Baker and D. W. Turner, J. Chem. Phys. 51, 52 (1969).

75. C. R. Brundle, D. W. Turner, M. B. Robin and H. Basch, Chem. Phys. Lett. 3, 292 (1969).

76. J. A. Pople and D. L. Beveridge, Approximate Molecular Orbital Theory. McGraw Hill, New York, 1970.

77. M. J. S. Dewar, The Molecular Orbital Theory of Organic Chemistry. McGraw Hill, New York, 1969.

78. R. Hoffman, J. Chem. Phys. 39, 1397 (1962); 40, 2474, 2480, 2745 (1964); Tetrahedron 22, 521, 539 (1966).

79. D. W. Davies, Chem. Phys. Lett. 2, 173 (1968).

80. P. E. Cade, K. D. Sales and A. C. Wahl, J. Chem. Phys. 44, 1973 (1966).

81. A. B. Cornford, D. C. Frost, C. A. McDowell, J. L. Ragle and I. A. Stenhouse, J. Chem. Phys. 54, 2651 (1971).

82. D. R. Lloyd and N. Lynaugh, in Electron Spectroscopy (D. A. Shirley, ed.), p. 445. North-Holland, Armsterdam, 1972.

83. A. Veillard, Chem. Comm. 1022; 1427 (1969).

84. M. M. Rohmer and A. Veillard, Chem. Comm. 250 (1973).

85. W. G. Laidlaw and F. W. Birss, Theoret. Chim. Acta 2, 181 (1964).

86. F. W. Birss and W. G. Laidlaw, Theoret. Chim. Acta 2, 186 (1964).

87. W. G. Richards, Int. J. Mass Spectrom. and Ion Phys. 2, 419 (1969).

88. F. Brogli, P. A. Clark, E. Heilbronner and M. Neuenschwander, Angew. Chem. (internat. edit.) 12, 422 (1973).

89. L. S. Cederbaum, G. Hohlneicher and S. Peyerimhoff, Chem. Phys. Lett. 11, 421 (1971).

90. F. Ecker and G. Hohlneicher, Theoret. Chim. Acta 25, 289 (1972).

91. G. Hohlneicher, F. Ecker and L. S. Cederbaum, in Electron Spectroscopy (D. A. Shieley, ed.), p. 647. North-Holland, Armsterdam, 1972.

92. L. S. Cederbaum, G. Hohneicher and W. von Niessen, Chem. Phys. Lett. 18, 503 (1973).

93. L. S. Cederbaum, G. Hehlneicher and W. von Niessen, Mol. Phys. 26, 1405 (1973).

94. L. S. Cederbaum, Theoret. Chim. Acta 31, 239 (1973).

95. B. Kellerer, L. S. Cederbaum and G. Hohlneicher, J. Elect. Spect. 3, 107 (1974).

96. L. S. Cederbaum, Chem. Phys. Lett. 25, 562 (1974).

97. R. D. Mattuck, A Guide to Feynman Diagrams in the Many-Body Problem. McGraw Hill, New York, 1967.

98. K. F. Freed, Ann. Rev. Phys. Chem. 22, 313 (1971).

99. B. T. Pickup and O. Govcinski, Mol. Phys. 26, 1013 (1973).

100. D. P. Chong, F. G. Herring and D. McWilliam, Chem. Phys. Lett. 25, 568 (1974).

101. D. P. Chong, F. G. Herring and D. McWilliam, J. Chem. Phys. 61, 478 (1974) and others in press.

102. J. O. Hirschfelder, W. B. Brown and S. T. Epstein, Adv. Quant. Chem. 1, 255 (1964).

103. G. Berthier, in Molecular Orbitals in Chemistry, Physics and Biology (P. O. Löwdin and B. Pullman, eds.),

p. 57. Academic, New York, 1964.

104. C. C. J. Roothaan, Rev. Mod. Phys. 32, 179 (1960).

105. C. C. J. Roothaan, Rev. Mod. Phys. 23, 69 (1951).

106. J. A. Pople and R. K. Nesbet, J. Chem. Phys. 22, 571 (1954).

107. A. B. Cornford, D. C. Frost, F. G. Herring and C. A. McDowell, J. Chem. Phys. 54, 1872 (1971).

108. A. B. Cornford, D. C. Frost, F. G. Herring and C. A. McDowell, Chem. Phys. Lett. 10, 345 (1971).

109. C. R. Brundle, D. Neuman, W. C. Price, D. Evans, A. W. Potts and D. G. Streets, J. Chem. Phys. 53, 705 (1970).

110. M. Born and R. Oppenheimer, Ann. Physik 84, 457 (1927).

111. G. Herzberg, Molecular Spectra and Molecular Structure, Vol. 1, second ed., p. 203. Von Nostrand, New York, 1950.

112. D. P. Craig, J. Chem. Soc. 2146 (1950).

113. J. B. Coon, R. E. Dewanes and C. M. Loyd, J. Mol. Spect. 8, 285 (1962).

114. W. L. Smith and P. A. Warsop, Trans. Fara. Soc. 64, 1165 (1968).

115. T. Anno and A. Sado, J. Chem. Phys. 32, 1611 (1960).

116. T. E. Sharp and H. M. Rosenstock, J. Chem. Phys. 41, 3453 (1964).

117. F. Duschinsky, Acta Physicochim.U.R.S.S. 7, 551 (1937).

118. E. B. Wilson, J. C. Decius and P. C. Cross, Molecular Vibrations. McGraw Hill, New York, 1955.

119. F. Ansbacher, Z. Naturforsch. 14a, 889 (1959).

120. E. A. Hylleraas. Z. Physik 48, 469 (1928).

121. J. C. Lorquet and C. Cadet, Int. J. Mass Spect. Ion Phys. 7, 245 (1971).

122. L. C. Lorquet and M. Desouter, Chem. Phys. Lett. 16, 136 (1972).

123. R. N. Dixon and S. E. Hull, Chem. Phys. Lett. 3, 367 (1969).

124. M. Okuda, Dis. Fara. Soc. 54, 140 (1972).

125. M. Okuda and N. Jonathan, J. Elect. Spect. 3, 19 (1974).

126. S. Cradock and W. Duncan, Mol. Phys. 4, 837 (1974).

127. D. C. Frost, S. T. Lee and C. A. McDowell, J. Chem. Phys. 59, 5484 (1973).

128. A. W. Potts and T. A. Williams, J. Elect. Spect. 3, 3 (1974).

129. G. Herzberg and E. Teller, Z. Physik. Chem. B21, 410 (1933).

130. D. W. Turner, Proc. Roy. Soc. (London) A307, 15 (1968).

131. J. A. R. Samson, Rev. Sci. Inst. 40, 1174 (1969).

132. O. Edqvist, E. Lindholm, L. E. Selin and L. Åsbrink, Physica Scripta 1, 25 (1970).

133. L. Moore, Brit. J. Appl. Phys., (1968), p. 237.

134. S. G. Rautian, Soviet Phys.--Uspekhi, 66, 245 (1958).

135. G. G. Petrash, in Research in Molecular Spectroscopy (D. V. Skobeltsyn, ed.), p. 3. Proc. of the P. N. Lebedev Phys. Int., Vol. 27, 1965.

136. J. D. Morrison, J. Chem. Phys. 39, 200 (1963).

137. R. G. Dromey, J. D. Morrison and J. B. Peel, Chem Phys. Lett. 23, 30 (1973).

138. A. B. Cornford, Ph. D. Thesis, The University of Brithish Columbia, 1971.

139. H. Boersch, J. Geiger and W. Stickler, Z. Physik. 180, 415 (1964).

140. T. Ichinokawa, Japan J. Appl. Phys. 7, 739 (1968).

141. E. M. Purcell, Phys. Rev. 54, 818 (1938).

142. J. A. Simpson, Rev. Sci. Inst. 35, 1698 (1964).

143. A. M. Skerbele and E. N. Lassettre, J. Chem Phys. 40, 1271 (1964).

144. J. A. Simpson and C. E. Kuyatt. J. Appl. Phys. 37, 3805 (1966).

145. C. E. Kuatt and J. A. Simpson, Rev. Sci. Inst. 38, 103 (1967).

146. H. Z. Sar-El, Rev, Sci, Inst. 41, 561 (1970).

147. M. Zelikott, P. H. Wychoff, C. M. Anshenbrand and R. S. Loomis, J. Opt. Soc. Amer. 42, 818 (1952).

148. D. A. Vroom, Ph. D. Thesis, The University of British Columbia, 1966.

149. J. A. R Samson, Techniques of Vacuum Ultraviolet Spectroscopy. Wiley, New York, 1967.

150. T. R. Dyke, B. J. Howard and W. Klemperer, J. Chem. Phys. 56, 2442 (1972).

151. a. L. C. Martin, Proc. Roy. Soc. (London) A89, 127 (1913).

b. W. Jevons, Proc. Roy. Soc. (London) A117, 351 (1928).

c. F. H. Crawford and W. A. Shurcliff, Phys. Rev. 45, 860 (1934).

d. V. Kondratiev, Compt. rend. U.S.S.R. 20, 547 (1938).

e. G. Porter, Proc. Roy. Soc. (London) A200, 284 (1950).

f. R. F. Barrow, Dis. Fara. Soc. No. 9, 81 (1950).

g. P. J. Dyne and D. A. Ramsay, J. Chem. Phys. 20, 1055 (1952).

h. R. C. Mockler and G. R. Bird, Phys. Rev. 96, 1837 (1955).

i. S. J. Silvers, T. H. Bergeman and W. Klemperer, J. Chem. Phys. 52, 4385 (1970).

j. R. J. Donovan, D. Husain and C. G. STevenson, Trans. Faraday Soc. 66, 1 (1970).

k. R. W. Field and T. H. Bergeman, J. Chem. Phys. 54, 2936 (1971).

152. a. H. D. Smith and J. P. Blewett, Phys. Rev. 46, 276 (1934).

b. L. P. Blanchard and P. Legoff, Can. J. Chem. 35, 89 (1951).

153. a. N. Jonathan, A. Morris, M. Okuda, D. J. Smith and K. J. Ross, Chem. Phys. Lett. 13, 334 (1972).

b. G. H. King, H. W. Kroto and R. J. Suffolk, ibid., 13, 45 (1972).

154. After the completion of this work, a similar study was also reported by N. Jonathan, A. Morris, M. Okuda, K. J. Ross and D. J. Smith, Faraday Discussions 54, 48 (1972).

155. B. McCarroll, Rev. Sci. Instr., 41, 279 (1970).

156. Marcel Horani, Private Communication.

157. E. Lindholm, Arkiv Fysik, 40, 11 (1969).

158. W. G. Richards, Trans. Faraday Soc. 63, 530 (1967).

159. N. Jonathan, A. Morris, M. Okuda, D. J. Smith, and K. J. Ross, in Electron Spectroscopy (D. A. Shirley, ed.), p. 345. North-Holland. Publ. co., Armsterdam. 1972.

160. D. C. Frost, S. T. Lee and C. A McDowell, Chem. Phys. Lett. 17, 153 (1972).

161. D. C. Frost, S. T. Lee and C. A McDowell, Chem. Phys. Lett. 22, 243 (1973).

162. C. E. Moore, Ionization Potentials and Ionization Limits Derived from the Analysis of Optical Spectra. NSRDS-NBS 34, Sept. 1970

163. P. W. Schenk and R. Steudel, Angew. Chem. (internat. edit,) 4, 402 (1965).

164. Ref. 2, Appendix D.

165. A. V. Jones, J. Chem. Phys. 18, 1263 (1950) and ref. therein.

166. D. J. Meschi and R. J. Myers, J. Am. Chem. Soc. 78, 6220 (1956); J. Mol. Spect. 3, 405 (1959); U. Blukis and R. J. Myers, J. Phys. Chem. 69, 1154 (1964).

167. D. O. Cowan, R. Gleiter, O.Glemser and E. Heilbronner, Helv. Chim. Acta 55, 2418 (1972).

168. D. O. Cowan, R. Gleiter, O.Glemser, E. Heilbronner and J. Scharblin, Helv. Chim. Acta 54, 1559 (1971).

169. R. N. Dixon, G. Duxburg, G. R. Fleming and J. M. V. Hugo, Chem. Phys. Lett. 14, 60 (1972).

170. R. L. Dekock, D. R. Lloyd, A Breeze, G. A. D. Collins, D. W. J. Cruickshank, and H. J. Lempka, Chem. Phys. Lett. 14, 525 (1972).

171. P. W. Schenk and R. Steudel, Z. Anorg, Allgem, Chem. 342, 253 (1966).

172. J. H. D. Eland and C. J. Danby, Internat. J. Mass Spectrom. Ion Phys. 1, 111 (1968).

173. D. C. Frost, S. T. Lee and C. A. McDowell, unpublished CNDO/2 results.

174. R. Hageman, Compt. Rend. 225, 1102 (1962).

175. N. Wiberg. H. Bachhuber and G. Fischer, Angew. Chem. Int. Ed.) 11, 829 (1972).

176. N. Wiberg. G. Fischer and H. Bachhuber, Chem. Ber. 197, 1456 (1974).

177. C. Willis and R. A. Back, Can. J. Chem. 51, 3605 (1973).

178. S. N. Foner and R. C. Hudson, J. Chem. Phys. 28, 719 (1958).

179. E. J. Blau and B. F. Hochneimer, J. Chem. Phys. 41, 1174 (1964).

180. K. Rosengren and G. C. Pimentel, J. Chem. Phys. 43, 507 (1965)

181. A. Trombetti, Can. J. Phys, 46, 1005 (1968).

182. V. E. Bondybey and J. W. Nibler, J. Chem. Phys. 58, 2125 (1973).

183. J. W. Nibler and V. E, Bondybey, J. Chem. Phys, 60, 1307 (1974).

184. M. Carlotti, J. W. C. Johns and A. Trombetti, Can. J. Phys. 52, 340 (1974).

185. R. A. Back, C. Willis and D. A. Ramsay, Can. J. Chem. 52, 1006 (1974).

186. M. B. Robin, R. R. Hart and N. A. Kuebler, J. Am. Chem. Soc. 89, 1564 (1967).

187. D. P. Wong, W. H. Fink and L. C. Allen, J. Chem. Phys. 52, 6291 (1970).

188. G. Wagniére, Theo. Chim. Acta, 31, 269 (1973).

189. N. C. Baird and J. R. Swenson, Can. J. Chem. 51, 3097 (1973).

190. K. Osafune, S. Katsumata and K. Kimura, Chem. Phys. Lett. 19, 369 (1973).

191. C. R. Krüger and H. Niederprüm, Inorg. Synthesis Vol. 8, p. 15 (1966).

192. U. Wannagat and H. Niederprüm, Chem. Ber., 94, 1540 (1961).

193. R. J. Boyd, J. C. Bünzli, J. P. Snyder and M. L. Heyman, J. Am. Chem. Soc. 95, 6478 (1973).

194. E. Haselback, J. A. Hashmall, E. Heilbronner and V. Homung, Angew. Chim. (Int. Ed.) 8, 878 (1969).

195. E. Haselback and E. Heilbronner, Helv. Chim. Acta, 53, 684 (1970).

196. E. Haselback, E. Heilbronner, A. Mannschreck and W. Seitz, Angew. Chem (Int. Ed.) 9, 902 (1970).

197. E. Lindholm, Arkiv für Fysik 40, 97 (1968).

198. E. M. Kosower, Acc. Chem. Res. 4, 193 (1970).

199. M. N. Ackermann, J. L. Ellenson and D. H. Robinson, J. Am. Chem. Soc. 90, 7173 (1968).

200. M. N. Ackermann, Inorg. Chem. 10, 272 (1971).

201. M. N. Ackermann, M. R. Hallmark, S. K. Hammond and A. N. Roe, Inorg. Chem. 11, 3076 (1972).

202. D. Sellmann, A. Brandl and R. Endell, Angew. Chem. (Internat. Ed.) 12, 1019 (1973).

203. W. Steinmetz, J. Chem. Phys. 52, 2788 (1970).

204. M. N. Ackermann, J. L. Burdge and N. C. Craig, J. Chem. Phys. 59, 203 (1973).

205. D. C. Frost, S. T. Lee and C. A. McDowell, Chem. Phys. Lett 4, 472 (1973).

206. T. E. Gier, J. Am. Chem. Soc. 83, 1769 (1961).

207. J. W. C. Johns, H. F. Shurvell and J. K. Tyler, Can. J. Phys. 47, 893 (1969).

208. J. B. Roberts, H. Marsmann, I.Absar and J. R. Van Wazer, J. Am. Chem. Soc. 93, 3320 (1971).

209. G. Herzberg, Molecular Spectra and Molecular Structure, Vol. 3. von Nostrand, N.Y. 1966.

210. H. M. Rosenstock, Int. J. Mass Spect. Ion Phys. 7, 33 (1971); and refs. therein.

211. D. J. Ives, R. W. Pittman and W. Wardlaw, J. Chem. Soc., 1080 (1947).

212. T. G. Pearson and P. L. Robinson, J. Chem. Soc., 652 (1932); R. H. Prucell and F. D. Zahoorbux, ibid, 1029 (1937).

213. L. Ya. Markoviskii, N. V. Vekshina and T. K. Voivodskaya, Zh. Prikl. Chim. 43, 1149 (1970).

214. T. Wentink, Jr., J. Chem. Phys. 29, 788 (1958); 30, 109 (1959).

215. E. Ishiguro and M. Kobori, J. Phys. Soc., Japan, 22, 263 (1967).

216. T. N. Radwan and D. W. Turner, J. Chem. Soc. (A), 85 (1966).

217. J. T. Herron and H. I. Schiff, J. Chem. Phys. 24, 1266 (1956).

218. G. R. Cook, in Recent Developments in Mass Spectrometry, (K. Ogata and T. Hayakawa, eds.), p. 761, University Park Press, 1970.

219. S. Rottenberg and H. F. Schaefer, III, Mol. Phys. 21, 317 (1970).

220. C. Petrongolo, E. Scrocco and J. Tomasi, J. Chem. Phys. 48, 457 (1968).

221. S. D. Peyerimhoff and R. J. Buenker, J. Chem. Phys. 47, 1953 (1967).

222. O. Edgvist, E. Lindholm, L. E. Selin, L. Asbrink, C. E. Kyuatt, S. R. Mielczarek and J. A. Simpson, Physica Scripta 1, 172 (1970).

223, I. H. Hillier and V. P. Saunders, Mol. Phys. 22, 193 (1971).

224. R. N. Dixon, G. Duxbury, M. Horani and J. Rostas,

Mol. Phys. 22, 977 (1971).

225. J. C. D. Brand, J. L. Hardwick, R. J. Pirkle and C. J. Selisker, paper C6, 28th Symp. on Mol. Struct. and Spect., Columbus, Ohio, June 1973.

226. F. G.Herring, private communication.

227. L. Pauling, The Nature of the Chemical Band, 3rd ed. P. 345. Cornell University Press, 1960.

228. S. D. Peyerimhoff and R. J. Buenker, Theo. Chim. Acta 9, 103 (1967).

229. D. P. Chong, F. G. Herring and D. Williams, to be published.

230. L. Landau and W. H. Fletcher, J. Mol. Spect. 4, 276 (1960).

231. H. Basch, A. Viste and H. B. Gray, Theo. Chim. Acta 3, 458 (1965).

232. R. J. Boyd and M. A. Whitehead, J. Chem. Soc. (A), 2598 (1969).

233. H. Johnston and R. Graham. J. Phys. Chem. 77, 62 (1973).

234. R. Kaplan and H. Shechter, Inorg. Syn. 4, 52 (1953).

235. R. Ryason and M. K. Wilson, J. Chem. Phys. 23, 2000 (1954).

236. H. Cohn, C. K. Ingold and H. G. Poole, J. Chem. Soc., 4275 (1952).

237. R. E. Dodd, J. A. Rolfe and L. A. Woodward, Trans. Fara. Soc. 52, 145 (1956).

238. J. W. Rabalais, J. Chem. Phys. 57, 960 (1972).

239. J. Berkowitz, in Elemental Sulfur (B. Meyer, ed.) Chap. 7. Interscience, New York, 1965.

240. T. L. Leggett and D. A. Kohl, J. Chem. Phys. To be published.

241. R. C. Ivey, P. D. Schulze, T. L. Leggett and D. A. Kohl, J. Chem. Phys. 60, 3174 (1974).

242. D. R. Johnson and F. L. Lovas, Chem. Phys. Lett. 15, 65 (1972).

243. O. L. Chapman and C. L. McIntosh, Chem. Commun., 770 (1971); P. A. Baron and R. D. Brown, Chem. Phys. 1, 444 (1973).

244. K. Hagen and K. Hedberg, J. Am. Chem. Soc. 95, 1003; 1010 (1973).

APPENDIX

```
CCCC              THIS PROGRAM CALCULATES FRANCK-CONDON FACTORS USING
CCCC   HARMONIC OSCILLATOR APPROXIMATION BY THE PROCEDURE OUTLINED IN
CCCC  SECTION 2.3.3 IN THIS THESIS.
CCCC              REFERENCES:
CCCC  1. D. C. FROST, S. T. LEE AND C. A. MCDOWELL, JCP 59, 5484 (1973).
CCCC  2.  H. M. ROSENSTOCK JCP 41, 3454 (1964); IBID 44, 1271 (1966).
CCCC  3.  J. B. COON ET AL. J. MOL. SPECT. 8, 285 (1962).
CCCC       PROGRAM WRITTEN BY SHUIT-TONG LEE IN 1972 AT THE DEPARTMENT
CCCC  OF CHEMISTRY, THE UNIVERSITY OF BRITISH COLUMBIA
CCCC
CCCC                      INPUT DATA
CCCC  1ST CARD IDENTIFICATION (20A4)
CCCC  2ND CARD (3(F15.7,5X),2I2)
CCCC     1ST ENTRY    VIBRATIONAL FREQUENCY OF THE MOLECULE IN WAVE NO.
CCCC     2ND ENTRY    VIBRATIONAL FREQUENCY OF THE ION IN WAVE NO.
CCCC     3RD ENTRY    CHANGE IN NORMAL COORDINATE IN (GM**0.5*CM*10D20),
CCCC                  IF EQUAL TO 0, IT IS INITIALIZED INTERNALLY,
CCCC                  SEE 5TH ENTRY BELOW
CCCC     4TH ENTRY    MAX NO. OF VIBRATIONAL PEAKS FOR WHICH CALN IS
CCCC                  DONE.....MAX NO. = 16
CCCC     5TH ENTRY   IO = 2   RATIO OF V = 2 TO V = 1 IS USED TO
CCCC                          CALCULATE THE CHANGE IN NORMAL COORD.
CCCC                 IO = 1   RATIO TO V = 1 TO V = 0 IS USED TO
CCCC                          CALCULATE THE CHANGE IN NORMAL COORD.
CCCC                 IO = 0   BOTH CASES ABOVE ARE CALCULATED AND THEIR
CCCC                          MEAN IS TAKEN.
CCCC  3RD CARD  READ IN EXPERIMENTAL FRANCK-CONDON FACTOR  (8(10D4))
CCCC  4TH CARD (I2,3X,F12.8,2X,I2)
CCCC     1ST ENTRY   NO OF INCREMENT
CCCC     2ND ENTRY   STEP OF INCREMENT
CCCC     3RD ENTRY   THE NO OF THE MOST INTENSE PEAK   MAXVIB= VIB NO + 1
CCCC                 IF MAXVIB = 0  FRANCK-CONDON FACTORS ARE CALCULATED,
CCCC                 OTHERWISE RATIO OF FCF ARE CALCULATED
      DOUBLE PRECISION BETA,GAMA,X,Y,Z,RFCF,FCF,A,TEST,ERROR
      DIMENSION RFCF(20),FCF(20),IDEN(20),TEST(20)
      READ(5,10) (IDEN(I),I=1,20)
      WRITE(6,20) (IDEN(I),I=1,20)
   10 FORMAT(20A4)
   20 FORMAT('1',' FRANCK-CONDON FACTORS OF THE MOLECULE',2X,20A4//)
      READ (5,30) FREQM,FREQI,D,NOVIB,IO
      WRITE(6,40) FREQM,FREQI,D,NOVIB
   30 FORMAT(3(F15.7,5X),2I2)
   40 FORMAT(' MOLECULAR VIB FREQ = ',F7.2,'CM-1',10X,
     1'ION VIB FREQ = ',F7.2,'CM-1'//' CHANGE IN NORMAL COORDINATE = ',
     2F7.4//' MAX VIB PEAK CALCULATED = ',I2//)
      READ(5,600) (TEST(I),I=1,16)
  600 FORMAT(8D10.4)
      READ(5,80) N,DINC,MAXVIB
   80 FORMAT(I2,3X,F12.8,2X,I2)
      WRITE(6,90) N,DINC
   90 FORMAT(' NO OF INCREMENT = ',I2/' STEP OF INCREMENT = ',F7.4//)
```

```
      BETA=FREQM/FREQI
      X=1.-BETA
      Y=1.+BETA
      IF (D.GT.0.0) GO TO 159
      D1=0.0
      D2=0.0
      TEST1=TEST(1)
      TEST2=TEST(2)
      TEST3=TEST(3)
      IF (IO.EQ.2) GO TO 31
      R=SQRT(TEST2/TEST1)
      Z=R*Y/SQRT(2.)
      D1=Z/(BETA*0.1336466*SQRT(FREQI))
      IF (IO.NE.0) GO TO 61
   31 R=SQRT(TEST3/TEST2)
      S=R**2*Y**2-2*X
      Z=(R*Y+SQRT(S))/2.
      D2=Z/(BETA*0.1336466*SQRT(FREQI))
   61 D=(D1+D2)/2.
  159 DO 1000 K=1,N
      IF (K .GT. N) GO TO 1100
      IF (K .EQ. 1) GO TO 160
      D=D+DINC
  160 WRITE(6,95) D
   95 FORMAT('1',' CHANGE IN NORMAL COORDINATE = ',F7.4///)
      GAMA=0.1336466*SQRT(FREQI)*D
      Z=BETA*GAMA
      I=1
      RFCF(1)=1.
      I=I+1
      IF (I .GT. NOVIB) GO TO 800
      RFCF(2)=2.*Z**2/Y**2
      I=I+1
      IF (I .GT. NOVIB) GO TO 800
      RFCF(3)=(2.*Z**2/Y+X)**2/(2.*Y**2)
      I=I+1
      IF (I .GT. NOVIB) GO TO 800
      RFCF(4)=(2.*Z**3/Y+3.*X*Z)**2/(3.*Y**4)
      I=I+1
      IF (I .GT. NOVIB) GO TO 800
      RFCF(5)=(16.*Z**4/Y**2+48.*Z**2*X/Y+12.*X**2)**2/(24.*16.*Y**4)
      I=I+1
      IF (I .GT. NOVIB) GO TO 800
      RFCF(6)=(32.*Z**5/Y**2+160.*Z**3*X/Y+120.*X**2)**2/
     1  (120.*32.*Y**6)
      I=I+1
      IF (I .GT. NOVIB) GO TO 800
      RFCF(7)=(64.*Z**6/Y**3+480.*Z**4*X/Y**2+720.*Z**2*X**2/Y
     1  +120.*X**3)**2/(720.*64.*Y**6)
      I=I+1
      IF (I .GT. NOVIB) GO TO 800
      RFCF(8)=(128.*Z**7/Y**3+1344.*Z**5*X/Y**2+3360.*Z**3*X**2/Y
     1 +1680.*Z*X**3)**2/(5040.*128.*Y**8)
      I=I+1
      IF (I .GT. NOVIB) GO TO 800
```

```
      RFCF(9)=(256.*Z**8/Y**4+3584.*Z**6*X/Y**3+13440.*Z**4*X**2/Y**2
     1  +13440.*Z**2*X**3/Y+1680.*X**4)**2/(40320.*256.*Y**8)
      I=I+1
      IF (I .GT. NOVIB) GO TO 800
      RFCF(10)=(512.*Z**9/Y**4+9216.*Z**7*X/Y**3+48384.*Z**5*X**2/Y**2
     1 +80640.*Z**3*X**3/Y+30240.*Z*X**4)**2/(362880.*512.*Y**10)
      I=I+1
      IF (I .GT. NOVIB) GO TO 800
      RFCF(11)=(1024.*Z**10/Y**5+23040.*Z**8*X/Y**4+161280.*Z**6*X**2/
     1  Y**3+403200.*Z**4*X**3/Y**2+302400.*Z**2*X**4/Y+30240.*X**5)**2/
     2  (3628800.*1024.*Y**10)
      I=I+1
      IF (I .GT. NOVIB) GO TO 800
      RFCF(12)=(2.048D3*Z**11/Y**5+5.632D4*Z**9*X/Y**4+
     1  5.0688D5*Z**7*X**2/Y**3+1.77408D6*Z**5*X**3/Y**2+
     2  2.2176D6*Z**3*X**4/Y+6.6528D5*Z*X**5)**2/
     3  (3.99168D7*2.048D3*Y**12)
      I=I+1
      IF (I .GT. NOVIB) GO TO 800
      RFCF(13)=(4.096D3*Z**12/Y**6+1.35168D5*Z**10*X/Y**5+
     1  1.52064D6*Z**8*X**2/Y**4+7.09632D6*Z**6*X**3/Y**3+
     2  1.33056D7*Z**4*X**4/Y**2+7.98336D6*Z**2*X**5/Y+6.6528D5*X**6)**2
     3 /(4.790016D8*4.096D3*Y**12)
      I=I+1
      IF (I .GT. NOVIB) GO TO 800
      RFCF(14)=(8.192D3*Z**13/Y**6+3.19488D5*Z**11*X/Y**5+
     1  4.39296D6*Z**9*X**2/Y**4+2.635776D7*Z**7*X**3/Y**3+
     26.918912D7*Z**5*X**4/Y**2+6.918912D7*Z**3*X**5/Y+
     3  1.729728D7*Z*X**6)**2/(6.2270208D9*8.192D3*Y**14)
      I=I+1
      IF (8 .GT. NOVIB) GO TO 800
      RFCF(15)=(1.6384D4*Z**14/Y**7+7.45472D5*Z**12*X/Y**6+
     1  1.2300288D7*Z**10*X**2/Y**5+9.225216D7*Z**8*X**3/Y**4+
     2  3.2288256D8*Z**6*X**4/Y**3+4.8432384D8*Z**4*X**5/Y**2+
     3  2.4217592D8*Z**2*X**6/Y+1.729728D7*X**7)**2/
     4  (8.71782912D10*1.6384D4*Y**14)
      I=I+1
      IF (8 .GT. NOVIB) GO TO 800
      RFCF(16)=(3.2768D4*Z**15/Y**7+1.72032D6*Z**13*X/Y**6+
     1  3.354624D7*Z**11*X**2/Y**5+3.075072D8*Z**9*X**3/Y**4+
     2  1.3837824D9*Z**7*X**4/Y**3+2.90594304D9*Z**5*X**5/Y**2+
     3 2.4216472D9*Z**3*X**6/Y+5.189184D8*Z*X**7)**2/
     4  (1.307674368D12*3.2768D4*Y**16)
      WRITE (6,99)
   99 FORMAT(' FRANCK-CONDON FACTORS'/)
  800 DO 200 I=1,NOVIB
      J=I-1
      WRITE(6,100) J,RFCF(I)
  100 FORMAT(' RFCF(',I2') = ',D11.4)
  200 CONTINUE
      IF(MAXVIB.NE.0) GO TO 560
      A=0.0D00
      DO 400 I=1,NOVIB
      A=A+RFCF(I)
  400 CONTINUE
```

```
      WRITE(6,410) A
  410 FORMAT(//' SUM OF RFCF = ',D11.4//)
      GO TO 550
  560 A=RFCF(MAXVIB)
      M=MAXVIB-1
      WRITE(5,570) M,A
  570 FORMAT(/' RFCF(',I2,') =',D11.4,3X,'  IS TAKEN AS THE REFERENCE'/)
      WRITE(6,520)
  520 FORMAT(6X,'CALCULATION',16X,'EXPERIMENT'/)
  550 DO 500 I=1,NOVIB
      J=I-1
      FCF(I)=RFCF(I)/A
      WRITE(6,510) J,FCF(I),TEST(I)
  510 FORMAT(' FCF(',I2,') = ',D11.4,10X,D11.4)
  500 CONTINUE
CCC    STANDARD DEVIATION=ERROR IS USED AS A CRITERION FOR THE BEST FIT
      ERROR=0.0D00
      DO 900 I=1,NOVIB
      ERROR=ERROR+(FCF(I)-TEST(I))**2
  900 CONTINUE
      WRITE(6,910) ERROR
  910 FORMAT(//' STANDARD DEVIATION = ',D11.4)
 1000 CONTINUE
 1100 STOP
      END
```

Publications

1. S. T. Lee and K. Morokuma, 'Ab-Initio Molecular Orbital Calculation of Nitrenium Ion and Its Implications', J. Amer. Chem. Soc. 93, 6863 (1971).

2. D. C. Frost, S. T. Lee and C. A. McDowell, 'The High Resolution Photoelectron Spectrum of CS', Chem. Phys. Lett. 17, 153 (1972).

3. D. C. Frost, S. T. Lee and C. A. McDowell, The Photoelectron Spectra of OCSe, SCSe and CSe_2', J. Chem. Phys. 59, 5484 (1973).

4. D. C. Frost, S. T. Lee and C. A. McDowell, 'The Photoelectron Spectrum of S_2O', Chem. Phys. Lett. 22, 243 (1973).

5. D. C. Frost, S. T. Lee and C. A. McDowell, 'The Photoelectron Spectrum of HCP and Comments on the First Photoelectron Band of HCN', Chem. Phys. Lett. 23, 473 (1973).

6. D. C. Frost, S. T. Lee and C. A. McDowell, 'The High Resolution Photoelectron Spectrum of Ozone', Chem. Phys. Lett. 24, 149 (1973).

7. D. C. Frost, S. T. Lee, C. A. McDowell and N. P. C. Westwood, 'The Photoelectron Spectrum of Diazene (Diimine)', to be published.

8. D. C. Frost, S. T. Lee and C. A. McDowell, 'The High Resolution HeI Photoelectron Spectrum of SO', to be published.

9. D. C. Frost, S. T. Lee and C. A. McDowell, 'Photoelectron Spectroscopic Studies of the Oxyhalides of Nitrogen. I The Nitrosyl Halides (XNO, X= F, Cl, Br)', to be published.

10. D. C. Frost, S. T. Lee, C. A. McDowell and N. P. C. Westwood, 'Photoelectron Spectroscopic Studies of the Oxyhalides of Nitrogen. II The Nitryl Halides (XNO_2, X= F, Cl) and Nitric Acid', to be published.

11. D. C. Frost, S. T. Lee and C. A. McDowell, 'A Fast Pumping, Versatile Photoelectron Spectrometer', to be published.